INVESTIGATION OF FATIGUE LOADING ON MECHANICAL JOINTS IN FIBER-REINFORCED COMPOSITE LAMINATE

Thesis Submitted for the Award of the Degree of

DOCTOR OF PHILOSOPHY

in

Mechanical Engineering

By

AKASH GUPTA

Registration No: 41800545

Supervised By

Dr. Manjeet Singh (21545)

School of Mechanical Engineering (Associate Professor)

Lovely Professional University

LOVELY PROFESSIONAL UNIVERSITY, PUNJAB

2024

DECLARATION

I, hereby declared that the presented work in the thesis entitled "**INVESTIGATION OF FATIGUE LOADING ON MECHANICAL JOINTS IN FIBER-REINFORCED COMPOSITE LAMINATE**" in fulfillment of the degree of **Doctor of Philosophy (Ph. D.)** is an outcome of research work carried out by me under the supervision Dr. Manjeet Singh, working as Associate Professor, in the School of Mechanical Engineering of Lovely Professional University, Punjab, India. In keeping with the general practice of reporting scientific observations, due acknowledgments have been made whenever the work described here has been based on the findings of other investigators. This work has not been submitted in part or full to any other University or Institute for the award of any degree.

(Signature of Scholar)

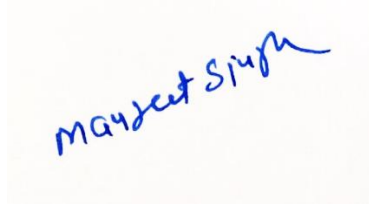Name of the scholar: Akash Gupta

Registration No.:41800545

Department/School: School of Mechanical Engineering

Lovely Professional University,

Punjab, India

CERTIFICATE

This is to certify that the work reported in the Ph. D. thesis entitled "**INVESTIGATION OF FATIGUE LOADING ON MECHANICAL JOINTS IN FIBER-REINFORCED COMPOSITE LAMINATE**" submitted in fulfillment of the requirement for the reward of the degree of **Doctor of Philosophy (Ph.D.)** in the School of Mechanical Engineering, is a research work carried out by Akash Gupta, 41800545, is a bonafide record of his/her original work carried out under my supervision and that no part of the thesis has been submitted for any other degree, diploma or equivalent course.

(Signature of Supervisor)

Name of supervisor: Dr. Manjeet Singh

Designation: Associate Professor

Department/School: School of Mechanical Engineering

University: Lovely Professional University

ABSTRACT

Fiber-reinforced composites are experiencing a growing utilization as structural materials in the aerospace and automotive industries, primarily because of their enhanced mechanical properties, reduced weight compared to traditional materials, and exceptional capacity to endure harsh weather conditions while maintaining long-lasting durability. Mechanical joints hold significant importance in the process of assembling and disassembling individual components of composite materials or large composite structures. Joints are essential to analyze structures, serving the purpose of connecting different parts. Factors such as load-bearing capacity, durability, and resistance to stress concentrations, types of loading need to be carefully considered when analyzing mechanical joints. These joints are studied by various authors under static loading but fatigue loading is a significant consideration in various applications, particularly aerospace and automotive industries. The behavior of joints differs significantly in fatigue loading from static loading conditions.

The primary objective of this study is to assess the behavior of pin joints made from glass fiber-reinforced polymer composites (GFRP) under fatigue loading conditions. Additionally, the study investigates the impact of Nano-silica incorporation on the fatigue performance of these pin joints. Furthermore, the evaluation of these joints' performance involves a thorough analysis of various geometric and material factors. The study specifically considers a pin joint configuration under fatigue loading, where two ratios are examined: the edge to circular cavity diameter ratio (E:D) and the width to circular cavity diameter ratio (W:D). These ratios are varied within the range of 3 to 5, respectively. Similarly, effective failure strength (EFS) was considered to decide the stress levels for various pin joint configurations *i.e.* 50% to 90% of EFS. The numerical analysis of pin joint failures was conducted using the FEA package, and the results were verified through experimental findings. Hand lay-up and compression moulding techniques were utilized to fabricate the composite laminates.

Fatigue tests were conducted using a tension-tension load control mode. The applied load had a sinusoidal waveform with a constant amplitude and a frequency of 2 Hz. In total five

stress levels have been considered to model the S-N curve *i.e.* 50% to 90% of the ultimate tensile strength (UTS) as per ASTM D3479. S-N curves were generated for the neat and modified GFRP composite laminates using Weibull distribution. The fatigue life of the laminate at different stress amplitudes was estimated by plotting these S-N curves, utilizing a trendline with a linear fit. The experimentally recorded cycles to failure were gathered by subjecting both neat and modified GFRP laminates under cyclic loading until failure or up to 10^6 cycles at each stress level. Furthermore, a numerical analysis of laminates was carried out to simulate and examine the behavior of composite materials under cyclic loading. This analysis was conducted using the same geometrical and fatigue loading setup and was subsequently compared with the experimental results.

In the preliminary phase, a pilot study was undertaken to identify the ideal Nano-silica weight fraction necessary for fabricating modified GFRP composite laminate. The Nano-silica content varied between 1% to 5 wt. % of epoxy resin. The study revealed that the addition of 3 wt. % of Nano-silica led to improvements in tensile strength, fatigue strength, and fracture toughness. A higher toughness not only increases the material's ability to withstand repeated loading but also provides a greater capacity to resist crack growth, ultimately contributing to improved durability and reliability. A further increase in Nano-silica content *i.e.* beyond 3 wt. % leads to a noticeable decline in tensile strength. The decrease in performance can be ascribed to the clustering of Nanoparticles, which hinders the mobility of epoxy chains and introduces structural defects in the material. For the subsequent analysis of pin joints under fatigue loading for the modified GFRP, a Nano-silica content of 3 wt. % has been selected.

The comparison between Neat GFRP and Modified GFRP composite laminate clearly shows that Neat GFRP has a steeper slope in the S-N plot, indicating lower fatigue resistance and higher vulnerability to failure under cyclic loading with fiber breakage and matrix cracking damage pattern. In contrast, the Modified GFRP composite laminate exhibits a shallower slope in the S-N plot, signifying higher fatigue resistance, extended fatigue life, and improved durability under cyclic loading conditions. The combination of fiber breakage, matrix cracking along with fiber pull-oull was observed. The stress-strain

hysteresis loop in composite materials reflects energy losses during each loading cycle, where absorbed energy is dissipated as heat. An increase in hysteresis is caused by various damages, including fiber-matrix interaction failure. This accumulated heat weakens shear strength at the interface, leading to the disruption of the bond between fibers and the matrix. As the stress level rises, the hysteresis loop's area expands due to increased friction between separated surfaces, resulting in greater energy dissipation. Cyclic loading causes a reduced slope in the stress-strain loop, indicating dynamic modulus degradation. High stress leads to aggressive damage, causing quicker modulus reduction than lower stress levels.

The study concentrated on evaluating the bearing strength of GFRP pin joints separately under low cycle fatigue (LCF) and high cycle fatigue (HCF) conditions. The geometric parameters, specifically the W:D and E:D ratios, were identified as the sole determining factors for the damage behavior of pin joints. When E:D values are small, net-tension failure was observed, and with small W:D values, shear-out failure occurred. These failures manifested suddenly and without any prior warning. On the other hand, the desired progressive mode of failure, which is the bearing mode, was observed in pin joints with W:D and E:D ratios greater than or equal to 4, indicates a non-catastrophic failure. The numerical results are closely aligned with the experimental findings. Modified GFRP pin joints exhibited a shallow slope in the S-N plot at higher W:D and E:D ratios, indicating enhanced fatigue strength in comparison to neat GFRP pin joints. The addition of Nano-silica enhances the bonding between the fibers and matrix through strong interlocking between fiber and matrix, while also effectively resisting crack propagation which is highly suitable for fatigue loading to increase the bearing strength and enable the material to withstand cyclic loads for an extended number of cycles.

For neat GFRP pin joints at E:D and W:D equal to 3, the obtained bearing strength in the LCF regime is approximately 70% of the static bearing strength. In contrast, at E:D and W:D equal to 5, the improved strength observed in the LCF and HCF regimes is 93% and 15.5% of the static bearing strength, respectively, exhibiting the bearing failure mode. Moreover, it was observed that when E:D is equal to 3 and W:D is equal to 3, 4, and 5, the joints do not demonstrate positive bearing strength under the HCF regime, leading to

catastrophic failure mode. The addition of Nano-silica has resulted in a transition of the damage mode from pure tension to shear damage mode, leading to a moderate fatigue life before failure. E:D and W:D equals 5 revealed extending fatigue life with improved bearing strength as compared to neat GFRP under the same geometric configuration *i.e.* 96.6% and 17.5% of static bearing strength under LCF and HCF regimes respectively. Among all the pin joint configurations, at E:D and W:D equals 5 the joints made from modified GFRP show the most significant increase in bearing strength, with an improvement of approximately 28.3% compared to Neat GFRP under LCF regime. Furthermore, it was noticed that by setting E:D to 5 and W:D to 4, a significant 37.02% increase in bearing strength was attained compared to the Neat GFRP pin joint under the HCF regime. However, this improvement was accompanied by a progressive damage mode.

`ACKNOWLEDGEMENT

TABLE OF CONTENT

LIST OF TABLES

LIST OF FIGURES

CHAPTER 1 - INTRODUCTION

1.1   Composite Materials

The focus of today's world has shifted toward the adverse earth's climatic conditions and the availability of limited natural resources. As a result, major automobile, marine & aircraft industries are either transitioning from gasoline-powered to electric vehicles or working to improve fuel efficiency. In several industries, there is currently a great demand for materials that may boost strength without adding a lot of weight. Extensive global research is being conducted to develop new materials to meet these requirements. Due to their great strength, low cost, and simplicity of processing, traditional metals and their alloys have historically been the main materials used in a variety of industries. However, these materials do have certain drawbacks, including poor corrosion resistance and a substantially lower strength-to-weight ratio [1]. To get over these restrictions, composite materials were developed. These materials have unique qualities including great strength and stiffness at a decreased weight with remarkable mechanical performance [2]. Fiber-reinforced composite (FRC) materials have found extensive application across diverse industrial sectors including aircraft, automobiles, space, submarines, civil structures, and more.

Composite materials are formed by combining different materials *i.e.* matrix constituent and reinforcement constituent to tailor a new material. The unique characteristics of its constituent elements are coupled to enhance their utility within the novel material. The ability to combine various materials to make composite material opens up many doors in various structural and non-structural applications. These individual materials, or constituents, are typically different in composition and/or physical properties and are combined in a way that optimizes the required strengths of composite material.

The development of composite materials also comes into existence along with their advancement. Engineers are required to design the product, choose the candidate material

based on the analysis, and then outline the fabrication technique. Engineers can generate composite components with finer tolerances due to advances in manufacturing techniques, and researchers in the material field are constantly developing new composite materials.

1.2   Classification of Composite Materials

The categorization of composite materials are divided according to the type of reinforced material and matrix material. Additionally, they can be further subdivided into classifications based on the specific reinforcement and matrix materials utilized.

1.2.1 Classification Based on Reinforcement

The classification of composites is based on the reinforcing technique, which includes structural, fiber reinforced composite (FRC), and particle-reinforced composites, as depicted in Figure 1.1. Within the category of FRC, there are two distinct types: discontinuous fibers and continuous fibers.
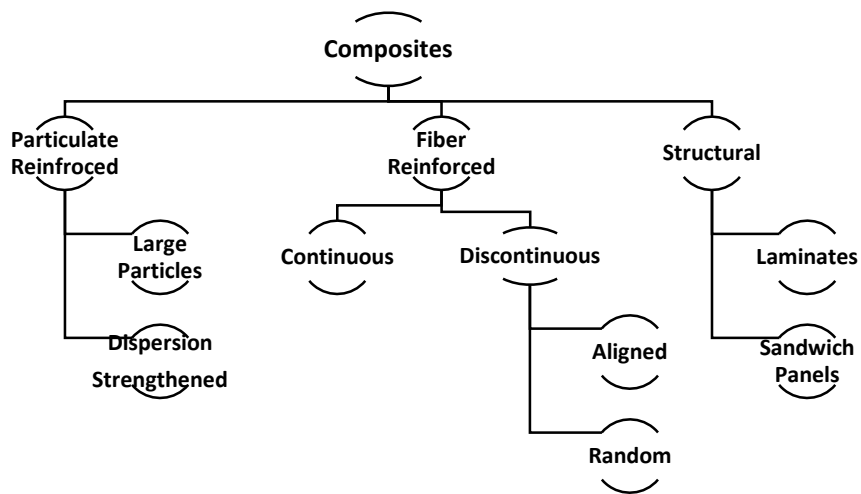
Figure 1.1 Classification of composite material in terms of strengthened form [3]

Reinforcement in composites provides strength and stiffness. It falls into two categories, and the remarkable advances in fiber development contribute to the significant improvements in composite properties compared to traditional materials. Figure 1.2 illustrates the primary types of reinforcements utilized in composite materials. The reinforcements comprise continuous aligned fibers, discontinuous fibers, particles,

2

whiskers, and diverse fiber patterns like textiles and braids. Among these, continuous, aligned fibers are the most popular and efficient, especially in high-performance applications. Continuous fibers are often transformed into various reinforcing forms to simplify the manufacturing process and attain specific features, such as improved impact resistance [4].
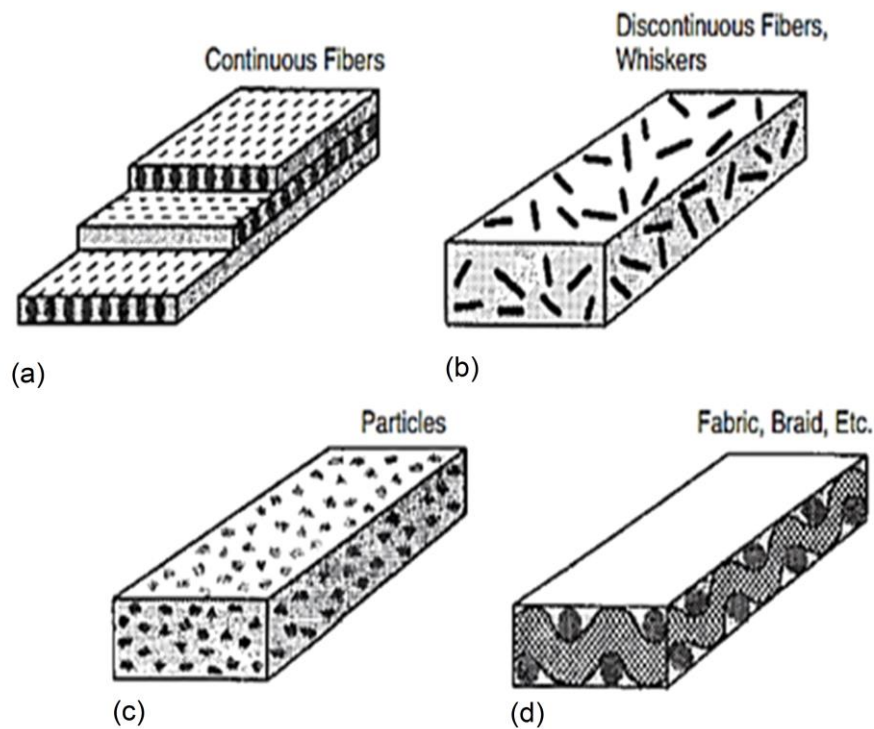
Figure 1.2 Various forms of reinforcement (a) Continuous fiber (b) Discontinuous fiber (c) Particles (d) Fabric, Braid, Etc. [5]

The majority of fibers used in structural applications are natural and synthetic fibers *i.e.* glasses, carbons (also known as graphite), various ceramic varieties, high-modulus organic fibers, basalt fibers, etc. Most fibers are initially formed as bundles of multiple filaments, commonly known as strands or ends when untwisted, and as yarn when twisted, although the specific terminology may vary across classifications. Monofilaments, which can be employed in fiber production, typically have considerably larger diameters compared to filaments in strands. Table 1.1 provides information about the characteristics of various reinforcements [5].

Table 1.1 Properties of various reinforcements [5]

Fiber	Density (g/cc)	Longitudinal Modulus (GPa)	Tensile Strength (MPa)	Coefficient of Thermal Expansion (ppm/K)	Thermal Conductivity (W/m/-K)
E-Glass	2.6	70	2000	5	0.9
S-Glass	2.5	83	4200	4.1	0.9
Aramid	1.4	124	3200	-5.2	0.04
Boron	2.6	400	3600	4.5	--
Carbon	1.8	290	7000	-1.5	160
Aluminum Oxide (Al_2O)	3.9	370	1900	7.9	--
High-Density Polyethylene (HDPE)	0.97	172	3000	--	--
Basalt	2.7	100	2900	5.5	1.7

1.2.2 Classification Based on Matrix Material

The class of composite materials can also be grouped into three primary types depending on the matrix material:

1. Polymer Matrix Composites (PMCs): These are composite materials in which the matrix material is a polymer (resin). Typically, the reinforcing material consists of fibers, such as glass, kevlar, carbon, basalt, e*tc.* that are embedded with a polymer resin to form a composite material possessing exceptional strength and stiffness. Common matrix materials are epoxy resins, vinyl ester resins, Polyester resins, phenolic polyurethane, acrylic, polyolefin, acrylonitrile butadiene styrene (ABS), etc. Thermoset polymers are commonly preferred for numerous reasons, particularly in the context of commercial aircraft. Thermoset polymer composite has been utilized in the aerospace industry for approximately the last three to four decades. in the construction of the fuselage of Boeing 787 using an epoxy-based polymer [6].

2. Metal Matrix Composites (MMCs): These are composite materials in which a metal, such as aluminum or titanium, is used as the matrix material. The reinforcing material is typically ceramic fibers or particles such as silicon carbide (SiC) or alumina (Al_2O3), boron fibers, etc. which are embedded in the metal to create a composite material with high strength, stiffness, and thermal properties [7].

3. Ceramic Matrix Composites (CMCs): These composite materials employ a ceramic material as the matrix, such as silicon carbide, carbon, alumina, zirconia, among others. Ceramic fibers, such as silicon carbide or alumina, are typically used as the reinforcing material and embedded within the ceramic matrix to form the composite material. CMCs are extensively utilized in the aerospace industry for critical components such as rocket nozzles, heat shields, brake discs, and turbine engine parts. These materials are also sought-after in various other applications, including cutting tools and biomedical implants, due to their exceptional properties [8].

Nowadays, composite materials known as PMCs are extensively utilized. Other matrix materials have notable applications, showcasing their substantial potential in both structural and non-structural applications [9]. Typically, a PMC is created through the fusion of matrix and reinforced constituents. In a composite material, the matrix plays a crucial role in maintaining the arrangement and orientation of fibers, providing structural integrity by securely holding the reinforcements in a solid form. Its functions include load transfer, protection of reinforcements from environmental damage, and the addition of functionality, polish, texture, and color [2][5][6]. Matrix materials can be classified into four groups: carbon, ceramics, metals, and polymers. Each of these classes exhibits distinct properties that significantly differ from one another, impacting the properties of the composites. Table 1.2 list the characteristics of specific matrix materials for each category.

1.2.1 Polymer Matrix Composites (PMCs)

Polymer matrix composites are made of composite materials with a polymer acting as the matrix component and fibers or particulate components acting as reinforcement [10]. In this type of composite, the polymer matrix acts as a binder that holds the fibers together, providing support and transferring loads between the fibers.

Table 1.2 Properties of Matrix materials [5]

Material	Type	Density (g/cc)	Modulus	Tensile Strength (MPa)	Thermal Conductivity (W/m-K)	Coefficient of Thermal Expansion (ppm/K)
Epoxy	Polymer	1.2	3.5	70	0.1	60
Aluminum (AA-6061)	Metal	2.7	69	300	180	23
Silicon Carbide	Ceramic	2.9	520	--	81	4.9
Carbon	Carbon	1.8	20	--	5-90	2

On the other hand, the fibers within the composite contribute to its strength and stiffness. High-strength materials like aramid, carbon, or glass fiber are frequently used as reinforcement in FRP composites. These fibers are embedded in a polymer matrix, which is usually a thermosetting resin (e.g., epoxy, polyester, and vinyl ester) or a thermoplastic resin (e.g., polyethylene, polypropylene). The combination of the strong fibers and the lightweight polymer matrix results in a material that has an excellent strength-to-weight ratio, high stiffness, and good fatigue resistance. FRP composites can be tailored to meet specific performance requirements by selecting appropriate fiber types, orientations, and volume fractions, as well as the choice of the polymer matrix [11]. Thermoset and thermoplastic materials are two broad categories of polymers, each with its advantages and applications.

- Thermosets: Thermosets are widely used resins to impart strength in structural applications. Thermoset materials are characterized by a cross-linked structure in which the molecules are bonded through covalent bonds. These materials undergo a curing process during fabrication, resulting in a hardened state that cannot be reshaped upon heating [12]. It offers high-temperature resistance, dimensional stability, chemical resistance, high strength, rigidity, etc.

- Thermoplastics: The molecules that make up thermoplastic materials are branched or linear chain molecules with strong intra-molecular connections but only moderately

strong intermolecular links [10]. It can be reshaped with the application of heat and pressure [12]. The choice of resin depends on the demands of the design as well as on manufacturing considerations. Thermoplastics polymer offers various benefits *i.e.* ease of processing, chemical resistance, high toughness, impact resistance, and low processing temperature. Table 1.3 presents the various properties of the commonly used polymer matrix material.

Table 1.3 Various properties of the polymer matrix material [10].

Material	Polymer	Density (g/cc)	Modulus (GPa)	Tensile Strength (MPa)	% Elongation (%)	Thermal Conductivity (W/m-K)	Coeff. Of Thermal Expansion (ppm/K)
Epoxy	Thermoset	1.1-1.4	3-6	35-100	1-6	0.1	60
Polyester	Thermoset	1.2-1.5	2-4.5	40-90	2	0.2	100-200
Polypropylene	Thermoplastic	0.9	1-4	25-38	>300	0.2	110
Nylon	Thermoplastic	1.14	1.4-2.8	60-75	40-80	0.2	90
Polycarbonate	Thermoplastic	1.06-1.20	2.2-2.4	45-70	50-100	0.2	70
Polysulfone	Thermoplastic	1.25	2.2	76	50-100	--	56
Polyetherimide (PEA)	Thermoplastic	1.27	3.3	110	60	--	62
Polyphenylene sulfide (PPS)	Thermoplastic	1.36	3.8	65	4	--	54
Polyetheretherketone (PEEK)	Thermoplastic	1.26-1.32	3.6	93	50	--	47

Epoxy resins find extensive use in structural applications owing to their exceptional adhesive properties, high strength, and durability. The common applications where epoxy resin is used in structural applications are construction, infrastructure, automotive, aerospace, marine, *etc*.[13].

1.2.2 Glass Fiber-Reinforced Polymer Composite

Composite materials made of a polymer matrix reinforced with glass fibers are known as glass fiber-reinforced polymers (GFRP). Due to their exceptional strength and adaptability,

glass fibers are highly valued in structural applications. The common applications where GFRP composites are used in various sectors as shown in Table 1.4

Table 1.4 Application of GFRP composite in various sectors [14][15][16]

Sector	Application	Desired Properties
Automotive Industry	• Body panels • Bumpers • Interior components • Structural reinforcements	• Lightweight solutions • High Strength • High Stiffness • Improved fuel efficiency • Overall vehicle performance
Aerospace Industry	• Aircraft interiors • Fairing • Wing components • Radomes	• Overall weight reduction • Enhanced fuel efficiency • High strength and stiffness
Construction Industry	• Roofing materials • Panels • Pipes • Structural reinforcements for buildings	• Durability • Corrosion resistance • Dimensional stability
Marine Industry	• Boat • Hulls • Decks • Other structural components	• Excellent resistance to water • Corrosion resistance • Fatigue resistance
Sports and Recreational equipment	• Tennis rackets • Golf clubs • Hockey sticks • Bicycle frames	• Lightweight • Stiff structures • High strength • Durable
Wind energy	• Turbine blades	• High strength • Fatigue resistance • Lightweight • Higher Efficiency
Industrial equipment and infrastructure	• Tanks • Pipes • Bridges • Structural supports.	• Corrosion resistance • High strength • Durability

The secret to success in this industry is the design of lighter, stronger materials. These materials are intended for use at high temperatures and offer a superior level of corrosion resistance as compared to metals [17]. Consequently, composite materials are experiencing

growing utilization in a diverse array of structural applications, spanning from buildings and bridges to wind turbines, aerospace structures, and many more. Figure 1.3 illustrates the comparison between composite materials and conventional materials [18].
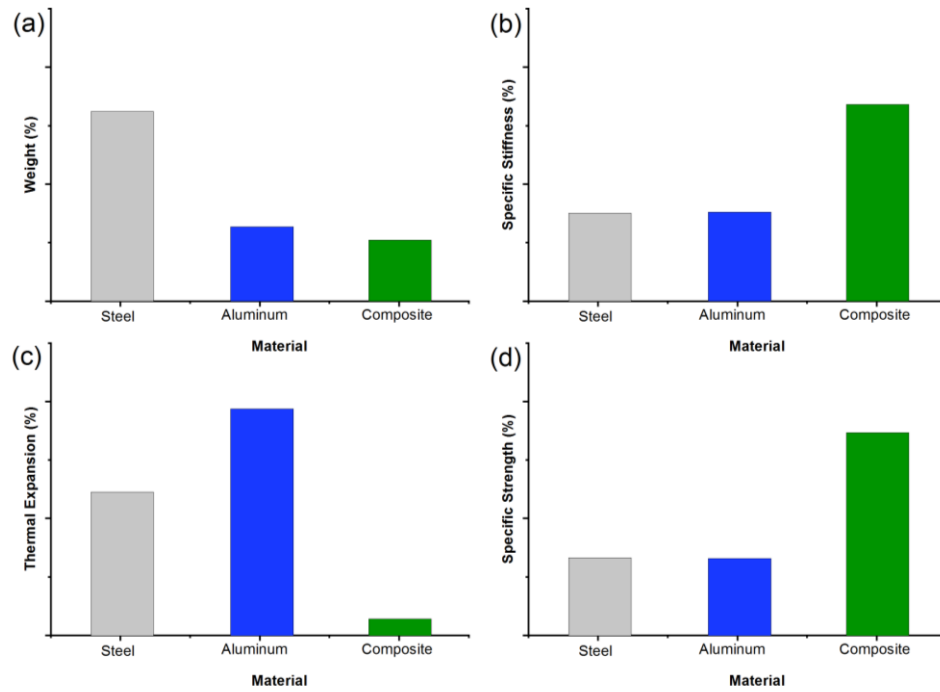
Figure 1.3 Comparison of material properties conventional material with respect to composite in terms of (a) Weight (%) (b) Specific Stiffness (%) (c) Thermal Expansion (%) (d) Specific Strength (%) [18]

1.3   Advantages of Composite Materials

Composite materials are often used instead of metals for several reasons, including:

- High Strength-to-weight ratio: In structural applications where weight is an issue, such as those in the aircraft or automotive sectors, composite materials outperform metals in terms of strength to weight ratios [9].
- Design flexibility: Composite materials can be tailored to possess specific mechanical properties, enabling enhanced design flexibility and more efficient utilization of material [18].
- Corrosion resistance: FRP composite materials are highly resistant to corrosion, which can be a major issue for metals in harsh environments. This makes

9

composites an ideal choice for applications where corrosion is a concern, such as marine or offshore structures [9].

- Fatigue resistance: FRP Composite materials are often more resistant to cyclic loading under working conditions, especially in aircraft structures are often more resistant to fatigue that can withstand repeated loading without developing cracks or other damage [19].
- Thermal insulation: Fiberglass composite materials can provide excellent thermal insulation, which can be important in applications where temperature control is critical [20].

1.4   Joining Techniques for Composites

Joining procedures are vital to guarantee the strength and performance of the entire composite structure. Joints in a structure have the potential to be one of its weakest parts, which influences the overall strength [21]. The appropriate joining method is considered to connect the component [22]–[24]. Joints are categorized into two types: (1) Adhesive Bonded Joints, and (2) Mechanical Joints. Figure 1.4 shows the types of joint configurations of composite laminates.

1.4.1 Adhesive Bonded Joints

Bonded joints are created by using adhesives to bond two or more composite components together. This type of joint offers excellent load transfer and is widely used in composite structures. By utilizing adhesive materials the interfaces are formed between two substrates referred to as adherents [25]. The selection of adhesives is based on factors such as hygrothermal conditions, composite type, and purpose of application. Cohesive failure and adhesive failure are common types of failure that can occur in adhesive joints. Adhesive failure pertains to the failure that happens at the interface between the adherents and the adhesive material itself. Cohesive failure takes place when there is a strong bond between the substrate material and the adhesive, but the inherent strength of either the substrate or the adhesive is low [26]. However, the surface preparation of the component parts and the adhesive curing conditions have a significant impact on how well the adhesive bonds.

Therefore, proper surface preparation and curing are crucial for creating strong and durable bonded joints [23]. There are various drawbacks as well for adhesive-bonded joints *i.e.* environmental sensitivity, limited joint thickness, surface preparation requirement, difficult disassembly, and limited joint strength as compared to mechanical fasteners.
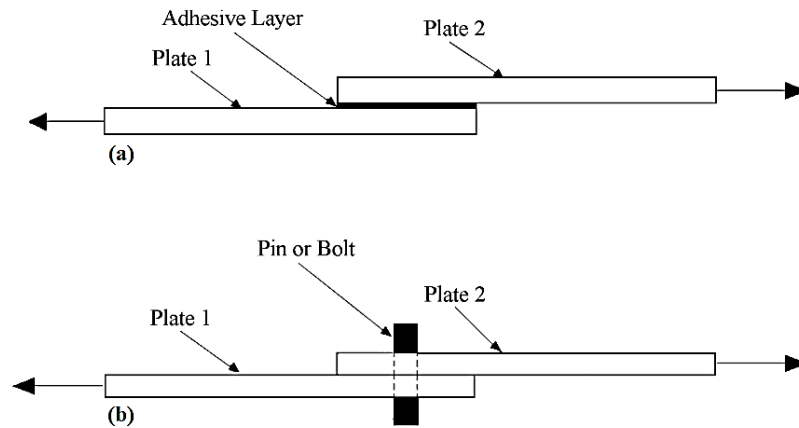
Figure 1.4 Joint Configurations: (a) Adhesive Bonded Joint, (b) Mechanical Joint

1.4.2 Mechanical Joints

In all the above applications joints are particularly important in manufacturing large components or structures because it can be challenging and sometimes impossible to fabricate or transport them as a single component [16]. By using joints to connect smaller components, manufacturers can create larger and more complex structures while also maintaining the ability to disassemble or replace parts if necessary. Additionally, joints can be designed to distribute forces and stress more evenly throughout a structure, improving its overall strength and durability. Properly designed and constructed joints can also help to prevent fatigue, cracking, and other types of damage that can occur in materials subjected to repeated stress or load. Mechanical fasteners like bolts, screws, and rivets are used to connect composite or metal parts, forming temporary or semi-permanent connections in mechanical joints [27]. Fasteners are put into pre-drilled holes in the joining components of mechanical connections. Mechanical joints offer ease of installation and inspection, in contrast to bonded joints [28]. However, mechanical joints can cause stress concentrations

11

and can compromise the structural integrity of the composite material if not properly designed [29][30].

1.5   Design Consideration of Mechanically Fastened Joints

There are two possible reasons for mechanical joint failure, first is the composite plate that contains the joint may fail, or the fastener itself may fail. In cases where the strength of the pin is comparatively larger than the composite plate, the analysis focuses on the design of laminate as per studied literature *i.e.* bearing strength and damage pattern of the composite plate. Pin joints are commonly employed for this purpose due to their ease of study and analysis [31].

1.5.1 Pin Joint

Pin joints are designed to investigate the failure behavior of FRP composite plates. This is because pin joints are assembled and disassembled without applying any external force on the composite plates [32]. To form a pin joint, one or multiple holes are drilled into the polymer composite plate, and a pin is inserted into each hole. Nevertheless, the utilization of pin joints can introduce localized damage and stress concentration, potentially leading to a decrease in the overall strength of the joint [33], [34]. Analyzing failure near the vicinity of a hole in a pin joint is a critical aspect of joint design.

1.5.2 Failure Modes in Pin Joints

It refers to the fundamental types of failure that can occur in a pin joint made of composite materials. Failure modes in pin joints can be categorized into two types. *i.e.* (a) Catastrophic failure modes, and (b) Progressive failure modes.

(a) Catastrophic failure modes: Failures resulting from net-tension and shear-out are categorized as catastrophic failures, occurring suddenly without warning, and leading to the complete collapse of the joint [35]. When experiencing net-tension failure, the separation happens perpendicular to the longitudinal edges. This particular type of failure often occurs when the specimen's breadth and hole diameter possess very low ratios. [29]. In a shear-out failure, separation occurs along the line extending from the hole toward the

12

transverse edge. In such cases, as the load increases gradually, the material in front of the hole pushes outward [32].

(b) Progressive failure modes: Bearing and Cleavage failure modes are considered non-catastrophic failure modes in nature due to the gradual failure of joints [15]. When a plate is unable to withstand the excessive crushing force exerted by a pin, it results in bearing failure. In such cases, the hole expands in the direction of the applied force [36]. Cleavage failure is a prevalent mode of failure in composite materials due to their anisotropic nature [36]. The composite material generally exhibits the highest failure strength in the fiber direction, while it tends to have lower strength in the transverse direction. In a pin joint, the stress is concentrated at the drilled area, and if a transverse load is applied, the stress concentration could be excess for the material's transverse strength, resulting in cleavage failure [21]. Figure 1.5 illustrates the typical failure modes observed in pin joints of composite materials.

1.6   Loading in Composite Structural Applications

The external forces and loads that are applied to composite materials are employed in various structural applications. Understanding the loading conditions is crucial for the design, analysis, and performance of composite structures. Because of their unique qualities and advantageous strength-to-weight ratio, composite materials are well-suited for a variety of structural applications. However, they must be able to withstand the specific types of loading they will experience during their operational life. Composite structures can experience different types of loading, including tensile, compressive, bending, shear, impact, and fatigue loading.
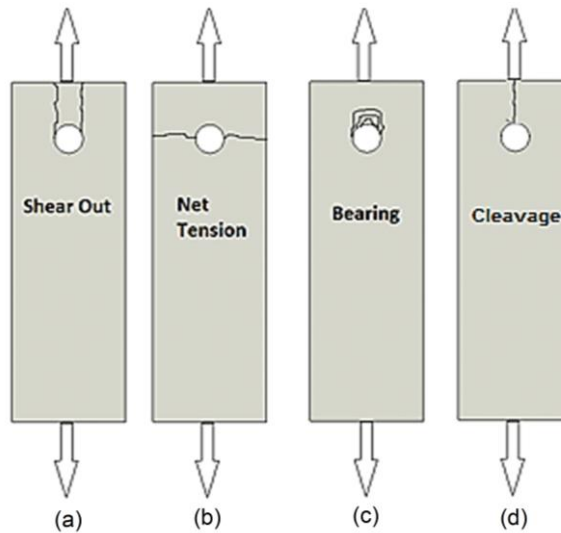
Figure 1.5 Basic damage pattern (a) Shear-out (b) Net tension (c) Bearing and (d) Cleavage [28]

Each type of loading imposes unique stresses and strains on the composite material, which must be accounted for during design and analysis. The common types of loading considered in composite structures are as follows:

- Static loading: If a material is subjected to a constant load or force over time, it can eventually fail due to gradual deformation or stress. For example, a bridge may fail due to static loading if it is not designed to handle the weight of the traffic passing over it.

- Cyclic loading: Cyclic loading can also cause fatigue and eventual failure in materials or structures over time. For example, a turbine blade in a jet engine may fail due to cyclic loading if it is subjected to repeated cycles of high-speed rotation and thermal expansion/contraction.

In general, failure due to loading types can occur when the applied load exceeds the material or structure's capacity to withstand it. The specific mode of failure will depend on factors such as the type and duration of the loading, the material properties, and the design and construction of the structure or component. To prevent failure, it is important to carefully consider the loading conditions and design materials and structures to withstand them. Static loading can cause gradual deformation or damage to a material or structure

14

over time, while cyclic loading can cause fatigue and eventually lead to failure, even at loads lower than the material's static strength.

1.6.1 Cyclic Loading in Structures

In mechanical systems, machine structures often experience cyclic loading. It is widely acknowledged that the fatigue strength of these structures is lower than their static strength, primarily due to structural degradation that occurs over repeated fatigue cycles [9]. Contrary to isotropic materials like metals and polymers, composite materials exhibit a different fatigue behavior. In composites, micro-cracks tend to develop at the early stages of loading, yet these materials can still withstand the applied load until they reach ultimate failure [37].

Different types of fatigue loading, including

- Low-cycle fatigue (LCF): LCF involves subjecting a material to a significant amount of stress during a relatively short amount of cycles, usually less than 10^5 cycles. LCF is common in applications involving high-temperature environments or rapid changes in loading conditions.
- High-cycle fatigue (HCF): HCF involves loading a material with a low magnitude of stress over a large number of cycles, typically more than 10^5 cycles. HCF is common in applications such as rotating machinery, where the material is subjected to repeated stress cycles at relatively low magnitudes.

In various applications, mechanical components experience varying forces that fluctuate in magnitude over time. Such forces induce stresses known as fluctuating stresses, which are responsible for approximately 80% of mechanical component failures due to fatigue. In practice, the pattern of stress variation is often erratic and unpredictable, as seen in the case of stresses caused by vibrations. To analyze the design of such components, simple models that describe the relationship between stress and time are used. The sine curve is the most commonly used model for this purpose. To represent cyclic stresses mathematically, three different mathematical models are generally considered: (a) fluctuating or alternating stresses; (b) repeated stresses; and (c) reversed stresses [38].

1.7   Overview of the Thesis

As per the study, Glass fiber-reinforced composites find widespread applications across various fields. Mechanical joints are commonly employed in these applications for assembly and disassembly purposes. Creating a mechanical joint involves drilling a hole for inserting a fastener. However, these joints may constitute a potential weak point in the structure, leading to unexpected failures. Therefore, a thorough analysis of mechanical joints in composites is crucial for efficient structural design. The challenge lies in the anisotropic nature of composites and the stress concentration around the drilled hole, evaluating this behavior complex.

The current thesis focuses on investigating failure in pin joints within glass fiber-reinforced polymer composites under fatigue loading conditions. This investigation takes into consideration various geometric and material aspects to optimize the performance of pin joints. Neat and modified GFRP laminates were developed for the analysis, and pin joints were constructed with and without the incorporation of Nanoparticles in the laminates to enhance their mechanical properties. The numerical analysis of pin joint failures was complemented by experimental testing, validating the findings of the study.

CHAPTER 2 - REVIEW OF LITERATURE

In this chapter, a comprehensive literature review is presented to identify existing gaps and establish the research objectives for the current study. Fiber-reinforced polymer composites are extensively used in load-bearing applications. Choosing an appropriate joining technique is essential for connecting various composite structures. Nevertheless, the stress concentration occurring around the drilled holes utilized for these joints creates vulnerable areas that can lead to the failure of structures. Identifying the appropriate fasteners is crucial in fiber-reinforced polymer composites due to their anisotropic properties. The strength and damage pattern of the composite is severely influenced by the material and geometrical parameters of the fastener. Strengthening the laminates can lead to improved joint strength. The literature review has been conducted in the following three primary categories:

- The behavior of pin joints of the fiber-reinforced composite under various parameters.
- The impact of Nano-materials on polymer composite laminates, which have the potential to be used in the fabrication of pin joints.
- The behavior of composite laminates under fatigue loading conditions.

2.1 Influence of Different Parameters on the Strength of Pin Joints.

The strength of pin joints in composite plates is influenced by various variables such as material properties, fiber stacking sequence, geometrical parameters, multi-holes, and the direction of the applied force. Numerous studies have examined the influence of these parameters on joint performance, employing both experimental and numerical approaches. The following sections present a literature review of pin joints, examining the influence of different parameters.

Mccarthy *et al.*[39] developed a three-dimensional finite element model of a single-lap composite bolted joint to examine the impact of looseness near circular cavity in

graphite/epoxy composites on the strength of bolted joints. The proposed model was examined against FEA solutions and experimental data to determine its validity. From the created model using FEA, it was concluded that it shows good agreement in terms of micro-strain obtained in experimental, numerical using quasi-isotropic layup at 5KN applied load. The authors further explore the three-dimensional effects of bolt tilting, secondary bending, and thickness deviation on stress and strain distribution. Baba [17] investigated the pin geometry and fiber placement that affect the failure mode and strength of a composite plate with pinned joints. The investigation has been done on E-glass/epoxy composite material and mechanical properties were analyzed in axial and in-plane shearing during the static loading environment. Consequences obtained that fiber alignment influences the mechanical strength near the hole periphery where failure is initiated. Furthermore, the study concluded that when the width of the joint was small and the end distance was large, net-tension failure was observed, while the shearing damage mechanism was observed in the opposite case. When the end distance increased, bearing mode as well as shearing damage mechanism were detected. However, the mechanical strength near the circular hole region was influenced by the E:D and W:D ratios, resulting in diverse damage mechanisms, but only up to a certain critical value. Icten *et al.*[33] used 2D FEA codes to predict the failure mode and strength of a mechanically fastened pin joint in a woven Kevlar-epoxy composite laminate. Three failure criteria, including maximum stress, Hashin, and Hoffman, along with the Progressive Damage approach, were employed in the analysis. The experimental and numerical results indicated that increasing the E/D and W/D ratios resulted in bearing strength mode up to a critical value. At an E/D ratio of 1, the observed failure mode was either shear-out or net-tension. Full bearing strength was observed at E/D =2 and W/D = 2. The result obtained numerically and experimentally shows good agreement in terms of failure mode and failure load. A similar study based on pin joint parameters was conducted by Karakuzu *et al.*[40]. The researchers investigated how geometric dimensions affected the bearing strength, failure mechanism, and failure strength of a circular void in a woven laminated glass-vinyl ester composite plate under tensile force. The investigation used 3D FEA with Hashin's failure criteria to obtain

numerical results. These results were validated by comparing them with experimental data from specimens tested at different E:D and W:D ratios. The numerical approach is matched with experimental results regarding progressive damage analysis and the joint's maximum strength. Positive confirmation was obtained by comparing the experimental results with the numerical predictions. The results demonstrated that there was an observation of the bearing strength mode with an increase in the E/D and W/D ratios up to a significant critical value. Tercan *et al.* [29] conducted experimental tests on grit woven 1 x 1 rib glass/epoxy composite plates with three different fiber orientations: 0º, 45º, and 90º. The study revealed that the bearing strength increased as the E/D ratio increased while maintaining a constant W/D ratio. The highest bearing strength was observed at E/D = 4 and W/D = 4 with a fiber orientation of 45º. Karakuzu *et al.* [32] examined how geometric parameters affected failure modes and failure strength in a knitted laminated glass-reinforced vinyl-ester composite plate with two parallel circular discontinuities. They used both experimental and numerical methods to assess the performance, utilizing Hashin's failure criteria. The results showed that increasing the E:D ratio while keeping the M:D and K:D ratios constant resulted in the highest bearing strength. The bearing strength attained numerically and experimentally was matched, but the failure modes obtained experimentally and numerically showed some variances. As well as Karakuzu *et al.* [41] studied the influence of geometric dimensions (edge/diameter ratio, width/diameter ratio, and distance from hole to hole) on failure modes, peak failure load, and bearing strength of a knitted laminated glass reinforced vinyl-ester composite plate with two adjacent circular voids. Experimental and numerical methods were employed, utilizing Hashin's failure criteria. The results showed that net tension mode was obtained at a lesser W/D ratio and the peak bearing strength was obtained at W/D = 3 when other parameters were kept constant. Sen *et al.*[28] investigated the effect of geometric parameters, E/D and W/D, on the bearing strength and failure mechanism of mechanically fastened bolted joints with clearance in a glass/epoxy laminated composite plate. Three different stack-up sequences were used. Preload moments of 0, 3, and 6 Nm were applied. The results showed that the bearing strength increased with increasing W/D and E/D ratios, and with increasing preload moment. When

E/D = 1, the failure mode was cleavage, net-tension, or shear-out. On the other hand, Asi [42] investigated the effect of linear densities of woven glass fiber on the bearing strength of a laminated composite plate containing a single circular cavity pin-loaded specimen. The results showed that bearing strength initially increased with increasing linear densities, but then decreased with further increases in linear densities. The ultimate bearing load was achieved at W/D = 4 and E/D = 4, which was attributed to higher void content and wrinkle levels of the specimens. Aktas *et al.*[43] conducted experimental and numerical analysis of the damage modes and bearing load of mechanically fastened pinned joints in glass-epoxy composite plates. They used ANSYS FEA with Yamada-Sun failure criteria to model the joints. The experimental results showed good agreement with the numerical predictions for the modes of failure and failure load. Similarly, Nanda Kishore *et al.*[21] examined the failure process and failure load of a multi-pinned joint in a glass-epoxy composite laminated plate. The study was supported numerically using FEA to foretell the failure along with the degradation rule. The modes of failure observed in both three-pin and four-pin joints, as determined through numerical and experimental analysis, exhibited similar results with an error percentage of 10%. If the P/D ratio increases and other S/D and E/D ratios are kept constant gives the failure mechanism of bearing mode. Moreover, Karakuzu *et al.*[44] investigated the behavior of three-pin loaded hole composite plates made of glass/epoxy composites with a stacking sequence of [0º/90º/±45º]S. Three parameters were considered: edge-to-diameter ratio (E/D), longitudinal distance of holes (F/D), and transverse distance of holes (G/D). The results showed that the maximum bearing strength is directly proportional to the E/D ratio when F/D is kept constant (F/D = 2). The G/D ratio had a minimal effect on the strength. Aluko [45] developed an analytical technique to estimate the bearing strength of pinned joints in composites. The technique used the Yamada-Sun failure criterion and the characteristic curve model. The characteristic dimensions were determined through stress analysis that did not consider bearing effects. The study showed that an increase in the W/D ratio led to an increase in joint strength. The analytical results were in good agreement with the experimental findings reported in previous literature. A geometric Parameter study was also conducted by Aktas [46] on the

impact of geometric variables on the failure mechanism and load capacity of serial pinned joints in knitted glass-epoxy composite material. Yamada-Sun failure criteria were employed to predict the damage pattern and bearing strength. The results were analyzed and validated through numerical and experimental methods. The findings revealed that the highest failure load was achieved at E/D and W/D equals 4, demonstrating a strong correlation between experimental results and numerical predictions. Qin *et al.*[47] conducted experimental and numerical investigations to examine the influence of various fasteners on the mechanical performance of pinned joints, particularly focusing on the failure mechanisms. Double-lap composite joints of bulge heads or auger fasteners were thoroughly analyzed. The impact of different fasteners on the strength, failure mechanism, and stiffness of double-lap joints was examined and established based on experimental results. The study revealed that the auger bolt exhibited approximately 32% lower non-linear onset strength but higher bearing strength near the circular hole in the direction of the bolt compared to the bulge head joint. Along with the experimental study, a statistical analysis was also performed by Khashaba *et al.*[27]. The influence of the stacking sequence on pinned joints in glass-epoxy composite laminates was investigated. The study involved failure analysis and reliability assessment using the Weibull distribution function, which was correlated with experimental results. The investigation focused on examining the impact of stacking sequence on parameters such as mean ultimate stress, bearing strength, bearing displacement, and stiffness. Four stacking sequence was considered $[0^\text{o}/90^\text{o}]_{2S}$, $[15^\text{o}/-75^\text{o}]_{2S}$, $[30^\text{o}/-60^\text{o}]_{2S}$ and $[45^\text{o}/-45^\text{o}]_{2S}$. The study findings led to the conclusion that $[45^\text{o}/-45^\text{o}]_{2S}$ maximum bearing strength was observed with maximum failure displacement. And at $[0^\text{o}/90^\text{o}]_{2S}$ stacking sequence has higher displacement and critical failure stress was perceived. There is a strong alignment between the theoretical model and experimental results. In a similar context, Olmedo *et al.*[48] conducted an analysis of an analytical model for pin joint strength prediction. Characteristic curve model and spring-mass theory were applied to foretell damage due to bearing mode. The presence of the bearing component replicated the bearing stiffness of entirely all plies to compute the damage load and foretell the bearing failure in each ply. The inaccuracy in foretelling preliminary stiffness was

21

almost 5%, and the maximum load was forecast with an error of almost 7%. Thus this theory can be adopted as a prognostic tool in the design of pin joints of composites. Another refined finite element model was presented by Turan *et al.*[49] investigated the failure mechanism and load capacity of pin joints in unidirectional carbon-epoxy composite laminates. They used both numerical and experimental methods. The numerical study used finite element analysis (FEA) with a progressive damage approach and Hashin's failure criteria. The results showed that the failure strength increases with increasing E/D and W/D ratios. This was consistent with both the numerical and experimental findings. Cesim [50] examined woven fabric composites pin joints at varous parameters, employing E/D and W/D ratios of 1:3 and 3:4, respectively. The study found that small weaving angles had a greater impact on the laminates with a multi-directional stacking sequence. Nevertheless, layups with identical orientations exhibited a lower load-carrying capacity in comparison to those with different directions. Another finite element method proposed by Pisano *et al.* [51] employed a limit analysis numerical technique at the lamina level to perform upper and lower bound estimates that secure orthotropic laminates under in-plane stress conditions. The failure loads estimated using the layer-by-layer formulation exhibited a lower percentage error compared with an experimental data from literature. The study also offered a more comprehensive understanding of the failure modes and progression of damage, taking into account the ply orientations.

Irisarri *et al.*[51] developed an enhanced finite element model to predict the load-carrying capacity of bolted joints in CFRP laminates. The model incorporated cohesive elements to capture the initiation and propagation of delamination. A viscoelastic model was employed by Irisarri *et al.* [52] to characterize the ply behavior, incorporating a progressive damage approach. The proposed model also considered the effects of material, stacking sequence, and geometric parameters, as well as friction and pin-hole clearance. The clamping forces' impact on the onset of damage and the bolted joint's bearing strength was partially accounted for by the model. Furthermore, A novel approach to investigate the damage development process in single pinned joints in glass-epoxy composite laminates was presented by Ondurucu *et al.* [52], which involved performing characterization on the

specimens tested under bearing loads. The investigation considered the effect of geometric parameters on both the damage mode and corresponding load-carrying capacity. The shear-out specimens exhibited cracks within the matrix in the direction of applied loads, while the bearing specimens displayed brittle fractures on the fibers. Li *et al.* [53] examined pin joints using a probability approach to perform deterministic progressive damage analysis with 2D FEA was employed. The study revealed that the degradation rules had a significant influence on the bearing strength of the joint. A design methodology using two limit analysis numerical procedures demonstrated by Pisano *et al.* [62] the Elastic Compensation Method and the Linear Matching Method, to validate numerical results. The numerical results were subsequently compared to a substantial amount of experimental data from the literature, demonstrating a strong agreement between them. In another study, Zhang *et al.* [55] proposed a model that utilizes progressive damage analysis (PDA) and the characteristic length method (CLM) for multi-pin joints in composite plates. The study found that the material degradation rules have a significant impact on the failure load, and it also shows coherence with experimental results. A numerical analysis of the clearance fit was conducted by Murthy *et al.* [56] studied the influence of hole clearance at the pin/bolt-hole interface in mechanical joints. In the absence of clearance, the contact status does not change with increasing loads, and the problem remains linear. And they conclude that the cosine distribution on the plate through the pin underestimates the progressive failure and overestimate the shearing and net-tension failure effect Esmaeili and Chakherlou [57] conducted a numerical investigation on the influence of bolt clamping of joints. The study utilized a novel experimental approach that involved a metal insert between the plate and the nut. This method allowed for the determination of the bolt clamping force resulting from different applied torques during the tightening process for both types of joints. The findings revealed that higher bolt torque resulted in decreased stresses, mainly due to the compressive stresses. Moreover, the stress concentration around the hole was notably diminished in the hybrid joints. The study concluded that, compared to simple joints, hybrid joints demonstrated superior static strength across all levels of bolt torque. Similarly, Qin *et al.* [47] investigated the mechanical behavior of composite bolted

joints influenced by various types of fasteners experimentally and numerically. The study focused on examining the mechanical behavior of joints assembled using protruding head and countersink fasteners, and finite element analysis was employed to validate the obtained results. The countersink fasteners resulted in lower initial failure loads compared to the protruding head fasteners. Additionally, the final failure displacement was 1 mm larger for the countersink joints than for the protruding head joints. Furthermore, the nonlinearity onset load was higher in the case of protruding head joints than in the countersunk head joints. Joints with protruding heads demonstrated 4.5% higher rupture strength than those with countersink heads.

2.2   Influence of Nano-material in the Polymer Composite Laminate

By adding Nanoparticles to the matrix materials of polymer composites, various mechanical properties can be improved. These enhanced materials have the potential to be used in the preparation of pin joints, resulting in stronger joints. This review presents a comprehensive overview of the literature on the use of different Nanoparticles in polymer composites.

Asi [35] conducted a study where Al2O3 was incorporated into the glass epoxy composite to enhance the load-carrying capacity of the pin joint. The Al2O3 particles were added in varying weight percentages of 7.5%, 10%, and 15%. The greatest bearing strength was achieved with a 10% wt. % of Al_2O_3. Conversely, the bearing strength declined beyond 10 wt. % of Al_2O_3. Similarly, Arun *et al.* [58] explored the influence of TiO2 and ZnS fillers on the matrix materials in the mechanical joints of glass fiber-reinforced polymer. The researchers found that the addition of these fillers increased the strength of the mechanical joints, with the greatest increase observed at filler volumes of up to 2%. Moreover, both composites based on Nano-SiO2/epoxy resin and standard SiO2/epoxy resin showed an initial increase and subsequent decrease in toughness as the filler content reached 4 wt.%. Nano-composites composed of silica and polyurethane (SiO2/PU) were synthesized by Zhu *et al.* [59]. The properties of the electrophoretically prepared membrane modified with SiO2/PU exhibited an improvement in terms of strength compared to unmodified and PU-

modified laminates. An experimental study on the macroscopic and microscopic fracture characteristics of SiO2/epoxy Nano composites was conducted by Yao *et al.* [60]. A three-point bending test was utilized. The digital speckle correlation method was employed to analyze the deformation at the crack tip in the Nano-composites at a full-field level. SEM and FE-SEM were employed to analyze the microscopic fracture characteristics and propagation of crack behavior. The authors investigated the impact of varying Nanoparticle SiO_2 on the toughness of the Nano-composites. The findings revealed that the Nano composite with a Nanoparticle content of 3 wt. % exhibited higher fracture toughness and improved resistance to deformation compared to the other Nano composite variations. Moreover, a study to investigate the influence of Nano-silica was conducted by Jumahat *et al.* [61]. To prepare the Nano-composites, a 40 wt. % Nano-silica/epoxy master batch was utilized, with Nano-silica content ranging from 5-25 wt. %. Additionally, they used TEM to characterization the dispersion of the silica within the epoxy matrix. The addition of 25 wt. % Nano-silica resulted in approximately 38% higher tensile modulus and 24% higher tensile strength compared to the unmodified epoxy. In a similar context, composites reinforced with TiO_2 for dental purposes were investigated by Hua *et al.* [62] by employing a validated Nano scale Representative Volume Element (RVE). Increasing the Nanoparticle content from 1 vol. % to 5 vol. % led to a nearly linear rise in the modulus and strength of the composite, as observed. The study emphasized the significant impact of interphase stiffness on the composite's modulus and strength. Likewise, Myskove *et al.* [63] examined the concentration of montmorillonite and temperature affects the curing rate and mechanical properties of composite materials. Modified clay was introduced into an epoxy-amine hardener system, and its impact on the curing reaction rate was observed. The inclusion of clay influenced the modulus of the epoxy systems in both the glassy and rubbery states, leading to enhanced tensile mechanical properties. A behavior of Nano clay with epoxy studied experimentally by Lam *et al.* [64] examined the effect of varying Nano clay content on the inter-laminar shear properties and hardness of Nano clay/epoxy composites was investigated. Different sizes of Nano clay/epoxy clusters were observed after extruder mixing. The study revealed that the addition of a small amount of Nano clay

led to an enhancement in the micro-hardness of the composites. However, beyond a certain threshold, the hardness declined as the content of Nano clay was increased, likely due to the clusters reaching a critical size limit, resulting in a decreased reinforcing effect of the Nano clay. The addition of Nano clay particles resulted in a decrease in the short beam shear strength of the epoxy, as revealed by the inter-laminar shear test. The fractured samples exhibited shiny surfaces of the clusters, indicating poor bonding between Nanoclay and matrix with lower strength. Brunner *et al.* [65] conducted a study to compare the impact of a Nano-modified epoxy matrix with an unmodified epoxy matrix on the fracture toughness. It was observed that toughness and energy release of approximately 40-50% and 10-20%, respectively, in the epoxy matrix modified with Nanoparticles. Moreover, the inclusion of 10 wt. % of functionalized organo-silicate clay resulted in a significant increase of over 50% in both the tensile and compressive modulus. Similarly, Chowdhury *et al.* [66] fabricated carbon fiber/epoxy laminates by incorporating Nanomer I-28E Nano clay-modified epoxy at varying weight percentages. They evaluated the flexural and thermo-mechanical properties of the resulting Nano-composites and compared them to the pristine samples. The microstructure of the composites was examined using Scanning Electron Microscopy. By adding 2 wt. % of Nano clay to carbon/SC-15 epoxy composites, a significant enhancement of approximately 31% in strength and 21% in modulus was achieved compared to the neat composite. In a similar study, Jawahar *et al.* [67] investigated the tribological properties of polyester and the objective was to assess the impact of Nano clay on the tribological performance of the composites and compare it with conventional clay-filled composites. The findings revealed that the Nano-composites demonstrated a remarkable improvement of up to 85% in wear resistance and a 35% reduction in the coefficient of friction. The Nano-composite with 3 wt. % clay exhibited the highest wear resistance and the lowest coefficient of friction. These results emphasize the potential advantages of incorporating Nano clay to enhance the tribological properties of thermoset polyester composites. Kim *et al.* [68] analyzed the fracture toughness of epoxy resin by adding Nano-particle additives, specifically carbon black and Nano clay. Fracture toughness was assessed using single-edge notched bend specimens at room temperature

(25°C) and cryogenic temperature (-150°C). The findings indicated an improvement in fracture toughness for the reinforced epoxy resin at room temperature, but a decrease at cryogenic temperature, despite the presence of the toughening effect. While the inclusion of Nanoparticles in the composite laminate matrix improved inter-laminar fracture toughness and impact characteristics at room temperature, the un-reinforced epoxy exhibited superior structural properties at cryogenic temperatures. Furthermore, the study revealed that the incorporation of Nano clay enhanced the adhesion between fibers and the matrix, resulting in improved mechanical properties of the composites. To evaluate the mechanical characteristics of FRP composite fabricated using Nano clay with polyester resin and E-glass fiber by Sundaram *et al.* [69]. The Nano-composite FRP displayed a high ultimate tensile strength, with a 50% enhancement observed at 5 wt. % of Nano clay. Likewise, the impact of the curing temperature of Nano-composites was investigated by Mohan *et al.* [74]. The study revealed that the curing temperature and clay content influenced the properties and structure of the Nano-composites. Higher curing temperatures led to improved mechanical properties compared to lower curing temperatures. Regardless of the curing conditions, the maximum enhancement in tensile properties was observed at a Nano clay concentration of 2 wt. %. Moreover, Li *et al.* [70] utilized the Nano-disassembling method to completely exfoliate epoxy/clay Nano-composites with comprehensive high performance. In this method, the incorporation of Nano-SiO2 into the mixture of montmorillonite and epoxy system served as a disassembling agent to interact with montmorillonite (MMT). Similarly, Singh *et al.* [71] conducted a study to analyze the impact of Nano clay on the bearing strength and failure mechanism of mechanical joints. The research encompassed both experimental and numerical analysis of different geometric parameters. The mechanical properties were assessed through shear, tensile, and flexural tests conducted on a universal testing machine. The properties were analyzed for different weight percentages of Nano clay. The experiment results are in positive association with the numerical outcomes based on Tsai-Wu failure criteria. The material degradation approach and characteristic curve model were applied to envisage the failure of the specimen. Sekhon *et al.* [72] conducted a study that

27

investigated the influence of Nanoparticles as fillers on the load-bearing capacity of glass-epoxy composites pin joints. The study utilized Nanoclay and Nano TiO2 in addition to the unfilled composite. It was concluded from the consequence obtained that the bearing strength of the pinned joint improved with Nano-clay as matched to Nano TiO2. Moreover, Singh *et al.* [73] examined the influence of geometric parameters on double pin joints in modified glass-reinforced epoxy with Nanoclay laminates. Both experimental and numerical analyses were conducted using the Tsai-Wu failure criteria and characteristic curve model. The study found that the bearing strength of the multi-hole pin joint configuration was mainly influenced by E/D and P/D, accounting for 62% and 65% of the impact, respectively. The experimental outcomes were positively correlated with numerical predictions. Singh *et al.* [74] utilized the Taguchi technique and Design of Experiments (DoE) to analyze the impact of geometric parameters on double pin joints of glass-epoxy Nano clay composites. Geometric parametric were taken to conduct experiments and numerical prediction using the Tsai-Wu failure criteria and characteristic curve model. The findings show that E:D is the key factor affecting the increase in bearing strength for longitudinal and transverse multi-hole cavities. It has a contributing factor of 84.5% for the series configuration and 64.23% for the parallel configuration. The experimental results show a strong correlation with the numerical predictions. In a similar context, Singh *et al.* [31] examined the influence of various ply alignments and the incorporation of Nano filler material to fabricate modified glass –epoxy on the load-bearing strength and damage mechanism of pin-loaded joints with a single hole cavity experimentally and numerically. The researchers employed Tsai-Wu failure criteria and the characteristics curve model to predict the failure modes. The specimen underwent tensile and shear tests to assess its mechanical properties at various ply orientations. It harmonized the experimental outcomes with the attained numerical solutions.

2.3   Influence of Static and Fatigue Loading Behavior of Composite Laminates

The influence of static and fatigue loading on composite materials has been the subject of numerous studies in the literature. Various researchers have explored the consequences of different loading conditions on the mechanical characteristics of composite laminates,

emphasizing aspects such as stiffness, strength, and failure mechanisms. The authors investigated the effects of static loading on composite laminates made of different fiber orientations and stacking sequences. The results demonstrated that the stiffness and strength of the laminates were influenced by various factors, including the type of fiber, fiber orientation, number of plies, and stacking sequences. The type of loading had an impact on the failure mode of the laminates, with certain laminates experiencing matrix cracking, fiber breakage, or delamination [17], [33], [75], [76]. In another study, the authors investigated the effects of fatigue loading on composite laminates made of different fiber types and orientations. The findings indicated that multiple factors, including loading frequency, stress amplitude, fiber orientation, and cycle count, had an impact on the fatigue behavior of the laminates. The existence of imperfections, such as voids or delamination, was found to significantly impact the fatigue characteristics of the laminates. These imperfections primarily led to crack initiation and propagation, serving as the primary mode of failure [77]–[79]. Ferdous *et al.* [80] examined the fatigue behavior of glass-vinyl ester based composite under tension-tension loading. The authors investigated the influence of fatigue parameters *i.e.* stress level, loading frequency, and stress concentration. Testing was conducted up to 80% of ultimate strength or 10^7 cycles. The prime objective of the study was to assess the fatigue life and corresponding damage pattern of the material. The finding revealed that the stress concentration effect plays a prime significant role under low stress levels conversely at high stress levels the mode of failure is due to pure tension. The researchers found that mean stress failure criteria were suitable for modeling low-stress conditions, while Goodman failure criteria were more appropriate for high-stress conditions. They also developed an analytical model that accurately predicted the fatigue life of GFRP composites in tension. Yadav *et al.* [81] proposed a fatigue damage model for woven glass fiber composites, which incorporated two material parameters. One parameter was directly related to fatigue life, while the other was inversely proportional to the fatigue loading level. Through their analysis of damage development, they obtained promising results indicating that the fatigue modulus exhibited an inverse relationship with fatigue strain. To validate the model, the researchers compared

29

it with experimental data from Tensile Fatigue Tests. The model accurately captured the evolution of damage in woven glass-epoxy composite laminates under various fatigue loadings, as demonstrated by its ability to predict the fatigue life of the composites. Similarly, Zhou *et al.* [82] developed a fatigue model to assess the progressive damage of fiber-reinforced composites, considering delamination and in-plane damage. The model utilized fatigue master curves and incorporated Hashin criteria for in-plane failure prediction and cohesive fatigue failure criteria for delamination. It accurately estimated the fatigue life of composites with different layup sequences and arbitrary stress ratios. The model also simulated interlayer delamination using a modified cohesive element. Experimental data from GFRP composite laminates and CFRP composite bolted joints supported the model's accuracy. Moreover, the fatigue behavior of woven GFRP laminates with different fiber orientations was analyzed by Ansari *et al.*[83]. Tensile and tension-tension fatigue tests were conducted on standardized test coupons. The off-axis laminates showed lower fatigue strength compared to on-axis laminates. Global damage was observed in on-axis laminates, while localized damage was prominent in off-axis laminates. Higher stress levels led to severe damage and shorter lifespans, while on-axis specimens exhibited better fatigue life. Giannopoulos *et al.* [84] investigated the influence of bolt clamping and fatigue behavior of AS7/8552 fiber-reinforced bolted joints. Damage initiation and final fatigue failure have been observed for the suitability of bolted joints for the aircraft industry. The finding indicated that the intensity of bolt clamping affects the strength, damage pattern, and fatigue life of FRP composite. Nakada *et al.* [85] formulated a model to predict the statistical life of CFRP subjected to creep and fatigue loads. The results indicated a decrease in long-term tensile fatigue strength with increasing cycles, while flexural fatigue strength was influenced by temperature and frequency instead of failure cycles. Similarly, Curtis [86] examined the effects of fatigue on continuous fiber composite materials, considering stress concentrators and environmental exposure, and compared them with metal fatigue. Genedy *et al.* [87] investigated the impact of MWCNTs on GFRP composite. Experimental findings showed that incorporating 0.5 wt% and 1.0 wt% MWCNTs significantly enhanced fatigue life. Specifically, 0.5 wt. % MWCNTs

increased GFRP fatigue life by 1143%, and 1.0 wt% MWCNTs improved it by 986% compared to neat GFRP. A model for developing the S-N curve has been proposed by Kassapoglou [88]. The methodology works on the premise that the number of cycles leading to failure is affected by the probability of failure happening in each cycle. This probability of failure is assumed to remain constant and is obtained from static test results with statistically determined variations. The researchers developed mathematical expressions for the cycles to failure based on the R ratio, eliminating the need for curve fitting or experimentally derived parameters. Moreover, the fatigue predictions do not require calibration through fatigue tests. After comparing the proposed model with various test cases documented in the literature, the findings demonstrated were very promising. In a similar context, Starikov and Schon [89] conducted a study on the impact of composite bolted joints under fatigue loading. They used titanium or composite fasteners to bolt composite plates, which were then subjected to fatigue loading with a stress ratio (R) of -1. Multiple measurement techniques were utilized to analyze the fatigue characteristics of the specimens, such as the implementation of strain gauges. The study's findings indicated that specimens utilizing titanium fasteners exhibited exceptional fatigue-resistance characteristics, typically resulting in bolt failure as the primary cause of failure. Furthermore, it was observed that bolt movement significantly increased over the course of fatigue life. Strain-gauge measurements also unveiled that different bolt rows exhibited varying degrees of load transfer due to fatigue degradation at those specific bolt rows. A mathematical model has been developed to describe fatigue damage in composite structures by Mao and Mahadevan [90]. They studied the properties of damage growth in composite materials and compared them to those of damage growth in uniform materials. They used the principles of continuum damage mechanics to assess the weakening of composite materials when subjected to cyclic loading. They introduced a novel damage model that consider the unique features of composite materials. The new model was demonstrated to be more precise than current models in modeling the quick damage growth that occurs early in the material's life and near the end of its fatigue life. The parameters for the new model were obtained by analyzing experimental data. A stiffness degradation

and permanent deformation of carbon fabric reinforced PPS investigated under fatigue loading by Baere *et al.* [91]. The failure of the specimen was observed to occur at the tab region rather than the gauge length, resulting in an underestimation of the fatigue life compared to the actual fatigue performance. In light of this, the proposed approach aimed to improve the geometry of the fatigue testing procedure due to the premature failure experienced by the specimen. Furthermore, the assessment focused not only on determining the cycles to failure but also on evaluating the degradation of stiffness and plastic deformation of the material. The study findings revealed that the 4-ply bi-directional woven laminate did not exhibit significant stiffness degradation, but only limited permanent damage was observed. This suggests that the material behaves in a highly brittle manner, with a very narrow stress range in the infinite life region, and failure occurring within low cycle fatigue region. Gerendt *et al.* [92] conducted a study in which they developed a progressive damage model for fiber-reinforced polymer pinned joints. The model was validated by comparing its predictions with the experimental test results, considering both static and fatigue behavior. The model demonstrated close agreement with the observed outcomes, indicating its effectiveness in accurately predicting the behavior of such joints. Sghaier *et al.* [93] conducted a study on the behavior of glass fiber-reinforced epoxy composites under high cycle fatigue conditions. The study employed a probabilistic approach and utilized Monte Carlo simulation to plot fatigue curves. The authors explore four different scenarios, considering different assumptions regarding the determinism or probabilistic nature of stress and the number of cycle values. Similarly, Samareh-Mousavi *et al.* [94] devised a fatigue model for carbon-epoxy pin joints that incorporated the influence of nonlinearity in the in-plane shear stress-strain relationship. This model encompassed a failure theory along with degradation rules for material properties. To ensure its accuracy, the fatigue model was compared to experimental tests. The results showed that considering nonlinearity led to shorter life predictions under high loads due to increased stress along the fiber length of on-axis plies. However, under lower loads, both linear and non-linear regimes exhibited similar stress states and fatigue life predictions. Dindar and Bektas [95] explored the effects of Nanosized multi-walled carbon

Nanotubes and Nanoclay into epoxy resin on the fatigue strength of glass-reinforced composite materials. The study involved incorporating both Nanoparticles at a concentration of 0.5 wt. % into the epoxy resin using an ultrasonic homogenization mixer. Composite plates were fabricated with and without MWCNT and Nano clay additions to evaluate the influence of Nanoparticles on material properties. Static and fatigue properties were compared between the two sets of specimens. The results demonstrated notable differences in both fatigue strength and tensile strength between the composite specimens with and without the Nanoparticles. The mechanical behavior of CFRP pin joints under various cyclic loadings, both on microscopic and macroscopic scales proposed experiment protocols by Sypt et al. [96] to systematically examine. During the drilling process, surface flaws are induced at the hole-bearing surface, which is subsequently tracked at the microscopic level, while the mechanical response of the laminate is evaluated macroscopically. The study aims to determine how different fatigue loading conditions affect the various damage mechanisms, which are identified by analyzing various configurations. Using this experimental approach, a general damage scenario is established for the tested material. In a similar context, Javaid et al. [97] analyzed the fatigue behavior of hybrid glass and carbon fiber composite joints in comparison to static loading, with a particular emphasis on the influence of different ply layups. Four different joint designs were investigated, namely scarf, interleaving, and two types of double scarf joints. The joints were created by co-curing unidirectional carbon fiber prepreg with 8H glass prepreg, utilizing an overlap-to-thickness ratio of 20:1. The study aimed to analyze the mechanical performance of these joint configurations under different loading conditions. The joints were tested under uniaxial tension in static tests and tension-tension fatigue in dynamic tests. Furthermore, FE analysis was employed to assess the distribution of stresses within each joint configuration. The findings indicated that the double scarf joint, with glass on the outer layer, exhibited the highest performance in both fatigue and static tension. In comparison, the interleaving joint demonstrated the second-best performance in static tension and fatigue, but it had the lowest fatigue performance among the tested joints. The study suggests that for joint designs exposed to highly stress cyclic loading conditions,

static tests alone may be insufficient to predict joint performance and fatigue tests should be conducted. Analysis of bolt and bolted connections by evaluating several thousand fatigue tests by Maljaars and Euler [98]. Their findings suggest that the current design standards need to be updated to incorporate the appropriate stress parameters and production methods to significantly reduce fatigue resistance variability. Furthermore, there is a need for updating the shape and positioning of the fatigue resistance (S-N) curves. These findings have been integrated into the latest revision of the European standard EN 1993-1-9. This article offers the context for the proposed changes focusing on Mode I cyclic loading investigated by Ramirez *et al.* [99]. SEM was utilized for a fractographic analysis to establish a connection between Stress-Intensity Range Ratio results and the failure mechanisms of the joints. The analysis demonstrated a positive bonding between the plate and adhesive in both the Co bonded and Secondary bonded joints. Padmaraj *et al.* [100] conducted a study to explore the fatigue behavior of glass epoxy laminates subjected to pure tension loading. Tension-tension sinusoidal loading tests were carried out under constant amplitude, with varying stress levels and R = 0.1, at 3 Hz. The degradation in stiffness was employed as a measure to quantify the growth of damage in the material. To anticipate the development of damage in the material, a phenomenological damage model based on cumulative stiffness degradation was employed. The results revealed that the material experienced a rapid decline in stiffness during the initial fatigue loading cycle, followed by a sustained degradation rate until failure. A wear-out model with two parameters, relying on the degradation of strength, was developed to forecast the fatigue behavior and residual strength of polymer-based composites proposed by D'Amore *et al.* [101] using data available in the literature. The authors contended that by examining the statistical distribution of cycles to failure under specific loading conditions, it is possible to derive the kinetics of strength degradation. The impact of loading frequency is a critical aspect to consider during fatigue testing of composites. When the test is conducted at low frequencies, it often requires lengthy test durations, which can introduce complicating factors like material creep. On the other hand, testing at high frequencies, typically above 10 Hz, may lead to elevated specimen temperatures, potentially causing softening of the

matrix material. Several research studies have been carried out to explore the impact of frequency on the fatigue life of composite materials [102]–[104]. Saff *et al.* [105] investigated the effect of loading frequency on the fatigue life of graphite-epoxy composite material. Increasing the load cycling frequency from 0.1 to 10 Hz resulted in more cycles required for failure. Hahn and Kim [37] observed a comparable pattern when testing a glass-epoxy composite across the frequency range of 4 Hz to 10 Hz. They also observed that the temperature rise in the tested composite samples was directly associated with the frequency. However, after analyzing the data within the specified frequency range, they concluded that the resulting temperature increase had a negligible impact on the composite's behavior [102].

2.4 Failure Modes and Strength Prediction

2.4.1 Failure Modes

Different types of failure modes can occur in a mechanically fastened joint under the tensile loading condition of composite material. Net-tension and shear types of failure modes are critical catastrophes, especially in comparison with bearing modes during compression. Such types of failure can be anticipated by raising the breadth (W) and end edge distance (E) of the composite material for a typically given size and depth. From all causal factors only bearing mode is permitted failure mode relative to other modes due to the anti-catastrophic nature and cannot be excluded by any change in configuration [41], [106]. The static compressive strength (σ_b) of a single pin-loaded composite joint can be estimated using equation (2.1).

$$\sigma_b = \frac{P}{D.t} \tag{2.1}$$

Where,

σ_b = Compressive strength

t = thickness of the plate

D = diameter of the hole

P = Load applied at the end of the plate

A significant surge was observed in the bearing strength proportionally with an alteration in the geometric variables *i.e.*, the proportion of the distance from side to cavity bore (E/D) and breadth to cavity bore (W/D), the bearing strength progressed positively [33], [72], [107]. There was a remarkable trend observed in the literature to predict the failure mode and strength using numerical and experimental methods.

2.4.2 Strength Prediction Approach

Most of the efficient approaches for predicting the modes of failure and strength are elastic limit design (ELD) [107], progressive damage analysis (PDA) [49], and characteristic curve method [108].

- *Progressive Damage Analysis*

This approach is most promising for the prediction of strength and modes of failure in composite laminated pin joints. From the existing literature, it has been found that many researchers [109]–[113] recommended the different degradation rules of material property which are shown in Table. 2.1, when failure had been identified at a point in a material [114], [115]. In PDA, the material properties of the ply were degraded by applying the degradation rule. Once the failure was detected in a ply, the ply is then disabled to bear the load and the further load is distributed to the other plies. The existing rules for the degradation of ply-by-ply material properties are empirical and based on assumptions arising from engineering constraints within the properties of composites [112], [113].

Table 2.1 Material property degradation factors [49], [109]–[112]

	E_{11}	E_{22}	E_{33}	G_{12}	G_{23}	G_{13}	v_{12}	v_{23}	v_{13}
(Camanho& Mathews 1999 (3D)	**Degradation factor**								
Tensile Matrix condition	-	0.2	-	0.2	0.2	-	-	-	-
Tensile Fiber condition	0.07	-	-	-	-	-	-	-	-
Compressive Matrix condition	-	0.4	-	0.4	0.4	-	-	-	-
Compressive Fiber condition	0.14	-	-	-	-	-	-	-	-
(Turan et al.2014) (3D)									
Tensile Matrix condition	-	$x10^{-5}$	-	-	-	-	$x10^{-5}$	-	-
Tensile Fiber condition	$x10^{-5}$	$x10^{-5}$	$x10^{-5}$	$x10^{-5}$	$x10^{-5}$	$x10^{-5}$	$x10^{-5}$	$x10^{-5}$	$x10^{-5}$
Compressive Matrix condition	-	$x10^{-5}$	-	-	-	-	$x10^{-5}$	-	-
Compressive Fiber condition	$x10^{-5}$	$x10^{-5}$	$x10^{-5}$	$x10^{-5}$	$x10^{-5}$	$x10^{-5}$	$x10^{-5}$	$x10^{-5}$	$x10^{-5}$
Fiber-matrix shear condition	-	-	-	$x10^{-5}$	-	-	$x10^{-5}$	-	-
(Icten and Karakuzu 2002) (2D)									
Fiber tensile Failure	0	-	-	-	-	-	0	-	-
Fiber compressive Failure	0	-	-	-	-	-	0	-	-
Matrix tensile Failure	-	0	-	0	-	-	0	-	-
Matrix compressive Failure	-	0	-	0	-	-	0	-	-
(Chan & Lee 1995) (3D)									
Failure detected in any condition	0	0	0	0	0	0	0	0	0
(Lessard&Shokrich 1995) (2D)									
Tensile Matrix condition	-	0	*	0	*	*	0	*	*
Tensile Fiber condition	0	0	*	0	*	*	0	*	*
Compressive Matrix condition	-	0	*	0	*	*	0	*	*
Compressive Fiber condition	10	10	*	10	*	*	10	*	*
(Kim et al.1998) (2D)									
Tensile Matrix condition	-	0	*	0	*	*	0	*	*
Tensile Fiber condition	0	-	*	-	*	*	0	*	*
Compressive Matrix condition	-	0	*	*	0	*	0	*	*
Compressive Fiber condition	0	-	*	-	*	*	0	*	*
- no reduction of moduli, * material property not applicable **Where, E_{11}, E_{22}, E_{33} are elastic modulus, G_{12}, G_{23}, G_{13} are shear modulus v_{12}, v_{23}, v_{13} are poison's ratio**									

Singh *et al.* [71] studied numerically and experimentally the influence of Nano-clay on the bearing strength and the damage mode of pin joint by ranging E:D and W:D values ranging from 2 to 5. Characteristic curve and PDA approach were used to predict the damage mode along with the failure strength as shown in Figure 2.1.
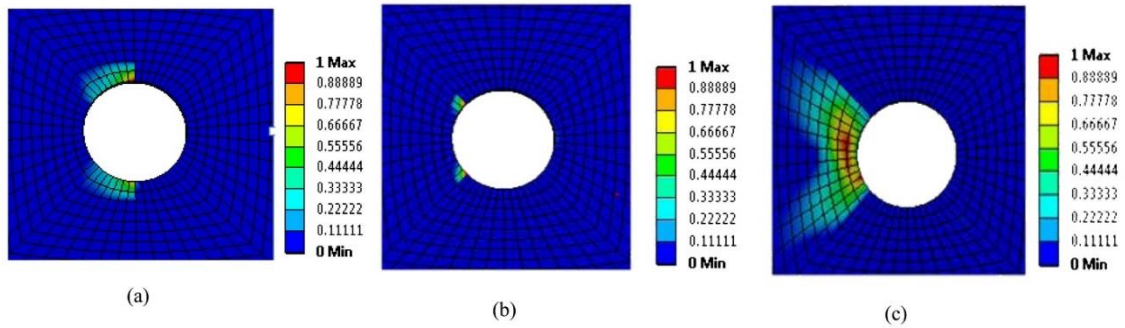
Figure 2.1 Different failure mode using PDA approach at (a) W/D and E/D equals 2; net tension (b) W/D= 4 and E/D= 2; shearing (c) W/D and E/D equals 4; shearing [71]

Camhano *et al.* [109] investigated the carbon fiber reinforced plastics by employing a 3D FE model to predict the damage progress rate along with the strength of the pin joint. The numerical predictions were compared with the experimental results as shown in Figure 2.2. A 3D model gives a more precise estimation as compared to a 2D model [116]. It is completely based on 3D failure criteria with damage-dependent constitutive equations to take into account elastic material properties to predict the joint's failure strength.
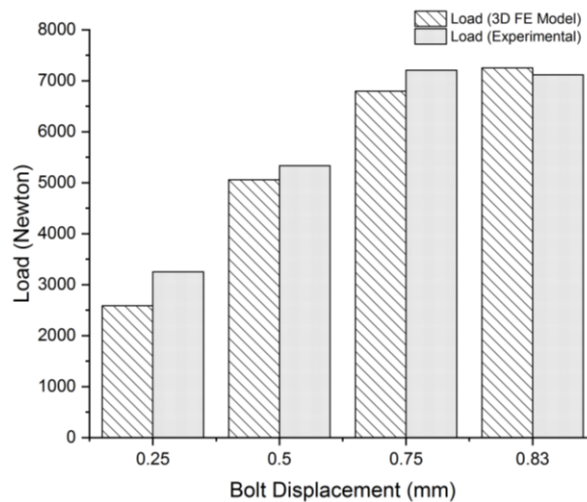
Figure 2.2 Comparisons of the load vs displacement between the 3D FE model and experiments [109]

Singh *et al.* [71] examined the influence of Nano-clay on the strength and the damage form of unidirectional glass epoxy Nano-clay-based composite laminate. The algorithm used for progressive damage analysis is shown in Figure 2.3 [71], [111], [117].

38
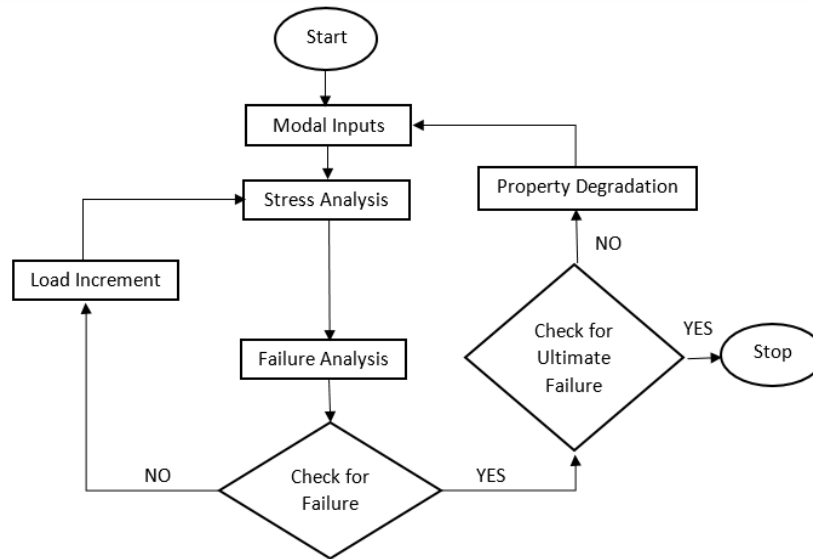
Figure 2.3 Algorithm for progressive damage analysis [71], [111], [117]

- *Characteristic Curve Method*

Whitney and Nuismer [118] introduced two methodologies viz. point and average stress method to estimate the extreme failure of the composite. In the point stress model, extreme failure was predictable to arise; if the stress was triggered at a particular location from the outskirts of the cavity. In the average stress process, for the estimation of extreme laminate failure (X_T^L), it was presumed that the average stress induced over the region from the outskirts of the void is equivalent to the particular distance [106], [118]. Chang *et al.* [108] suggested a characteristic curve model, for predicting the laminate's ultimate failure by considering two typical spans, *i.e.* one was in pulling maneuver (r_{ot}) and another one was in push maneuver (r_{oc}), using equation (2.2). The concept of the characteristic curve is shown in Figure 2.4 [31], [71].

39

R_ot, D, x, R_oc, θ, y

Characteristic curve
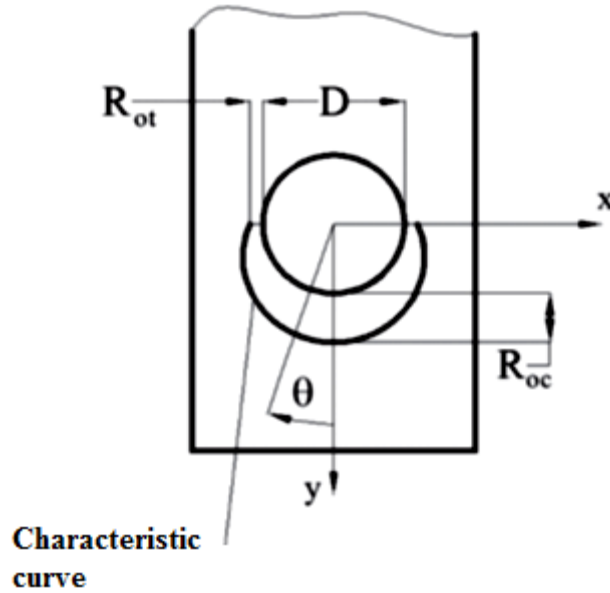
Figure 2.4 Characteristic distance concept proposed by Chang [31], [71], [108]

$$r(\theta) = R + r_{ot} + (r_{oc} - r_{ot}) \cos\theta \qquad (2.2)$$

Where θ varies from $-90° \leq \theta \leq 90°$

R = Radius of the hole

r_{ot} = Characteristic distance in tension

r_{oc} = Characteristic distance in compression.

When the value of angle (θ) lies between -15°<θ <15° and the failure index (FI) is unity on the above-mentioned curvature, the suggested failure mechanism is bearing mode. If it lies between 30°<θ<60° then the shear failure is observed, and if the angle is between 75°<θ<90°, then the net-tension failure mode is observed. A blend of failure modes can also be obtained if the angle is in the transitional range [45], [71], [119]–[122].

- *Cohesive Zone Model*

It was proposed that the failure mode *i.e.*, transverse matrix crack, axial splitting, and delamination are the major factor that decides the pin joint strength by altering the distribution of stresses at the critical zone near the hole periphery [123]–[125]. The correlation factor needs to be determined experimentally and analytically to foresee the

strength and sub-critical damage mode during loading conditions [109], [126], [127]. The cohesive zone elements were used for discrete modeling of the sub-critical domain to eradicate the correlation factor and lessen the scatter in the prediction [128]. Delamination is a major failure form in the composites because of the delicate head-to-head lamina strength. It's a major flaw in composite structural integrity. Shear micro-cracks, known as in-plane axial splits, had been obtained in the composite structure at the stacking sequence of $[0^\circ/-45^\circ/+45^\circ]$[129]. The principle of fracture mechanics was important for quantifying the potential energies between two states of the split through Virtual Crack Closure Techniques (VCCT) to portray delamination growth. [129]–[131]

- *Elastic Limit Design Methodology (ELD)*

The ELD technique works by locating pre-failure load throughout any laminate ply. It can be estimated by selecting correct failure conditions based on stress distribution using an analytical approach. Identification of ply's elastic properties was done using various experimental tests and the component of fracture toughness ended with stable propagation of cracks. Pinho *et al.*[132] offered a fusion of six expressions to foresee the catastrophe known as the LaRC04 failure criteria. The 3D model was considered under loading conditions for each failure using LaRC04 failure criteria. It deals with the performance of fracture mechanics of composite lamina, *i.e.* surge in probable in-plane shear strength when the average transverse loading is applied in compression and has consequences on fiber kinking [133],[134]. ELD approach for laminated composite pinned joint utilizing LaRC04 failure criteria as shown in Figure 2.5.

2.5   Material Failure Criteria for Composite Laminates

Failure study of the composite laminate is the researcher's primary motivation for the last few decades due to its practical significance. There are different varieties of factors, viz. fiber pull out, shear matrix cracking, and transverse matrix damage that governs lamina failure. In the approaches mentioned in the previous section, various forms of failure criteria were used to evaluate composite laminate failure. There is a broad classification of lamina failure criteria: (a) Limit Criteria, (b) Interactive Criteria, (c) Non- Interactive

41

Criteria, and (d) Others. Other criteria are Puck's Failure Criteria and the Multi-scale damage approach using Micromechanical analysis.
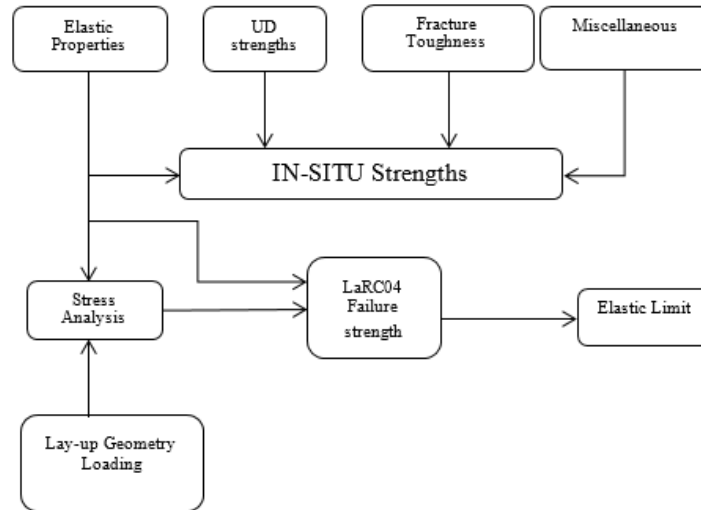
<div align="center">Figure 2.5 Schematic of elastic limit design procedure [106]</div>

2.5.1 Limit Criteria

Limit criteria are applicable to foretell the failing load and the corresponding failure mechanism by matching the lamina stresses or strains with the corresponding strength in a longitudinal direction (σ_{xx}), transverse direction (σ_{yy}), and as well as with shear stress (τ_{xy}) or shear strain (Y_{xy}) when the interaction of these two are not under consideration. Maximum stress criteria and Maximum strain criteria come under this category.

- *Maximum Stress Criteria* [117], [134]

This criterion encapsulates the performance of all those materials in which specific structural elements occupy stresses σ_1, σ_2, and τ_{12}. According to this principle, the catastrophe of the laminate follows when at least one principal stress element along with corresponding axes go beyond the corresponding stress in the same direction. This criterion was significant for composite laminate and does not consider the stress interaction and underpredict the strength in the existence of consolidated plane stress using equations (2.3-2.5).

For fiber damage $$\frac{\sigma_{11}}{X} = 1 \qquad (2.3)$$

For lateral matrix damage $$\frac{\sigma_{22}}{Y} = 1 \qquad (2.4)$$

For shear matrix damage $$\frac{\tau_{12}}{S} = 1 \qquad (2.5)$$

Where, σ_{11}, σ_{22}, τ_{12}, $X, Y,$ and S are the stresses acting in a longitudinal, transverse direction, and shear, respectively.

- *Maximum Strain Criteria* [117]

This criterion delivers outcomes closely similar to those from the maximum stress criterion. According to this principle, the catastrophe of the laminate follows when at least one strain component crosses the related strain in the same direction together with the principal material axis. The key limitation of maximum strain criteria allows some interaction with longitudinal and transverse directions due to the poison effect by employing equations (2.6-2.8).

For fiber damage $$\frac{\epsilon_{11}}{X_\epsilon} = 1 \qquad (2.6)$$

For lateral matrix damage $$\frac{\epsilon_{22}}{Y_\epsilon} = 1 \qquad (2.7)$$

For shear matrix damage $$\frac{\gamma_{12}}{S_\epsilon} = 1 \qquad (2.8)$$

Where, $\epsilon_{11}, \epsilon_{22}, \gamma_{12}, X_\epsilon, Y_\epsilon$ and S_ϵ are the strain acting in a longitudinal, transverse direction, and in-plane shear respectively.

2.5.2 Interactive Criteria

These criteria are having an interrelation among stress and strain factors using a high-order polynomial expression that contains overall stress or strain constituent. With the help of polynomial equations, the damage was presumed when the equation was satisfied. The modes of damage initiation have been observed by comparing the stress and corresponding strength ratio [75], [111], [119], [135], [136]. The commonly employed failure criteria for composite laminates within this category are Hill - Tsai Criteria, Tsai - Wu Criteria, and Yamada - Sun's Failure criteria.

- *Hill – Tsai Criteria* [75], [111], [137], [138]

It is a preliminary 2D form of Von-Mises yield criteria, Hill modified Von-Mises criteria for ductile material, and based on that Tsai formulated a theory for orthotropic composite laminate which is given by equation (2.9).

$$\left(\frac{\sigma_{11}}{X}\right)^2 + \left(\frac{\sigma_{22}}{Y}\right)^2 - \left(\frac{\sigma_{11}}{X}\right)\left(\frac{\sigma_{22}}{X}\right) + \left(\frac{\tau_{12}}{S}\right)^2 = 1 \qquad (2.9)$$

Where,

X is tensile strength in the fiber direction

Y is the tensile strength in the transverse direction

S is the shear strength, and

$\sigma_{11}, \sigma_{22}, \tau_{12}$ stresses in longitudinal, transverse and in-plane shear direction respectively. In the provided expression, there is no distinction between the strengths in tension and compression. Nonetheless, an appropriate strength value can be utilized in the expression mentioned above. Strength interaction has been considered in this theory due to the involvement of the quadratic form. The major limitation of the Tsai-Hill criteria is that it fails to discriminate between failure under tension and compression.

- Tsai – Wu Criteria [71], [136]

This criterion is grounded on Goldenblat and Koponov's model [139] and it has been amended by Tsai - Wu by presuming the existence of failure surface in stress space and in-plane shear strength. This criterion accounts for both tensile and compressive stress through linear terms. Tsai- Wu criteria are willingly amenable for a computational process as well as use stress Invariants. With these advantages, it is a widely accepted theory which is given in equation (2.10).

$$F_1\sigma_{11} + F_2\sigma_{22} + F_{11}\sigma_{11}^2 + F_{22}\sigma_{22}^2 + 2F_{12}\sigma_{11}\sigma_{22} + F_{66}\tau_{12}^2 = 1 \qquad (2.10)$$

Where

$$F_1 = \frac{1}{X} + \frac{1}{X'} \quad F_2 = \frac{1}{Y} + \frac{1}{Y'} \quad, F_{11} = \frac{-1}{XX'}, F_{22} = \frac{-1}{YY'}, F_{66} = \frac{1}{S^2},$$

F_{12} is experimentally determined strength

44

X′ is compressive strength in the fiber direction

Y′ is compressive strength in the transverse direction (perpendicular to fiber),

F_1, F_2, F_{11}, F_{22}, and F_{66} are Tsai-Wu polynomials.

Singh *et al.* [31] investigated the impact of ply orientation and a blend of Nano-filler on compressive strength and failure form at pin joints prepared from GFR composite by utilizing Tsai-Wu criteria along with a characteristic curve approach for estimating the damage modes as shown in Figures 2.6 & 2.7 respectively.
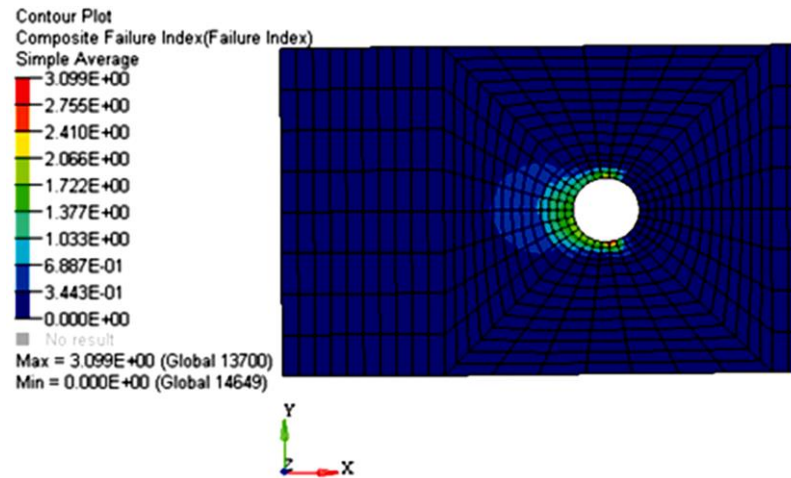
Figure 2.6 Failure Index value at W/D=4 and E/D=4 [31].
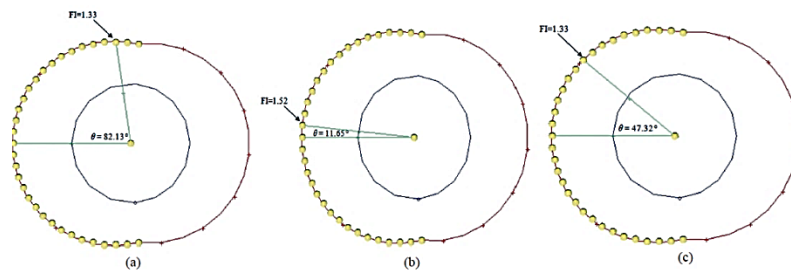
Figure 2.7 Failure Index and angle at the vicinity of hole [31].

- Yamada Sun's Failure Criteria [119], [121], [135]

The Yamada–Sun failure criterion was revised by exploring the in-plane shear stresses that influence the axial compression failure, but never the axial tensile failure. This criterion can be applied in two distinct methods *i.e.* point stress method and the average stress

method. Failure was assumed when these given equations were satisfied. If equations (2.11) and (2.13) are satisfied, then fiber breakage occurs. Equations (2.12) and (2.14) signify the state of matrix failure.

For Point Stress Method

$$\left(\frac{\sigma_{11}}{X_T}\right) - 1 \leq 0, \qquad \sigma_{11} \geq 0 \tag{2.11}$$

$$\left(\frac{\sigma_{11}}{X_C}\right)^2 + \left(\frac{\sigma_{12}}{S_L}\right)^2 - 1 \leq 0, \sigma_{11} < 0 \tag{2.12}$$

For Average Stress Method

$$\left(\frac{\sigma_{11}^{av}}{X_T}\right) - 1 \leq 0, \qquad \sigma_{11}^{av} \geq 0 \tag{2.13}$$

$$\left(\frac{\sigma_{11}^{av}}{X_C}\right)^2 + \left(\frac{\sigma_{12}^{av}}{S_L}\right)^2 - 1 \leq 0, \sigma_{12}^{av} < 0 \tag{2.14}$$

Where, $\sigma_{11}, \sigma_{12}, X_c, X_T$ and S_L are the stresses acting in a longitudinal, transverse direction, and C, T, and S represent compression, tension, and shear, respectively.

2.5.3 Non-Interactive Criteria

These criteria are separate from the fiber to the matrix damage criteria. The equations employed to foresee the failures are dependent on various stress components involved. The most commonly used separate criteria are Hashin's Criteria and Hashin –Rotem Criteria for the separate treatment of fiber and matrix failure mode.

- Hashin's Criteria [109], [117], [140]–[144]

This criterion was applicable to forecast the fiber damage, matrix damage, and strength of the pin-loaded composite laminates along with failure forms [145]. As per Hashin's failure criteria, it offers a good estimation for the fiber damage and matrix damage along with failure manner to forecast if, both failure modes were mutually independent. Yan *et al.* [146] investigated the experimental and prediction from finite element-based FRP composite joint under tensile loading at two different test geometries *i.e.* open hole and a filled hole under tensile test. It was concluded from the results that the clamping pressure influenced the net tension strength *i.e.* the clamping force exhibited an inverse relationship

with the net-tension strength of the composite laminate. Additionally, delamination between the fibers and matrix was observed, which affected the overall strength of the material by causing fiber matrix splitting. The expressions used for fiber and matrix damage are given in equations (2.15-2.18).

Fiber breakage, $\sigma_{11} \geq 0$

$$\left(\frac{\sigma_{11}}{X_T}\right)^2 + \left(\frac{\tau_{12}}{S_C}\right)^2 = 1 \qquad (2.15)$$

Fiber buckling, $\sigma_{11} < 0$

$$-\frac{\sigma_{11}}{X_C} = 1 \qquad (2.16)$$

Tensile matric cracking, $\sigma_{22} \geq 0$

$$\left(\frac{\sigma_{22}}{Y_T}\right)^2 + \left(\frac{\tau_{12}}{S_C}\right)^2 = 1 \qquad (2.17)$$

Compressive matrix failure, $\sigma_{22} < 0$

$$\left(\frac{\sigma_{22}}{Y_C}\right)^2 + \left(\frac{\tau_{12}}{S_C}\right)^2 = 1 \qquad (2.18)$$

Where, σ_{11}, σ_{22}, τ_{12}, X_C, X_T, Y_T, Y_C, S_C are the stresses acting in a longitudinal, transverse direction; and C and T denote compression and tension respectively.

- Hashin - Rotem Criteria [147], [148]

This criterion was explicitly formulated for fiber-matrix composite and does not apply to other anisotropic materials, given in equations (2.19-2.20). Hashin - Rotem criterion can predict the failure strength which was based upon three assumptions *i.e.*, (i) Fiber matrix composite material failure occurs either in fiber or matrix (ii) There are no inter-laminar stresses which may cause failure (iii) The matrix material is much weaker than fiber.

Fiber failure$\frac{\sigma_{11}}{X} = 1$ $\qquad (2.19)$

Matrix failure$\left(\frac{\sigma_{22}}{Y}\right)^2 + \left(\frac{\tau_{12}}{S}\right)^2 = 1$ $\qquad (2.20)$

- Puck Failure Criteria

In general, fiber-reinforced composites demonstrate brittle fracture mechanics in which the fracture happens unexpectedly without significant plastic deformation. A composite's macroscopic failure can be seen at the lamina scale. The Puck theory provides different equations for fiber failure (FF) and inter-fiber fracture (IFF) [149]. The failure of the fiber is normally known as the lamina's final failure. Fiber failure is characterized as a large number of elementary fibers being broken simultaneously. A maximum stress criterion was used to characterize fiber failure in the earlier versions of the Puck failure criteria [150].

2.5.4 Multi-Scale Damage Approach

This model employs and establishes a connection between, both the micromechanics and meso-mechanics of laminated composites [20], [151]–[153]. The constraints parameters are the descriptors of damage entities that can be achieved by micro-level analysis such as internal variables as compared to the traditional continuum damage mechanism treatment where internal variables are completely hidden [114], [154]–[156]. Transverse micro-cracking and micro-delamination were characterized by discrete cracks for which, according to finite fracture mechanics, minimum cracking surfaces were implemented [153], [157], [158]. This methodology can be used as a directory for virtual materials, *i.e.*, materials database. Several stress analyses were simulated and compared with experimental results for samples with or without a cavity.

2.5.5 Summary

Literature on various aspects of pin joints in the context of fiber-matrix composite structures has been deliberated. The failure strength and damage initiation primarily rely on material selection, geometric dimensions, stacking sequences of composite laminate, and the addition of Nanoparticles. There are various laminate failure criteria, which are categorized to foretell the strength and modes of failure in composite material regardless of the types of fibers on the macro and micro scale. Interactive failure criteria *i.e.*, Hill-Tsai criteria, Tsai-Wu criteria, Yamada – Sun's failure criteria, to anticipate failure, high-order polynomial expressions encompassing all stress or strain components were utilized while

employing limit stress criteria such as the Maximum stress criterion also widely used due to the use of linear equations. Several approaches have been applied by the researchers in the mechanically fastened pin joint to investigate the damage pattern and its initiation *i.e.* characteristic curve approach, progressive damage analysis (PDA), cohesive zone model (CZE), and elastic limit design. PDA along with Hashin's criteria was mostly the preferred methodology among all approaches to foretell failure strength and failure modes of fiber and matrix using the material degradation rule. Based on the conducted studies, it was concluded that the analytical approach was relatively consistent with the experimental results for predicting damage initiation and failure modes.

2.6 Scope of Study

Extensive research has been carried out on mechanical joints in fiber-reinforced composites, employing experimental and numerical methods. The main emphasis of this research has been on exploring the influence of geometric and material factors on the failure behavior of pin joints, particularly concerning the configuration of composite laminates. A polymer matrix composite (PMC) with the addition of Nanoparticles like multi-walled carbon Nanotubes (MWCNT)[159], grapheme [160], Nanoclay [76], TiO_2 [161], SiO_2 [162], and alumina [163], SiC [7] is a type of composite material where Nanoparticles are incorporated into a polymer matrix to enhance its mechanical, thermal, electrical, or other functional properties. Nevertheless, there has been a restricted exploration of failure analysis concerning polymer matrix composites (PMC) mechanical joints incorporating Nanofiller materials. It has been observed that the incorporation of Nanofiller Nanoparticles improves the static tensile strength of PMC, thereby allowing for an examination of the effects of different filler materials on both single and multi-pin joints. Additionally, it has been recognized that the strength of laminates is influenced by the fiber orientation. Numerous failure criteria have been developed to predict the failure strength and failure modes of mechanical joints in composite materials.

The different approaches using finite element analysis in conjunction with laminate failure criteria to predict joint failure and failure modes have been confirmed through experimental

validation [54], [71], [134], [140]. In static loading, very limited study was observed of the composite laminate under fatigue loading. Over the past three decades, computational techniques have turned their attention to several diverse application areas, ranging from aeronautical to mechanics of material analysis, CFD problems, dynamics analysis, heat flow, and optimization to the numerical solution using (partial) differential equations [164]–[166]. Figure 2.8 represents the research gap identification through a Venn diagram based on the literature.
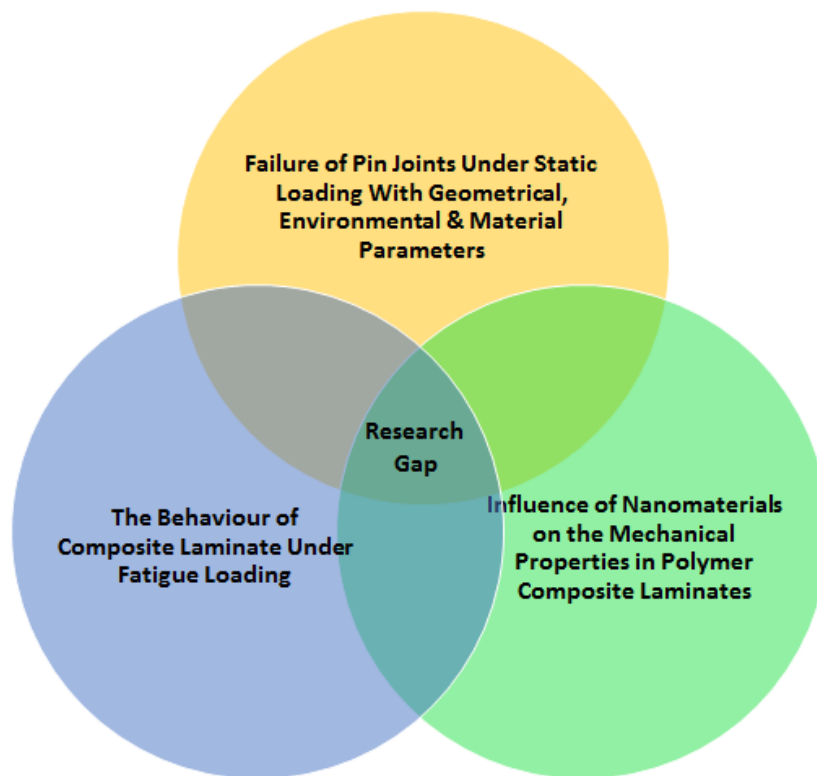
Figure 2.8 Research gap identification through Venn diagram

2.7   Gaps in the Existing Literature

The literature review has identified several significant research gaps in the current understanding of mechanical pin joints and fiber-reinforced composite laminates. These gaps can be summarized as follows:

2.7.1 Cyclic Loading Behavior of Composite Pin Joints:

Previous studies on mechanical pin joints have predominantly focused on factors such as hygrothermal and environmental effects under static loading conditions. However, the behavior of pin joints under cyclic loading, especially in structural applications, presents a distinct set of challenges that differ significantly from static loading. The existing body of research has inadequately addressed the impact of fatigue loading conditions on these joints. Therefore, there is a pressing need for comprehensive investigations that specifically explore the application of pin joints under cyclic loading conditions, considering various geometrical parameters.

2.7.2 Impact of Nanoparticles on Fiber-Reinforced Composite Laminates:

While prior research suggests that the incorporation of Nanoparticles can enhance the strength of fiber-reinforced composites, the available literature lacks in-depth analysis regarding the impact of Nanomaterials in fiber-reinforced composite laminates. The current knowledge is limited, and a more detailed examination is required to thoroughly understand and quantify the effects of incorporating Nanoparticles in composite materials. This research gap emphasizes the necessity for a comprehensive exploration of the role of Nanomaterials in enhancing the mechanical properties of fiber-reinforced composite laminates.

2.7.3 Nanoparticle Impact on FRP Pin Joints under Fatigue Loading Conditions

Existing studies on fiber-reinforced polymer (FRP) composite pin joints have primarily concentrated on their behavior under static loading conditions. To ensure accurate strength predictions and a more comprehensive understanding of their mechanical performance, further analysis is imperative. Specifically, there is a need to investigate the behavior of FRP composite pin joints under fatigue loading conditions. Additionally, a comparative analysis between joints with and without the addition of Nanoparticles is crucial to delineate the influence of Nanomaterials on the fatigue resistance of these joints. Such a comparative analysis will contribute significantly to assessing the performance, durability, and fatigue resistance of these joints, providing valuable insights for both theoretical understanding and practical applications in engineering and materials science.

2.8   Research Objectives

The research was planned with the following objectives based on the identified gaps in the literature:

- To fabricate fiber-reinforced composite laminate using Hand Lay and Compression Molding techniques for mechanical joint applications with and without the addition of Nanoparticles.
- To investigate the different mechanical properties of composite laminate for joint applications under fatigue loading.
- To analyze the mechanical joints under fatigue loading by considering different geometric and material parameters using experimentally and computationally.
- To compare the performance of mechanical joints of composite laminates with and without the addition of Nanoparticles under fatigue loading.

2.9   Research Process and Techniques

Initially, the research process commences with a thorough literature review in the realm of composite pin joints, aimed at identifying a specific problem statement. The literature analysis, in this context, focuses on the mechanical properties of pin joints, particularly emphasizing their behavior under fatigue loading conditions, thereby identifying a significant problem statement. After the identification of the problem statement, the research proceeds to the crucial phase of material selection, wherein the choice of fiber reinforcement and matrix material is made based on the intended application. Following the material selection, the fabrication of composite laminate is carried out utilizing both Hand Layup and Compression moulding techniques. Notably, the fabrication is conducted in two distinct categories: *i.e.* with and without the addition of Nanoparticles.

Upon the completion of composite laminates in both categories, the research extends to the mechanical characterization of fiber-reinforced polymer composites. This involves a comprehensive assessment of key mechanical properties such as tensile strength, shear strength, compressive strength, and fatigue strength, adhering to ASTM standards. The

subsequent step involves the meticulous selection of geometrical parameters for pin joints, specifically focusing on edge and width. The Design of Experiments (DoE) is employed to determine factors and their levels, guiding the preparation of pin joint specimens accordingly.

With the pin joint specimens prepared as per the designated runs in the DoE, experimental testing follows, encompassing both fatigue loading and static loading conditions. Simultaneously, the mechanical properties of the composite laminate, treated as engineering material data, are incorporated into Finite Element Analysis (FEA) software. This FEA analysis is aligned with the predetermined DoE and is conducted both experimentally and computationally. The research delves into a comprehensive examination of neat and modified composite pin joints *i.e.* with and without addition of Nanoparticles. Finally, the results obtained undergo a thorough validation process, culminating in the synthesis of a comprehensive research report.

2.9.1 Methodology

```
┌──────────────────┐        ┌────────────────────────────┐
│ Literature Review│───────▶│   Analysis of Problem      │
└──────────────────┘        │ (Analysis of Bolted Joint) │
                            └────────────────────────────┘
                                         │
                                         ▼
                            ┌────────────────────────────┐
                 ┌──────────│   Material selection on    │──────────┐
                 │          │     application basis      │          │
                 │          └────────────────────────────┘          │
                 ▼                                                   ▼
   ┌──────────────────────────┐              ┌────────────────────────────────────┐
   │   Fiber Reinforcement    │              │               Matrix               │
   │ Glass/ Carbon/ graphite/ │              │ (Resin, epoxy, polyester,          │
   │         Kevlar           │              │       Vinlyester, etc)             │
   └──────────────────────────┘              └────────────────────────────────────┘
                 │                                                   │
                 ▼                                                   ▼
┌──────────────────┐    ┌────────────────────────┐    ┌──────────────────┐
│ With addition of │───▶│   Composite Laminate   │◀───│ Without addition │
│   Nanoparticles  │    └────────────────────────┘    │ of Nanoparticles │
│     Material     │                                   │     Material     │
└──────────────────┘                                   └──────────────────┘
                                    │
                                    ▼
                  ┌──────────────────────────────────┐
                  │ Characterization of fiber        │
                  │ reinforced polymer laminate      │
                  └──────────────────────────────────┘
                                    │
                                    ▼
                  ┌──────────────────────────────────────────┐
                  │ Selection of Geometrical Parameters      │
                  │           for pin joints                 │
                  └──────────────────────────────────────────┘
                                    │
                                    ▼
          ┌────────────────────────────────────────────────────┐
          │ Preparation of pinned Joint Specimen considering   │
          │        different geometric parameters              │
          └────────────────────────────────────────────────────┘
                 │                                 │
                 ▼                                 ▼
   ┌──────────────────┐              ┌──────────────────────────┐
   │ Experimentations │              │ Computational Approach   │
   └──────────────────┘              │         (FEM)            │
                 │                   └──────────────────────────┘
                 │                                 │
                 ▼                                 ▼
              ┌────────────────────┐        ┌──────────────────┐
              │ Result Validation  │───────▶│  Report Writing  │
              └────────────────────┘        └──────────────────┘
```

CHAPTER 3 - MATERIALS, METHODS, AND TESTING

This chapter covers fiber-reinforced composite laminates are the subject of discussion, including the various materials, methods, and testing procedures considered.

3.1   Materials

For the preparation of fiber-reinforced composite pin joint specimens, a combination of various materials such as epoxy, hardener, glass fabric, and Nano-silica was employed.

3.1.1 Resin

In the current study, epoxy resin was chosen as the matrix material due to its superior adhesive bonding with glass fiber, with superior mechanical properties when compared to other thermoset materials. Huntsman Araldite LY556 epoxy, which is a medium viscosity, unmodified liquid resin made from Bisphenol-A. It was combined with the Aradur HY951 hardener, a low-viscosity aliphatic polyamine, in a mixing ratio of 10:1 which is supplied by C.F. Composites, New Delhi, India. Table 3.1, 3.2 & 3.3 shows the physical, mechanical, and processing properties respectively of the epoxy and hardener.

Table 3.1 Physical Properties of Resin

Description	Density (g/cm³)	Viscosity (mPa.s)
Epoxy LY556	1.15-1.20	10000-12000
Hardener HY951	0.97-0.99	10-20

Table 3.2 Mechanical properties of Resin LY556 and Hardener HY951

Properties	LY556 (100) + HY951 (10)
Tensile Strength (MPa)	71.1
Elastic Modulus (MPa)	3105
Elongation (%)	4.5

Table 3.3 Processing Properties of Epoxy

Property	Resin: Hardener Ratio (w/w)	Initial Mix Viscosity @40° C (mPa.s)	Minimum curing Schedule (Temperature/Hours)
Value	10:1	650	80° C/ 2-4 h
			100° C/ 1-2 h

3.1.2 Glass Fabric

The [0º/90º] bidirectional (plain weave) E-glass fiber 390 ± 10 GSM of a thickness of 0.4mm (+/- 0.04mm) was used as a reinforcement in the present study. Woven roving is produced by interweaving direct roving to create a bidirectional fabric. Woven roving is a high-performance reinforcement that is compatible with numerous resins such as polyester, vinyl ester, and epoxy resins. Techniques like hand lay-up, molding, and pultrusion are used to manufacture boats, automobile parts, furniture, sporting facilities, and other FRP products utilizing woven roving. Table 3.4 and Table 3.5 displays the physical and mechanical properties of the bidirectional glass fiber.

Table 3.4 Physical characteristics of fiberglass

Description	Type	Density (g/cm³)	Area Density (gsm)
Glass Fabric	Plain woven	2.56	390±10

Table 3.5 Mechanical characteristics of fiberglass

Description	Tensile Strength (MPa)	Tensile Modulus (GPa)	Elongation at breaking load (%)
Glass fabric	2000- 2200	76	4.1

3.1.3 Nano-silica

Nano silica material has been used SiO_2 Nano-powder is 99.9% purity with an average particle size (APS) 15-20 nm of density 2.4 g/cc which is supplied by Wilmington, Delaware, USA (https://www.Nanoshel.in). Nano-materials are used as a Nano-filler in

composites to enhance the mechanical properties of epoxy. Table 3.6 presents the typical properties of Nano-silica. Incorporating Nano-silica into a glass epoxy composite can enhance its mechanical, thermal, and physical properties.

Table 3.6 Typical Properties of Nano-silica

Composition	Appearance	Molecular formula	Average Particle Size (APS) (nm)	Purity (%)	Molecular Weight (g/mol)	Density (g/cc)
Silicon dioxide	White dry powder form	SiO_2	15-20	99.9	60.08	2.4

The objective of this study was to investigate the effect of fatigue loading on glass epoxy composite laminate and to compare the performance of the composite for neat and modified GFRP. The incorporation of Nano-silica enhances various aspects of the composite, including tensile strength, hardness, wear resistance, toughness, high-temperature stability, resistance to crack propagation, reduced friction, low thermal expansion, and improved interfacial bonding [61], [167]. It can also increase the composite's resistance to moisture, corrosion, and wear. Furthermore, Nano-silica can improve the fire retardancy and UV resistance of the composite. By introducing Nano-silica into the manufacturing process of composite pin joints, there is a promising opportunity to augment their mechanical properties. The incorporation of Nanoparticles, with their significant surface area-to-volume ratio, facilitates the enhancement of interfacial bonding between the composite matrix and reinforcing fibers. However, the optimal amount of Nano-silica to be added to the composite material depends on various factors such as the type of composite material, processing conditions, and the specific application requirements. Therefore, a thorough investigation is necessary to determine the most suitable amount of Nano-silica to incorporate into the composite pin joint to achieve improved mechanical properties. Hence, comprehending the impact of Nano-silica on the performance of glass epoxy composite laminates under varying loading conditions becomes crucial.

3.2 Methods

In the present study, the methods used for the preparation and characterization of the materials are described in the following sections.

3.2.1 Fabrication of Composite Laminate

To produce composite laminates reinforced with glass fibers, multiple processes are involved. Firstly, glass fabric sheets were precisely cut to match the mold's dimensions. Subsequently, the epoxy resin was prepared by dispersing Nano-silica into it through a combination of high viscous stirring and sonication. Once the epoxy resin was ready, the hand layup technique was utilized to fabricate the laminate then the uncured laminate was placed inside the compression molding. Further, the subsequent section outlines the other procedures utilized to manufacture composite laminates.

3.2.1.1 Preparation of Epoxy matrix

The mixing of resin and hardener is a crucial step in many applications, such as in the manufacturing of composite laminates. Precise measurement of the resin and hardener, following the specified mixing ratio of 10:1, is crucial. Subsequently, introduce the hardener into the resin and perform a thorough mixing process. Ensure meticulous blending of the resin and hardener to guarantee a complete and homogeneous mixture. Once the resin and hardener are seamlessly integrated, it is imperative to utilize the mixture promptly for the preparation of the laminate. This urgency is essential because the curing process initiates promptly upon the combination of the two constituents of the matrix.

3.2.1.2 Preparation of Modified Epoxy with the addition of Nano-silica

As previously mentioned, the process for preparing a resin and hardener mixture was carried out in accordance with the specified mixing ratio. When preparing epoxy with Nano-silica, the same procedure has been followed, with the addition of some extra steps that need to be incorporated.

- *Agitation:* A highly viscous stirrer was employed to prepare the mixtures of hardener and Nano-silica, operating at 8000 rpm for 15 minutes until the

58

constituents were evenly dispersed throughout the mixture. Notably, the hardener possessed a lower viscosity than the epoxy resin, which facilitated the thorough mixing of the Nano-silica into the resin. High-viscosity stirrers are employed to achieve laminar mixing of liquids possessing high viscosities, as turbulent mixing cannot be easily attained without generating a considerable amount of heat.

- *Sonication:* Sonication is a process that involves the use of high-frequency sound waves to agitate particles in a liquid medium. The sound waves create pressure changes that cause small bubbles to form and then collapse rapidly, generating intense local heating and physical disruption of the particles. This can lead to various effects such as the dispersion of solids [168]. The process of sonication was carried out for a duration of 70 minutes using an Oscar sonicator, applying a current of 0.6 Amp, with pulse on-off times set at 10 and 2 seconds, respectively. Once the sonication process was complete, the hardener was added to the epoxy-Nano-silica mixture, while maintaining a hardener-to-resin ratio of 10:1. The resulting mixture was subjected to homogenization for 15 minutes at 8000 rpm to ensure thorough mixing. After this, the resin was ready to be used for preparing laminated composites.

3.2.1.3 Hand Layup Technique

The oldest and simplest method for manufacturing polymer composite materials involves open molding. The hand layup technique offers the flexibility to tailor the laminate according to specific design requirements, enabling customization of fiber orientation, ply count, and resin type. During this procedure, the glass fiber was initially cut into the necessary dimensions using a cutter. Subsequently, the first layer of glass fiber was positioned on a Teflon sheet, followed by the application of a resin layer using a brush. The second layer of glass fiber was then placed atop the first layer, and this process was repeated until the desired thickness was attained. To ensure proper adhesion and eliminate any trapped air particles, a hand roller is employed. The prepared laminates are then placed inside a compression molding setup for curing. Subsequently, the laminates are left to cure

for an additional 24 hours at room temperature. Figure 3.1 represents the schematic of the hand layup technique.
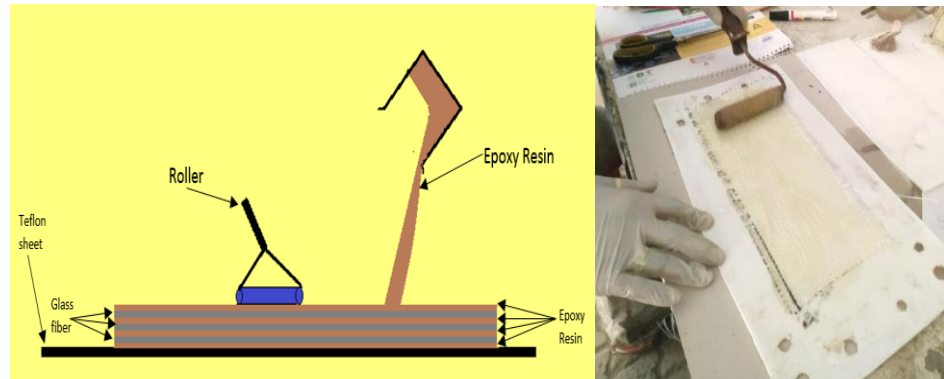
Figure 3.1 Schematic of Hand layup technique for preparation of composite laminate

3.2.1.4 Compression Molding

Mold has been specially prepared for the fabrication of composite laminate to obtain the controlled thickness along with heating plate features using 10 heating elements and a PLC controller to control the temperature for curing purposes. EN95 material is used to fabricate the composite mold and can be easily reusable. Schematic of hydraulic compression molding machine with mold setup to fabrication composite laminate as shown in Figure 3.2. Compression molding is a manufacturing process for composites where pressure is utilized to shape a material within a sealed mold. In this procedure, a laminate is positioned between metal plates and subjected to constant pressure while being heated to the specified temperature. By subjecting the laminate to heat and pressure in this process, it acquires a high fiber volume fraction and minimal void content. Once the laminate has cooled, it is removed from the hydraulic machine. The experimental setup employed for compression molding in this study has a capacity of 200 kN. ASTM standards have been used to prepare the sample for testing. ASTM D3039-76, ASTM D3410-75, ASTM D3479 and ASTM D5379, standards have been used for tensile, compressive, fatigue endurance, shear testing respectively. The geometry of the specimen for various testing as per ASTM standards is represented in Table 3.7.
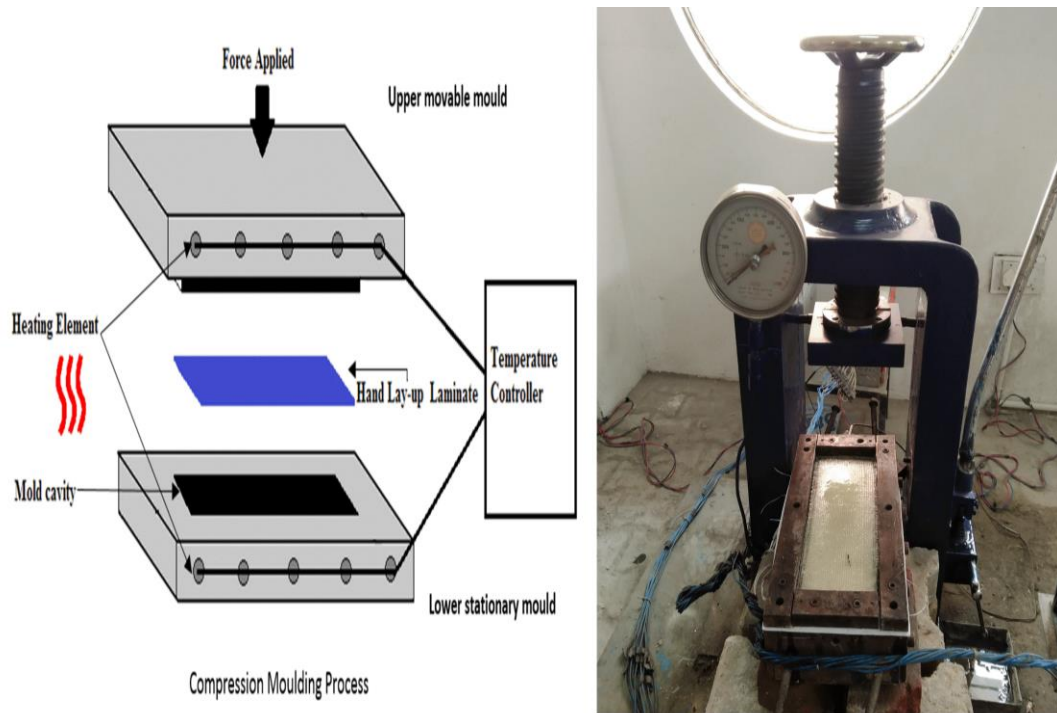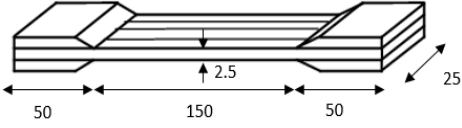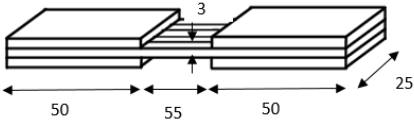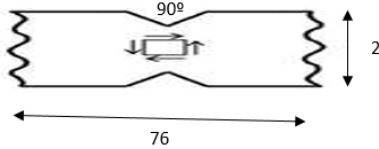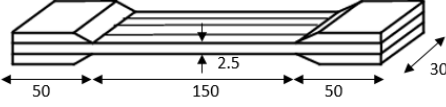
Figure 3.2 Mold setup for the compression molding process

3.3   Composite Laminate Preparation and Mechanical Properties

Initially, composite laminates were prepared using Hand lay-up with compression molding technique. In order to examine the effects of Nano-silica on the performance of glass epoxy composite, two distinct materials were fabricated. One material consisted of glass fiber reinforcement in neat epoxy, while the other material involved fiber reinforcement in epoxy modified with Nano-silica. The volume fraction of glass fiber has been maintained at 42.5%, As per the study it has been observed that up to 42.5% of fiber volume content offers more strength to the composite laminate [169]. Using the hand-layup technique, a laminate with the desired thickness was created. After the composite laminate was completed the uncured laminate was subjected to pressure and temperature inside compression molding. Then laminate is kept for further curing at room temperature for 24 hours.

Table 3.7 Various ASTM standards for testing specimen

Test Type	To determine	Specimen Geometry with dimensions	ASTM standards
Tensile Test	Modulus and Tensile strength	2.5 / 25 / 50 / 150 / 50	ASTM D3039-76 [71]
Compressive Test	Compressive strength	3 / 25 / 50 / 55 / 50	ASTM D3410-75 [71]
Shear Test	Shear strength	90º / 20 / 76	ASTM D5379 [31]
Fatigue Endurance Test	Endurance limit strength	2.5 / 30 / 50 / 150 / 50	ASTM D3479 [170]

The curing parameters utilized in the compression molding machine were fine-tuned to optimize the mechanical properties of the laminates made from the selected material. These samples were then subjected to tensile testing using the International Equipment's Composite Universal Testing Machine - Vector Model at a controlled temperature of $25 \pm 2º$ C as per ASTM D3039. A crosshead speed of 2 mm/min was maintained for all the specimens during the testing process. The composite laminates underwent shear testing in accordance with ASTM D5379 standards. The specimens, illustrated in Table 3.7, were subjected to shear loads using a universal testing machine with a cross-head speed of 2 mm/min. Compression tests were conducted following the ASTM D3410 test standard specification, utilizing a Universal Testing Machine (International equipment). The

specimens, as depicted in Table 3.7, were equipped with end tabs, and a consistent cross-head speed of 1.3 mm/min was upheld.

3.4   Experimental Setup for Fatigue Test on Dynamic UTM

The specimens were precisely cut to adhere to the prescribed dimensions of 250 mm in length, 30 mm in width, and 2.5 mm in thickness. Additionally, 50 mm GFRP tabs were affixed to both ends of the specimens, while the gauge length of the specimen was set to 150 mm as shown in Figure 3.3. Fatigue tests were conducted under tension-tension sinusoidal loading with a frequency of 2 Hz using the computer-controlled servo-hydraulic Instron Dynamic UTM machine at IIT Mandi in Himachal Pradesh, India. The fatigue testing was carried out according to ASTM D3479-19 standards [13].
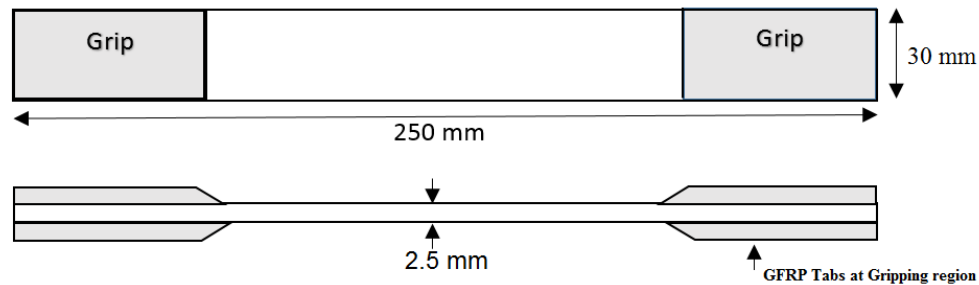
Figure 3.3 Specimen for fatigue test as per ASTM D3479-19

The stress level has been considered the value of the ultimate tensile strength (UTS) which ranged from 50–90%. Throughout the fatigue tests, measurements of load, displacement, and time were systematically recorded at predetermined intervals. The tests were halted either upon the failure of the specimens or upon reaching 10^6 cycles, whichever occurred first. All tests were conducted in the load control mode and maintained a stress ratio (R) of 0.1 with a constant amplitude. Figure 3.4 illustrates the loading scheme employed for the fatigue test.
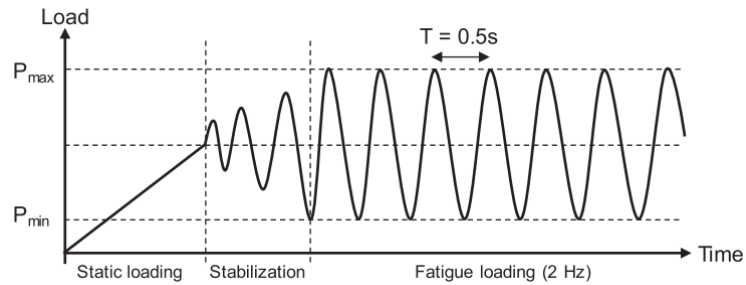
Figure 3.4 The tension-tension loading scheme utilized for the fatigue test

3.4.1 Steps to Perform Fatigue Test on Dynamic UTM

The typical procedure for conducting a fatigue test under tension-tension (T-T) loading conditions using a dynamic universal testing machine involves the following steps:

- *Preparation of Specimen*: Prepare the specimen according to the standard requirements. The specimen should be made of the required material with the dimensions specified by the testing standard.

- *Mounting the Specimen*: Mount the specimen in the grips of the testing machine. The grips should be properly aligned with the specimen and tightened to avoid any slippage.

- *Configuration of Load Control Parameters*: Configure the load control parameters, such as load range, frequency, and waveform, as per the testing standard.

- *Set-Up Data Acquisition System*: Configure the data acquisition system to capture essential data during the test, including load, displacement, and time.

- *Apply Preload*: Apply a preloading force to the specimen to guarantee appropriate contact between the grips and the specimen.

- *Start the Test*: Start the test by initiating the cyclic loading with the specified load range and frequency.

- *Monitor the Specimen*: Monitor the specimen during the test for any signs of failure or fatigue, such as cracks or deformation.

- *End the Test*: End the test when the specimen reaches the required number of cycles or when it fails.

Figure 3.5 shows the test setup for performing fatigue tests on a dynamic UTM machine. Significant research efforts in mechanically fastened joints have predominantly focused on experimentally and numerically analyzing the impact of geometric factors on joint strength. Researchers have extensively investigated the influence of parameters like end distance-to-diameter (E:D) and width-to-diameter ratios (W:D) on the performance of composite joints made of glass-epoxy under static loading conditions [29], [36], [171]. However, there has been comparatively less focus on studying the effects of these parameters under time-varying loading conditions.

Figure 3.5 Test Setup (a) Dynamic UTM (b) Specimen mounted in Dynamic UTM for fatigue test
(Courtesy: IIT, Mandi)

To investigate the effects on load-bearing capacities and joint failure mechanisms under static and fatigue loading scenarios, the ratios of E:D and W:D were adjusted within the range of 3 to 5., while other geometric parameters thickness 't', length 'L', and diameter 'D' remained unchanged. The hole diameter was set to 4 mm, and the experiments were conducted at a room temperature of 25º C. The schematic of the pin joint used for fatigue testing is presented in Figure 3.6. Each pin joint was subjected to loading until the pin had

displaced 10 mm from its initial position. Each geometric configuration specimen performed three tests to get the average bearing strength values.
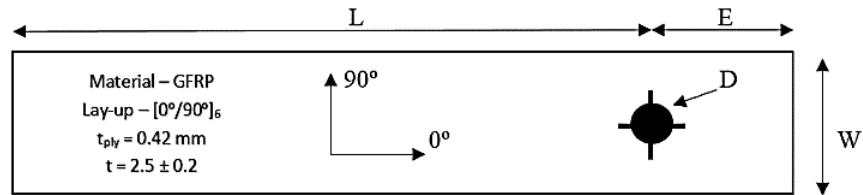
Figure 3.6 Schematic of pin joint specimen for fatigue test on dynamic UTM

In the dynamic UTM, the upper jaw is designed to move, while the lower jaw remains stationary. Consequently, the pin fixture is positioned in the upper jaw, and the composite pin joint samples are mounted in the fixture for fatigue testing of GFRP pin joints at various joint configurations.

3.5   Summary

In this chapter, the materials parameters and basic procedures employed for the preparation of laminates were discussed. For this investigation, bi-directional woven glass fiber epoxy composite laminates were manufactured using a combination of hand layup and compression molding techniques. Two sets of laminates were created: one without the addition of Nano-silica and the other with the inclusion of Nano-silica. Furthermore, several ASTM standards were discussed and employed to evaluate the mechanical properties of the composite laminates. In the subsequent chapter, a comprehensive analysis of the mechanical properties of the composite laminates is conducted, encompassing both static and fatigue loading conditions. The investigation focuses on the analysis of two types of composite laminates: neat epoxy and modified epoxy glass fiber-reinforced polymer (GFRP) laminates.

CHAPTER 4 –FATIGUE BEHAVIOUR OF GLASS/EPOXY COMPOSITE LAMINATE

The objective of this chapter is to explore the mechanical properties and behavior of composite laminates under both static and fatigue loading conditions. The emphasis is placed on comparing the performance of Neat and Modified epoxy glass fiber-reinforced polymer (GFRP) composites. A key aspect of this study was to examine the optimal quantity of Nano-silica particles necessary to enhance the mechanical properties of epoxy. To assess the mechanical properties under fatigue loading, an SN curve was employed to illustrate the behavior of the composite laminate at different stress levels. ASTM D3039 and D3479 standards were employed to attain the tensile and fatigue strength of both the neat and modified GFRP composite laminates.

4.1 Characterization of Mechanical Properties in Glass/Epoxy Composite Laminates

The thickness and void content of composite laminates are key factors that greatly impact their mechanical properties. These factors are influenced by the temperature and pressure applied during the manufacturing process [172]. Additionally, the catalyst present in the epoxy resin begins to react at room temperature. The current procedure involves placing the uncured laminates in the compression mold and then leaving them to cure at room temperature for 24 hours. The pre-phase time, referring to the duration required for the curing temperature to reach its desired level within the compression mold, typically exceeds 30 minutes. Throughout this period, the laminates are retained within the mold. Hence, it was imperative to optimize the process parameters such as pressure, curing temperature, and dwell time for effectively curing composite laminates. In this study, two distinct categories of samples were prepared based on material parameters *i.e.* Neat epoxy and Nano-silica infused modified epoxy GFRP composite under the influence of static and fatigue loading.

In this study, the design of experiments was utilized to minimize the experimentation run and expense. Various techniques are available for the design of experiments, but the Taguchi method is the most widely used approach for reducing the number of experimental trials. Taguchi created a series of experimental matrices known as Orthogonal Arrays (OAs), which are fractional factorial in nature and can be employed in diverse scenarios to optimize the process parameters and enhance the results [74], [173]–[176]. To measure the deviation between the desired and experimental values of a performance characteristic, a loss function is established and then converted into a signal-to-noise (S/N) ratio. The current research aims to enhance the strength of the material, and to achieve this objective, the S/N ratios are computed using equation (4.1), which follows the principle of 'Larger is the better.'

$$\text{Larger is the Better: } \frac{S}{N} = -10 \ \log(\frac{1}{n}\sum_{i=1}^{n}\frac{1}{y_i^2}) \qquad (4.1)$$

For the current investigation, three factors, namely pressure, temperature, and holding time, have been chosen for analysis with three levels of each. The problem has a degree of freedom of 6. To conduct the study, a standard L9 orthogonal array with 8 degrees of freedom has been utilized, even though it is larger than the degree of freedom required for the present problem. Table 4.1 displays the various levels of control factors used in the experiment.

Table 4.1 Factors and levels values analyzed in the compression molding process.

Factor	Levels		
	1	2	3
A-Pressure (kN)	30	50	70
B-Temperature (ºC)	50	70	90
C-Holding Time (min.)	20	30	40

The calculated S/N ratio was utilized to conduct an analysis of means, which is presented in Table 4.2. Additionally, the table displays the ranking of the process parameters that impact the multi-performance response based on the Delta statistics.

Table 4.2 Tensile strength of the laminates cured at different levels using L9 orthogonal array

Run	Pressure (KN)	Temperature (ºC)	Time (min.)	Tensile Strength (MPa)	S/N Ratio
1	30	50	20	118	41.43764
2	30	70	30	124	41.86843
3	30	90	40	129	42.21179
4	50	50	30	134	42.5421
5	50	70	40	126	42.00741
6	50	90	20	136	42.67078
7	70	50	40	121	41.65571
8	70	70	20	129	42.21179
9	70	90	30	138	42.79758

It is evident from the S/N ratio graph depicted in Figure 4.1 that the mechanical strength of the composite material is significantly influenced by the curing temperature. With an increase in the mould set temperature, the degree of cure of the epoxy also increases, leading to improved mechanical properties. Table 4.3 represents the response of the signal-to-noise ratio along with the significant contribution. The S/N ratio plots reveal that the impact of curing time decreases significantly beyond 30 minutes. Additionally, increasing the pressure from 30 to 50 kN, as illustrated by the S/N ratio plots, enhances the strength of the composite material. The cure pressure has also displayed noteworthy advancements in the mechanical properties of the composite material by reducing the void content.

Table 4.3 Response for signal-to-noise ratios

Factors	Level 1	Level 2	Level 3	Delta (max. –min.)	Rank
Pressure (kN)	41.84	42.41	42.22	0.57	2
Temperature (ºC)	41.88	42.03	42.40	0.68	1
Time (min.)	42.11	42.40	41.96	0.44	3

Therefore, the ideal combination for achieving optimal strength was to use a pressure of 50 kN, a temperature of 90°C, and a holding time of 30 minutes. To determine the importance of the process parameters, an analysis of variance (ANOVA) was conducted, as demonstrated in Table 4.4. Overall, the significant contribution of the temperature factor

holds 45.16% followed by pressure with a contribution of 29.5% with less contribution among all *i.e.* holding time at 18.04%.
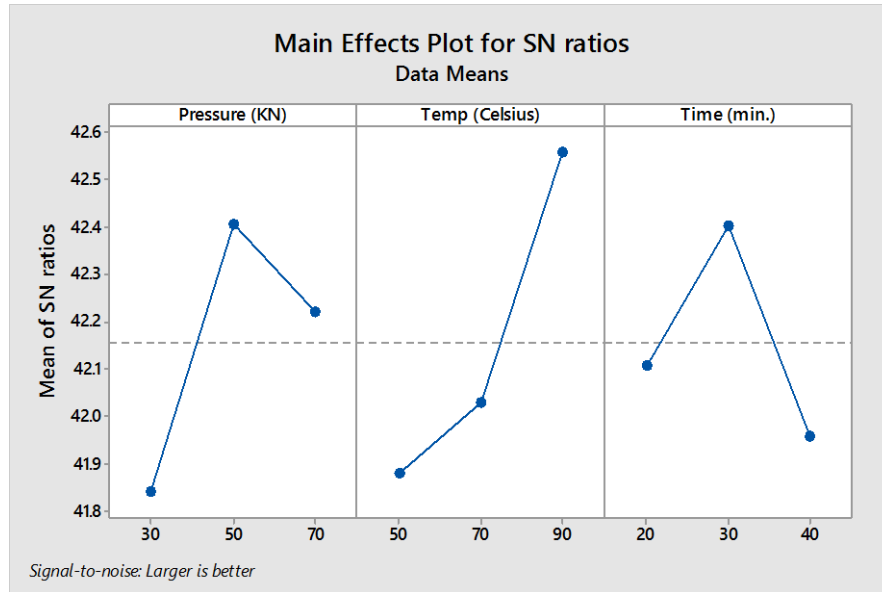
Figure 4.1 S/N ratio plots of tensile strength of the laminate cured at different levels of pressure, temperature, and holding time.

The p-values, which are less than 0.05 (at a 95% confidence interval), for all parameters, indicate that all were the significant parameters.

Table 4.4 Analysis of Variance for SN Ratios

Source	DF	Seq SS	Adj SS	Adj MS	F	P	Contribution (%)
Pressure (kN)	2	0.5025	0.5025	0.25125	4.04	0.019	29.5
Temperature (ºC)	2	0.7690	0.7690	0.38452	6.18	0.013	45.16
Time (min.)	2	0.3071	0.3071	0.15356	2.47	0.028	18.04
Residual Error	2	0.1244	0.1244	0.06218			7.30
Total	8	1.7030					

4.1.1 Static Analysis of Neat Glass Fiber Epoxy Composite Laminate

In this study, the design of experiments was utilized to determine the significant parameters. The static tensile test has been performed using ASTM D3039 standard. Figure 4.2 illustrates a schematic of the tensile testing specimen.

Figure 4.2 A tensile testing specimen of glass epoxy composite laminate (GFRP) as per ASTM D3039

In the current study, the laminates were fabricated by applying a pressure of 50 kN at a temperature of 90°C for a duration of 30 minutes. The combination of heat and pressure developed composite with a high volume fraction of fiber content with low void and thickness can be controlled. The tensile strength of neat GFRP as per ASTM D3039 obtained 144 MPa.

4.1.2 Static Analysis of Modified Glass Fiber Epoxy Composite Laminate

From the literature and through the investigation, it has been concluded that identification of the appropriate amount of Nano-silica plays an important role to offer improved mechanical strength [167]. To find the optimal weight percentage (wt. %) of Nano-silica to be added to the epoxy mixture, the concentration of Nano-silica was altered within the range of 0 to 5 wt.% [177]. Likewise, a similar process has been adopted for testing modified glass epoxy composite laminate. Figure 4.3 illustrates the average tensile strength of each Nano-composite as the Nano-silica content was varied between 0 and 5 wt. %. The findings demonstrate that the tensile strength of the Nano-composite material exhibits an increase as the Nano-silica content rises, reaching a peak at a concentration of 3 wt.%. This increase in strength is attributed to the larger specific surface area of the Nano-composite material.

71

Nevertheless, exceeding a Nano-silica concentration of 3 wt.% results in agglomeration formation, leading to a reduction in specific surface area and subsequently diminishing the tensile strength of the Nano-composite [178]. Agglomeration has a detrimental effect on the tensile strength of the Nano-composite. As Nano-silica particles agglomerate, the overall specific surface area available for interactions and bonding with the matrix decreases. The clustered particles behave like a defect within the material, making it more susceptible to failure under tensile loads. This reduction in tensile strength compromises the overall structural integrity of the composite.
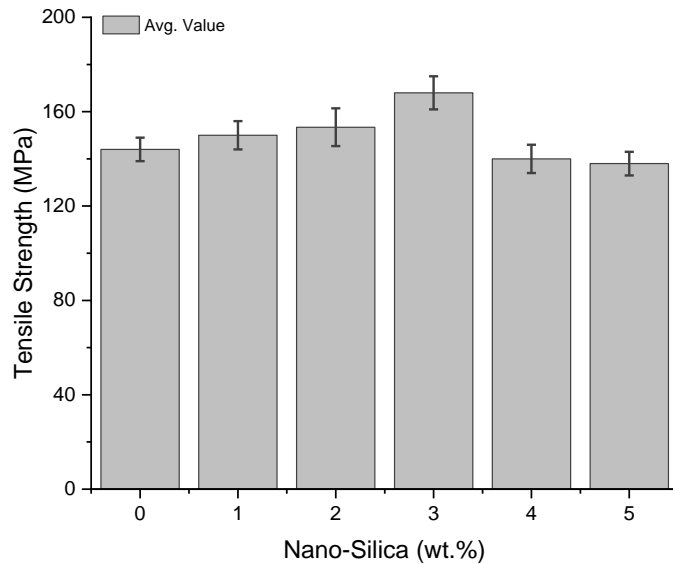
Figure 4.3 Tensile strength of modified GFRP at various wt. % of Nano-silica

Therefore in the present study, Nano-silica with 3 wt. % was used in epoxy to make modified epoxy for the preparation of modified GFRP pin joints for the analysis under static and fatigue loading. Figure 4.4 represents the stress-strain diagram for Neat and Modified Glass epoxy composite laminate with 3 wt. % of Nano-silica. The stress-strain curve clearly demonstrates a notable improvement in tensile strength when compared to the neat glass epoxy composite laminate. Furthermore, it is observed that the specimen experiences sudden failure after reaching the ultimate strength of the Neat GFRP composite laminate, just prior to specimen fracture. The occurrence of fiber breakage transpires when

the applied load on the GFRP surpasses the tensile strength of the individual fibers. Upon fiber breakage, the load-carrying capacity of the composite experiences a substantial reduction, resulting in localized failure of the composite laminate. Conversely, in the case of modified GFRP, there is a slight fluctuation in stress observed after reaching the ultimate strength before fracture, which indicates a combined failure mechanism involving both fiber breakage and fiber pullout.
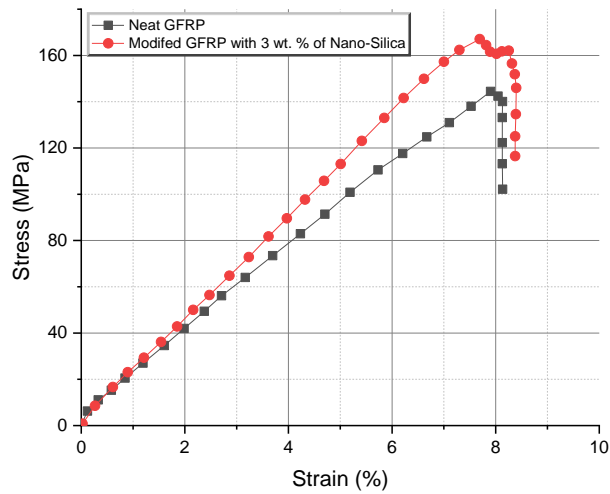
Figure 4.4 Stress vs Strain curve for neat & modified glass epoxy composite laminate

Through the comparison of the area under the curve illustrated in Figure 4.3, it becomes evident that the incorporation of Nano-silica not only notably enhances the tensile strength but also improves the toughness of the composite laminate. Under high loads, some fibers may break, while others may partially or completely pull out of the matrix. The extent and distribution of fiber breakage and pullout within the composite influence the mode and progression of failure. The incorporation of Nano-silica particles in the composite serves to reinforce the matrix and enhance the interfacial bonding between the fibers and the matrix. As a result, the overall stiffness of the material is improved. The mechanical properties of bi-directional glass epoxy composites, both with and without the inclusion of Nano-silica, are presented in Table 4.5. The assessment was conducted in accordance with ASTM standards ASTM D3039-76, ASTM D3410-75, and ASTM D5379. In order to evaluate the dispersion of Nano-silica within the epoxy, SEM and XRD analyses were

performed on the prepared resin and laminates. SEM images of the resin and laminates, both with and without the incorporation of Nano-silica, are shown in Figure 4.5. The images were obtained using SEM Carl Zeiss Sigma 500 FEG-SEM. When examining the fractography of neat Glass Fiber Reinforced Polymer (GFRP) using SEM as shown in Figure 4.5 (a), it has been observed that fiber and matrix fracture takes place in the specimen. Fiber fractures usually appear as clean, straight lines perpendicular to the fiber's longitudinal axis.

Table 4.5 Mechanical Properties of Neat and Modified GFRP

Property	Symbol (Units)	Neat GFRP	Modified GFRP with 3 wt.% of Nano-Silica
Longitudinal modulus in tension	E_1 (MPa)	4670	4903
Transverse modulus in tension	E_2 (MPa)	4670	4903
Longitudinal strength in tension	X_t (MPa)	144	167.4
Transverse strength in tension	Y_t (MPa)	144	167.4
Longitudinal strength in compression	X_c (MPa)	95.22	125.61
Transverse strength in compression	Y_c (MPa)	95.22	125.61
Shear strength	S (MPa)	35.8	42.1
Poisson ratio	v_{12}	0.15	0.16

The fracture surfaces may exhibit signs of fiber breakage due to applied stress on a composite material exceeding the strength of the fibers, resulting in the fracture of individual fibers. This signifies a debonding occurrence between the fiber and the matrix, which has the potential to diminish the load-bearing capability of the composite. Moreover, it also shows the fractured matrix regions surrounding the fibers. The matrix fracture surfaces typically exhibit irregular and rough morphology as shown in Figure 4.5(a). Conversely, along with the fiber breakage and matrix cracks, fiber pull-out was also observed in the fractography image of Modified GFRP as shown in Figure 4.5(b). Fiber pull-out arises when there is a weak interface between the fiber and the matrix, causing the fibers to partially or completely detach from the matrix under the influence of applied stress. This reveals that the failure of the laminate is not sudden due to the fiber pull-out and load redistribution to the remaining fiber which leads to localized stress and finally

74

fracture occurs in the specimen. The presence of fiber breakage with fiber pull-out enhances the material's resistance to crack propagation, improves its load-bearing capacity, and increases its ability to withstand dynamic loading conditions. As well as it also contributes to enhancing the toughness of fiber-reinforced composites by dissipating energy during deformation and fracture [179].
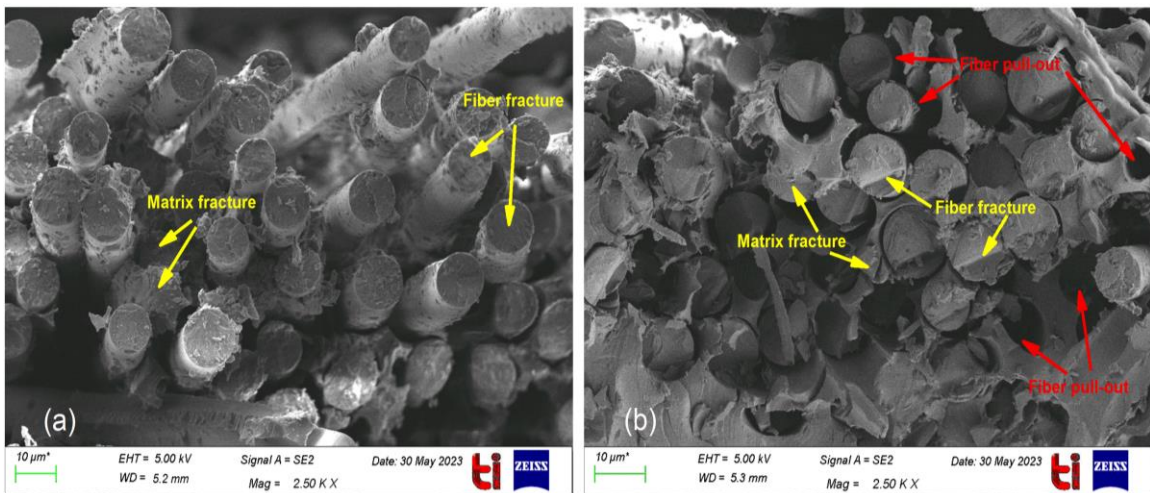
Figure 4.5 SEM images (a) Neat GFRP composite laminate (b) Modified GFRP composite laminate with 3 wt. % of Nano-silica

Furthermore, Figure 4.5(b) clearly demonstrates that the resin containing Nano-silica exhibited stronger bonding with the fiber in comparison to the neat epoxy. These observations suggest the development of a positive interfacial bond between the fiber and epoxy when Nano-silica is incorporated into the epoxy mixture. X-Ray Diffraction (XRD) experiments were performed on samples of both the pristine epoxy resin and the epoxy resin containing 3 wt. % of Nano-silica. Figure 4.6 illustrates the XRD pattern obtained from the pristine epoxy resin. The utilization of XRD analysis has been noted in the literature to aid in the observation of Nanoparticle (NP) dispersion and the degree of exfoliation/intercalation within the epoxy resin matrix [180]. Previous research studies have indicated the presence of broad peaks in pure epoxy resins. Each pattern exhibited broad diffraction ranging from 5° to 80°, with a couple of maxima peaks observed near 20° to 45°, which revealed the scattering behavior of the cured epoxy network and its

amorphous nature [180], [181]. In contrast, the modified epoxy resin containing 3 wt. % of Nano-silica content exhibits a prominent peak at 2θ = 19.52º, which corresponds to a d-spacing of 4.54 Å. Conversely, neat epoxy shows a broad peak at 21.11º with a d-spacing 4.21 Å as determined through Bragg's Law [182]. Broad peak with intensity implies it may have some degree of crystallinity, depending on the specific fabrication process and impurities present. Thus, the addition of 3 wt. % of Nano-silica could introduce additional diffraction peaks in the XRD plot.
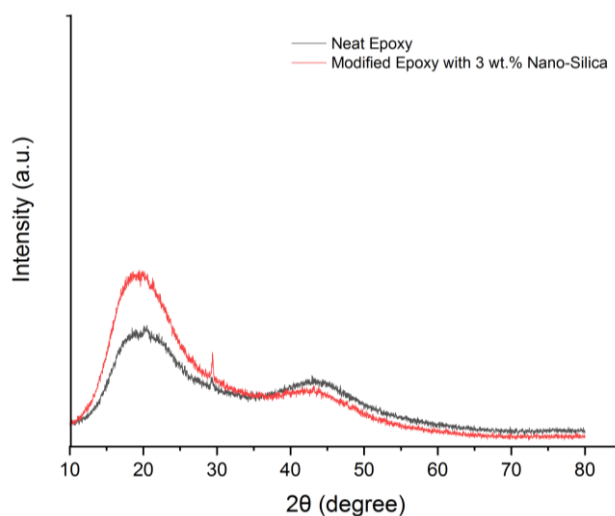
Figure 4.6 X-Ray diffraction pattern for neat and modified epoxy resin

The presence of Nano-silica can affect the scattering behavior of X-rays, resulting in alterations in peak intensities. These shifts could indicate changes in the local ordering or packing of the epoxy chains due to interactions with the Nano-silica particles [183]. These alterations can offer valuable insights into the even distribution of Nanoparticles within the epoxy. Nano-silica exhibits intercalation capability within epoxy chains, where intercalation denotes the insertion of one material between the layers or chains of another substance. In the context of epoxy, Nano-silica particles disperse within the epoxy matrix, resulting in the formation of a Nano-composite material. The interaction between Nano-silica particles and epoxy chains occurs through diverse mechanisms, such as hydrogen bonding or chemical bonding, contingent upon the surface functionalization of the Nanoparticles and the curing conditions of the epoxy. This intercalation of Nano-silica

within the epoxy chains contributes to the enhancement of the material's mechanical properties [184]. An increase in crystallinity or ordering can lead to improvements in the mechanical behavior of materials. This is because a more ordered structure often results in enhanced load transfer and improved interfacial interactions between the Nano-silica particles and the epoxy matrix. Increased crystallinity or ordering improves material mechanics by enhancing load transfer and interfacial interactions between Nano-silica particles and epoxy matrix.

4.2 Effect of Fatigue Loading on Glass Fiber Epoxy Composite Laminates

When dealing with composite materials, understanding their long-term behavior is a major challenge. Predicting fatigue behavior for homogeneous materials such as metals can already be difficult, but it is even more complex for composites. The reason for this is that changes in the microstructure of the materials, as well as changes in their interfaces and interactions, can lead to various forms of damage accumulation and modes of failure. Moreover, slight variations in temperature, loading conditions, material properties, or environmental factors can cause considerable changes in the material's performance. Fatigue life prediction for composite pin joints involves determining the amount of cyclic loading a joint can withstand before failure occurs. The performance of composite pin joints can be predicted through various approaches such as analytical modeling [78], [185], numerical simulation [186], and experimental testing [81]. Ensuring the long-term reliability and durability of composite structures in industries like aerospace, automotive, and marine applications is crucial, and therefore, accurate fatigue life prediction for composite pin joints is of utmost importance.

The Weibull distribution tool was utilized to model the extreme values of bearing strength under various geometric configurations. Two common arrangements of the Weibull distribution approach can be used *i.e.* two and three parameters based Weibull distribution. The general expression of three parameters based on Weibull distribution can be written as per eq. (4.2) [187]:

$$F(x; \gamma, n, \beta) = 1 - exp\left[-\left(\frac{x-\gamma}{n}\right)^{\beta}\right] \qquad (4.2)$$

$$\gamma \geq 0, \ n \geq 0 \ and \ \beta \geq 0$$

where, γ, n, and β are variables of position, scale, and shape, respectively. When $\gamma = 0$ in eq. (4.2) then it becomes two parameters-based Weibull distribution. The analysis employed a two-parameter-based Weibull distribution function to predict the load-bearing capacity of glass epoxy composite pin joints. The two-parameters Weibull function can be written as per eq. (4.3) [14], [188], [189]:

$$F(x; n, \beta) = 1 - exp\left[-\left(\frac{x}{n}\right)^{\beta}\right] \qquad (4.3)$$

$$n \geq 0 \ and \ \beta \geq 0$$

In this approach, the probability density function can be represented by F(x; n, β) which means the probability of bearing strength would be less than or equal to x.

$$F(x; n, \beta) + R(x; n, \beta) = 1 \qquad (4.4)$$

Where, R(x; n, β) in eq. (7.3) represents the reliability of the factor, which means the probability of bearing strength would be equal to or more than the value of x. from eq. (7.2) and (4.4), eq.(4.5) has been derived.

$$R(x; n, \beta) = exp\left[-\left(\frac{x}{n}\right)^{\beta}\right] \qquad (4.5)$$

The linear regression approach was adopted in eq.(4.5) to evaluate the scale and shape variables. Since this is the simplest technique that can be used to assess the Weibull variables. This approach allows transforming eq. (4.5) into a linear equation manner *i.e.* Y = mx + c. by taking double natural logarithmic on both sides of the expression.

$$ln\left[ln\left(\frac{1}{1-F(x,n,\beta)}\right)\right] = \beta ln(x) - \beta ln(n) \qquad (4.6)$$

To determine the F(x,n,β), Benard's approximation method is employed, and with the help of Median Rank (Q(t)), n and β will be evaluated using eq. (4.6).

78

Benard's Approximation (Median Rank)[27]

$$F(x,n,\beta) = Q(t) = \frac{i-0.3}{j+0.4} \tag{4.7}$$

Where i is the order of the specimen and j is the total size of the number.

4.2.1 Fatigue Analysis of Neat Glass Fiber Epoxy Composite Laminate

A fatigue test has been performed as per ASTM D3479 to check the behavior of Neat GFRP and modified GFRP with 3 wt. % of Nano-silica. The ASTM D3479 standard [97] was followed to conduct fatigue tests on dynamic UTM under tension-tension loading. The schematic of the Fatigue sample as per ASTM D3479 has been represented in Figure 4.7. Fatigue testing was performed on the specimens at five distinct stress levels, specifically 50%, 60%, 70%, 80%, and 90% of the Ultimate Tensile Strength (UTS) value.

Each specimen underwent three repeats at each stress level, and the cycle count until failure was recorded. Table 4.6 presents the experimental observations of the number of cycles to failure at various stress levels, along with the predicted number of cycles to failure at 90% reliability based on the Weibull distribution model.

Figure 4.7 GFRP Specimen for fatigue testing under tension-tension loading with 2 Hz frequency

Particularly in aerospace and automotive industries where demand for higher levels of safety and reliability plays a significant role which implies that there is a 90% probability

that the material or component will endure the specified number of cycles without failure [190][191]. The Weibull distribution function has proved to be a valuable and flexible way to characterize composite material properties when evaluating the reliability of composite structures [188].

Table 4.6 Fatigue Life of Neat GFRP Composite Laminate at Different Stress Levels (f = 2 Hz, R=0.1)

Neat ASTM D3479	At 50% of UTS	At 60% of UTS	At 70% of UTS	At 80% of UTS	At 90% of UTS
Max. Stress (MPa)	72	86.4	100.8	115.2	129.6
Coupon 1 – Nf (Cycles)	108945	6478	4312	1470	389
Coupon 2 – Nf (Cycles)	112413	5988	5893	1090	175
Coupon 3 – Nf (Cycles)	113788	7413	3843	1348	216
Predicted Life at 90% Reliability (Cycles)	107018	5450	3050	970	118

Two parameters based Weibull distribution have been employed on the experimental data obtained through dynamic UTM under tension-tension test to predict the survival life at 90% reliability of the GFRP composite at each stress level. Figure 4.8 illustrate the reliability plots at various stress level. Figure 4.9 presents the S-N (stress-life) curve for a GFRP composite laminate, conforming to the guidelines outlined in ASTM D3479-19. The plot showcases the relationship between stress and fatigue life. A trendline has been applied to the data points to provide a clear representation of the trend. To determine the 90% reliability of survival using a two-parameter Weibull distribution, a gray solid square indicates the data set used to fit the model parameters at each stress level. Additionally, a blue line represents the linear fitting, which was used as a linear fitting model achieving an accuracy level of 92.9% in terms of the adjusted sum of squares.
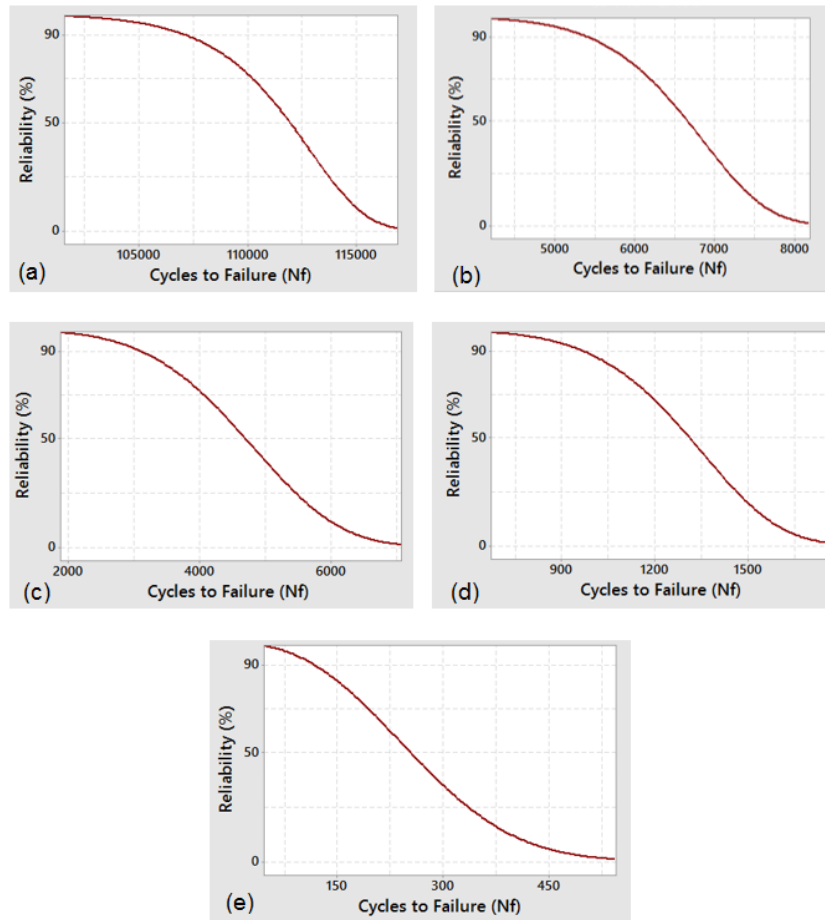
Figure 4.8 Reliability plot using Weibull Distribution at (a) 50% (b) 60% (c) 70% (d) 80% (e) 90% of UTS
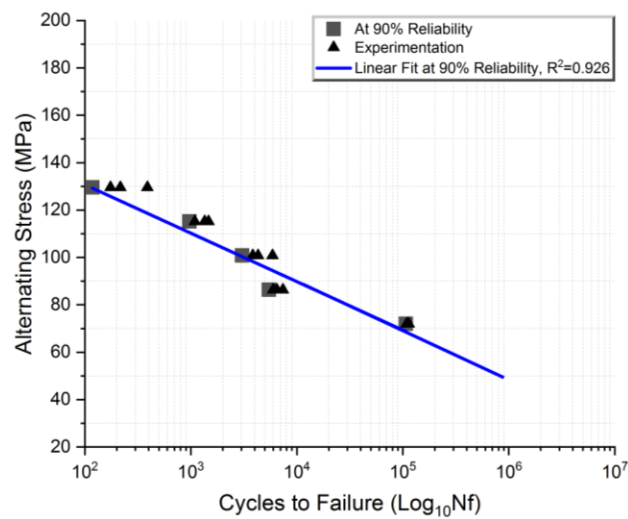
Figure 4.9 S-N curve for neat GFRP composite laminate as per ASTM D3479-19

Using the linear fitted model based on the mentioned S-N curve, a predicted endurance limit strength of 47.2 MPa has been derived, representing approximately 32.78% of the ultimate tensile strength of the GFRP composite laminate at 10^6 cycles. The maximum applied stress has a substantial impact on the fatigue failure of the samples. Additionally, the observed failure morphology in the tested laminates, as depicted in Figure 4.10, is also influenced by the stress amplitude. In comparison, the stiffness of glass fibers is higher than that of the surrounding matrix. Consequently, when the specimens are subjected to load, this difference in stiffness results in notable variations in strain, leading to elevated shear forces at the interface between the fibers and the matrix. The magnitude of these shear forces depends largely on the stress level, with high-stress conditions generating substantial shear forces that result in fractures primarily characterized by fiber pullouts. In contrast, under low-stress conditions, fiber breakage occurs instead of pullouts due to reduced shear stresses at the fiber-matrix interfaces. Conversely, samples subjected to high-stress amplitudes undergo more severe damage than those under low stresses. High stresses lead to the development of larger cracks that propagate and merge quickly, requiring fewer cycles to fail under cyclic loading. In contrast, low-stress conditions result in more numerous smaller cracks, which take more cycles to propagate, resulting in longer fatigue life for the samples. Under such circumstances, larger cracks propagate more quickly, generating a significant plastic zone in front of them. As these cracks advance within the matrix, they leave behind intact fibers that bridge the gaps. However, as cycling continues, the reinforcing fibers eventually break, resulting in pullouts even in the absence of matrix material [192]. In order to estimate the expected lifespan of GFRP composites subjected to fatigue loading, the reliability of the composites under these conditions was evaluated utilizing a Weibull distribution model.
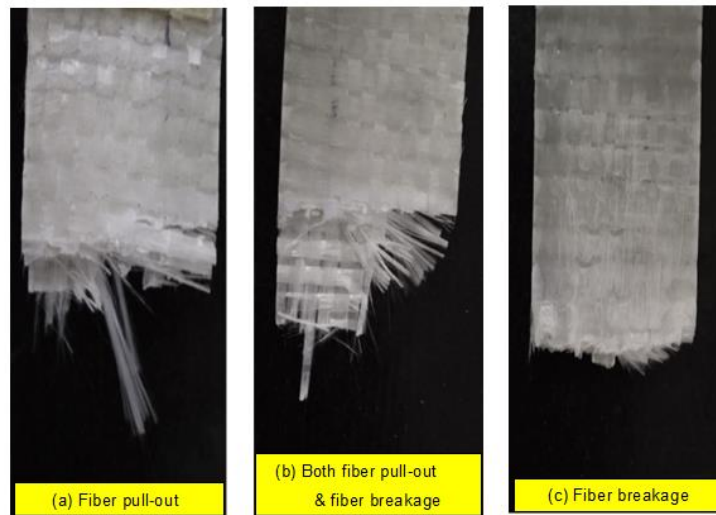
Figure 4.10 Fatigue failure morphology at (a) 90%, (b) 70%, (c) 50% of UTS

Observations have shown that when operating at a low frequency, specifically 2 Hz, longer test durations are often necessary. These extended durations can introduce complicating factors such as material creep. When polymers are exposed to fatigue, they exhibit substantial hysteresis loss due to their viscoelastic nature. Figures 4.11 (a)–(e) depict the evolution of stress-strain hysteresis for samples subjected to five specific stress levels, namely 50%, 60%, 70%, 80%, and 90% of the Ultimate Tensile Strength. The deformation resulted in significant damage to the matrix, fiber breakage, and debonding at crossover points. These failures are mostly irreversible, leaving little chance for the laminate to recover its original strength and stiffness upon unloading. Under fatigue conditions, the samples displayed lower strain levels for the corresponding stresses compared to their static loading. This behavior can be attributed to the strain rate-dependent properties that have been previously documented by the researcher [192].

The hysteresis produced during the last cycles can be observed in Figure 4.11 (a) - (e). These figures indicate that polymer composites undergo progressive damage. The increase in hysteresis was a result of multiple damages, including failure of the fiber-matrix interaction [193]. When plastics are exposed to alternating stresses, they generate heat due to significant hysteresis losses and low thermal conductivity. As a result, the accumulated

heat weakens the shear strength at the interface, leading to the eventual disruption of the bond between the fibers and the matrix [194].
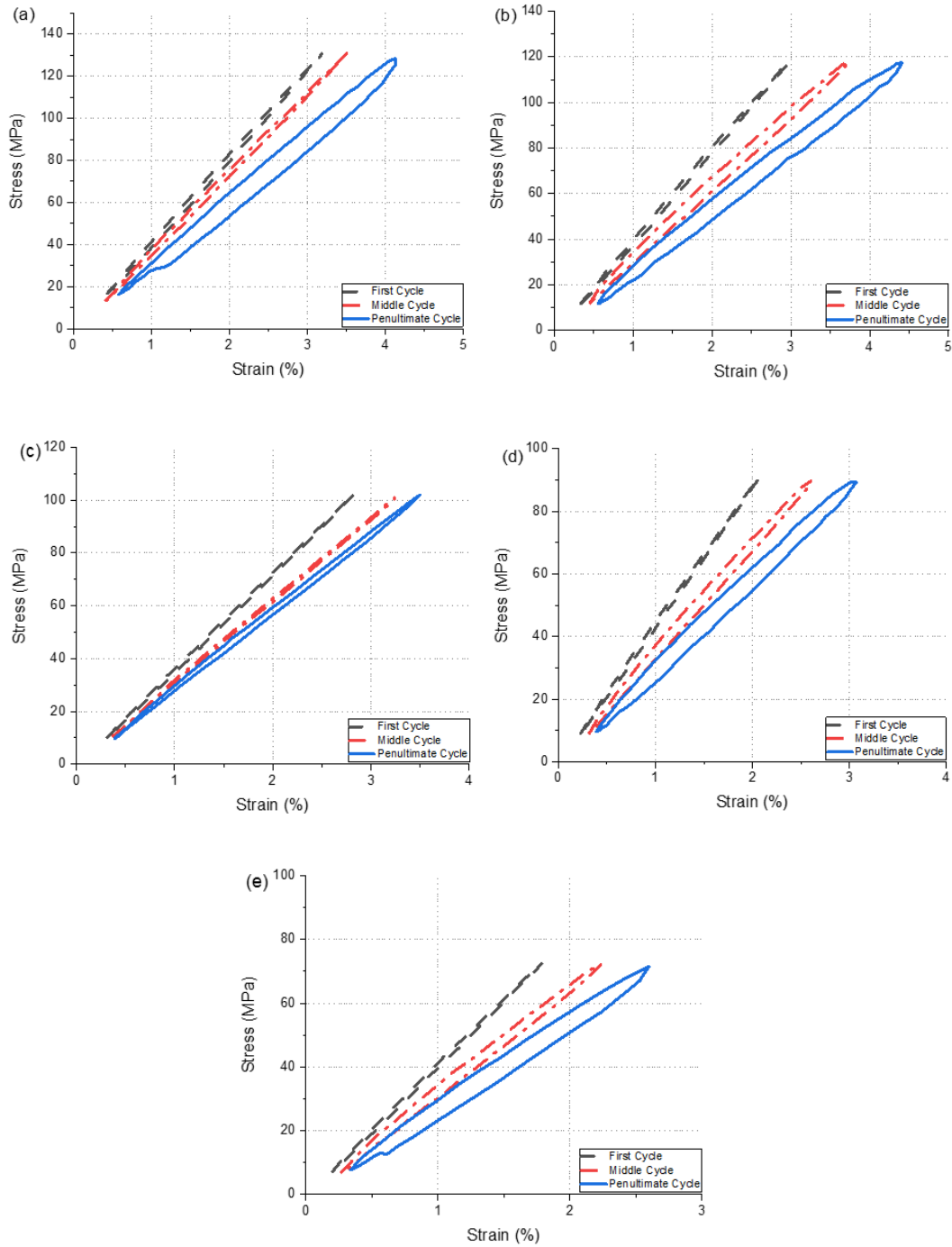
Figure 4.11 Hysteresis loop variations in Neat GFRP composite laminates under cyclic loading at (a) 90%, (b) 80%, (c) 70%, (d) 60%, and (e) 50% of ultimate tensile strength.

The observations indicate that as the stress level rises, the area of the hysteresis loop expands. This expansion can be attributed to the increased friction between separated and detached surfaces, resulting in a greater dissipation of energy [195].

4.2.2 Fatigue Analysis of Modified Glass Fiber Epoxy Composite Laminate

In a similar manner, a fatigue analysis was performed on a modified Glass Fiber Reinforced Polymer (GFRP) laminate that incorporated 3 wt. % of Nano-silica. The aim was to evaluate the fatigue properties of the modified composite laminate under identical environmental conditions. The experimental results, depicted in Table 4.7, display the failure cycles (N_f) obtained at different stress levels. Additionally, the survival probability was determined using Weibull distribution with a reliability of 90%.

Table 4.7 At various Stress levels, experimentation data along with the reliability data using Weibull distribution for Modified GFRP with 3 wt. % of Nano-silica

Modified GFRP (ASTM D3479)	At 50% of UTS	At 60% of UTS	At 70% of UTS	At 80% of UTS	At 90% of UTS
Max. Stress (MPa)	83.7	100.44	117.18	133.92	150.66
Coupon 1 – Nf (Cycles)	125287	7450	4959	1691	447
Coupon 2 – Nf (Cycles)	129275	6886	6777	1254	201
Coupon 3 – Nf (Cycles)	130856	8525	4419	1550	248
Predicted Life at 90% Reliability (Cycles)	119500	5990	3650	1090	150

A series of fatigue tests were conducted at each stress level, and the resulting SN curve was analyzed using statistical methods. From Figure 4.12 Modified GFRP with 3 wt. % Nano-silica showed the enhancement in strength. The endurance strength 57.4 MPa was observed, which is 34.3% of the Ultimate Tensile Strength (UTS). It is important to highlight that the modified GFRP, incorporating 3 wt. % of Nano-silica, demonstrated a notable increase of 21.61% in fatigue strength under tension loading conditions when compared to the fatigue strength of Neat GFRP at 1 million cycles. The inclusion of well-dispersed Nano-silica has been reported to enhance the ductility of the epoxy matrix [167], which may contribute to the slight improvement in fatigue strength.
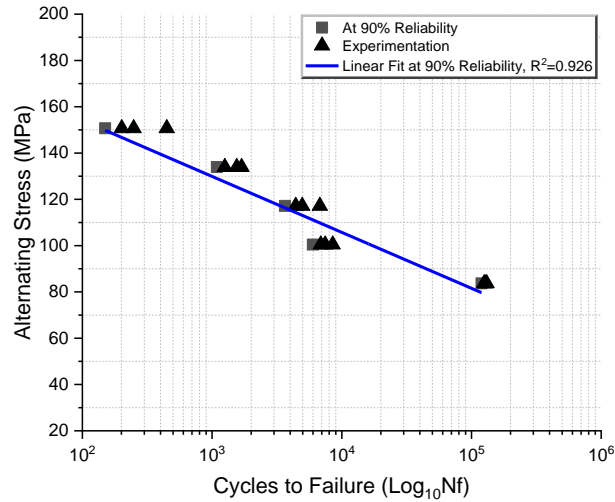
Figure 4.12 S-N curve for modified GFRP composite laminate with 3 wt. % of Nano-silica as per ASTM D3479-19

Figure 4.13 indicates that during the cyclic testing of the modified GFRP under tension loading, the hysteresis loop increases with higher stress levels. Significantly, the hysteresis loop at 90% of the Ultimate Tensile Strength (UTS) has been observed to be notably larger than at lower stress levels. The hysteresis loop in composite materials indicates the energy losses that occur during each loading cycle. It represents the amount of energy absorbed by the material, which is dissipated as heat. The hysteresis characteristics of thermoset epoxy-based FRP composites during fatigue are closely associated with the mechanisms of damage. The dissipation of energy during cyclic loading plays a pivotal role in determining the lifespan of a component. The stress-strain hysteresis loops can be directly derived from the stress-strain curve during fatigue processes, which are essential for understanding and assessing fatigue behavior [196], [197]. In brief, the area within the stress-strain loop corresponds to the total dissipated energy (TDE) per cycle, while the slope of the hysteresis loop reflects the change in elastic modulus as the number of cycles increases [198]. In summary, the dissipation of energy primarily arises from different types of damage, including fiber breakage, fiber bridging, and friction occurring at the unrestrained region within the matrix and at the interface between the matrix and fibers [195].
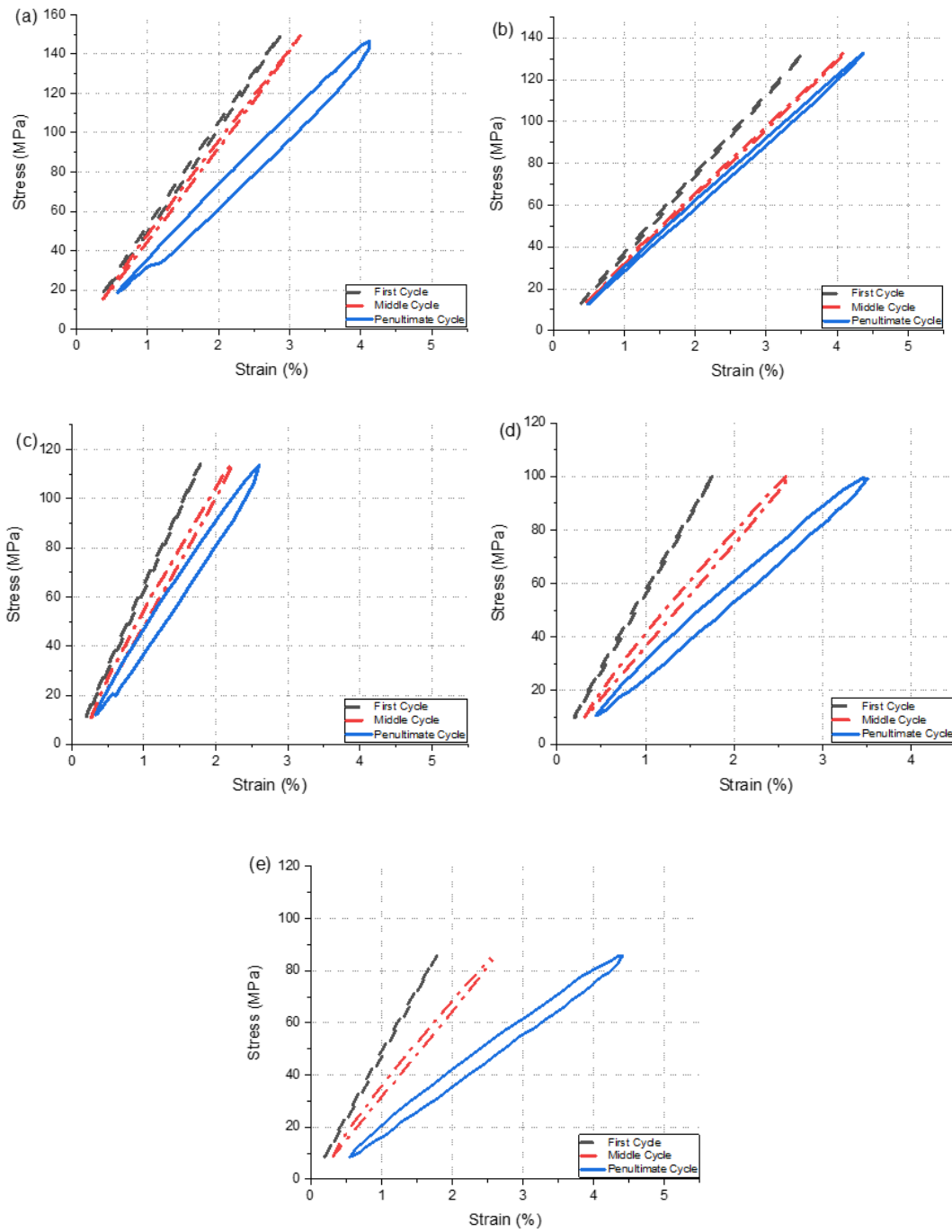
Figure 4.13 Hysteresis loop variations in Modified GFRP composite laminates under cyclic loading at (a) 90%, (b) 80%, (c) 70%, (d) 60%, and (e) 50% of UTS

Additionally, the presence of secondary bonds in the polymer contributes to increased energy dissipation due to their viscoelastic nature. These secondary bonds generate higher

frictional forces between the polymeric chains, resulting in greater energy dissipation during cyclic loading [199]. Based on Figure 4.14, it is evident that the Neat GFRP exhibits a steeper slope compared to the Modified GFRP composite laminate. This steeper slope signifies that the Neat GFRP has a lower fatigue resistance, making it more susceptible to failure under cyclic loading. Failure can occur even with relatively low-stress amplitudes after a relatively small number of cycles. On the other hand, the Modified GFRP composite laminate demonstrates a shallower slope, indicating higher fatigue resistance. These findings suggest that the Modified GFRP has the ability to endure higher stress amplitudes for a given number of cycles prior to failure. As a result, the Modified GFRP composite material demonstrates an extended fatigue life and enhanced durability under cyclic loading conditions.
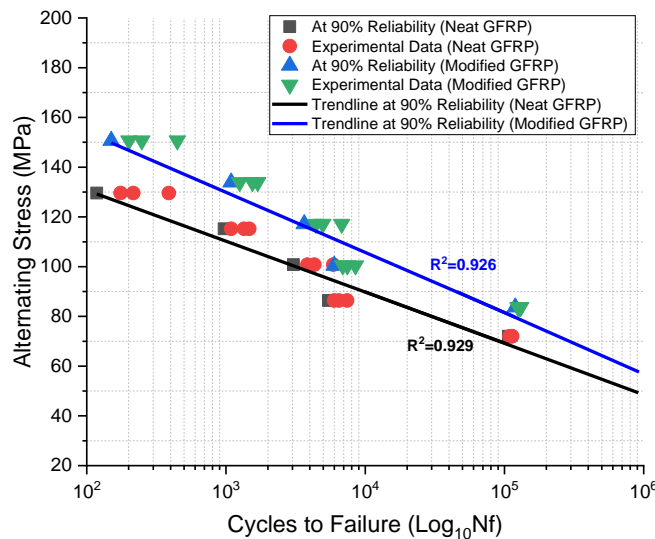
Figure 4.14 S-N curve for Neat and Modified GFRP composite laminate

Upon cyclic loading, there is a noticeable decrease in the slope of the stress-strain hysteresis loop, which signifies a reduction in the dynamic modulus of the specimen. This decrease in slope reflects the progressive softening or degradation of the material's stiffness during the cyclic loading process. Figure 4.15 presents the correlation between the evolution of the dynamic modulus and the normalized cycles (N/N_f), where N is the number of cycles at an instance and N_f is the cycle to failure. Notably, when subjected to a

88

maximum stress of 90% of the Ultimate Tensile Strength (UTS), the Modified GFRP laminates displayed the highest dynamic modulus. However, as the applied stress was reduced, the dynamic modulus gradually decreased. During the initial stage, which corresponds to a cycle ratio of approximately 0.05-0.1, the dynamic modulus undergoes a rapid decline. This decline can be attributed to the formation of multiple cracks within the material. When compared to the Modified GFRP laminates, the neat GFRP laminates experienced a significant decrease in the dynamic modulus. This difference can be attributed to the presence of Nano-silica in the Modified GFRP laminates, which enhances the interlocking between the fibers and epoxy. As a result, the interfacial stress is improved, leading to a notable impact on the dynamic properties of the laminate under fatigue loading. In the second stage (with a cycle ratio of 0.1-0.98), the modulus gradually decreased with an increase in fatigue cycles. The relationship between the modulus and cycle ratio was almost linear, and a significant portion of the fatigue life was associated. In this stage, crack growth in terms of count and length, along with inter-ply delamination, led to a gradual decrease in the modulus of the specimens. Towards the end of the second stage, the matrix crack reached its saturation point.
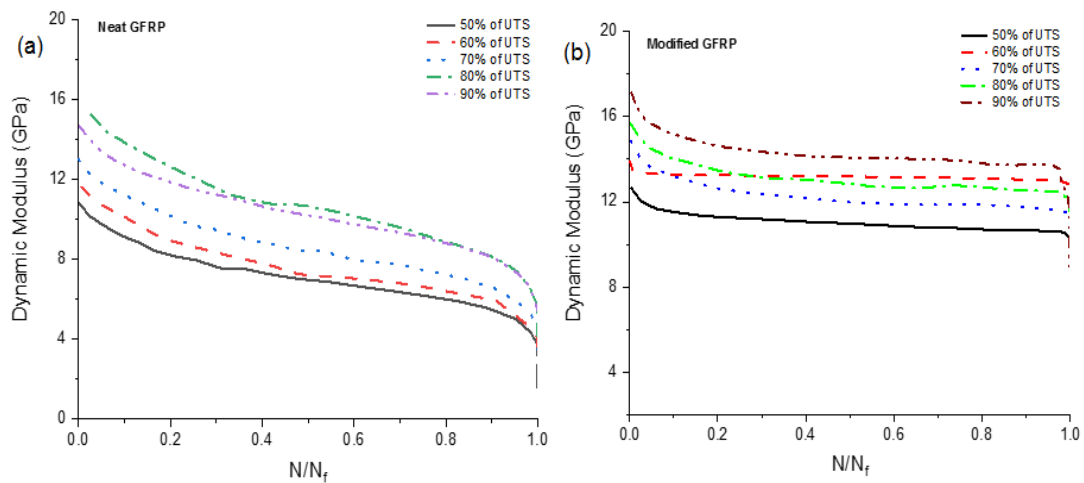
Figure 4.15 Dynamic modulus variation versus normalized cycles at different stress levels for (a) Neat GFRP and (b) Modified GFRP composite laminate

Subsequently, the laminates rapidly entered the third stage, which was marked by a continued decline in modulus until eventual failure. Notably, the Neat GFRP laminates exhibited a steep decline before reaching failure. Under high-stress levels, the laminates experienced aggressive damage, causing a more rapid decrease in stiffness compared to samples loaded under low-stress levels. Nevertheless, when examining the initial stage, a more pronounced decline in stiffness was observed at higher stress levels. In general, the modified GFRP composite laminate exhibits improved resistance to crack propagation and demonstrates minimal changes in dynamic modulus under cyclic loading, in contrast to the neat GFRP laminate. As a result, the modified GFRP laminate enhances fatigue strength and offers higher reliability.

4.3   Closure

The current chapter focuses on experimentally characterizing the mechanical properties of glass fiber epoxy composite laminates under fatigue loading conditions. Two types of materials are studied: neat bidirectional glass fiber-reinforced epoxy composite laminates and modified glass fiber-reinforced epoxy composite laminates. Initially, the impact of static loading is investigated for both types of composite laminates. It is worth mentioning that the incorporation of Nano-silica has a beneficial impact on the modified glass fiber-reinforced composite laminates, leading to a significant enhancement of 16.25% in tensile strength compared to the neat GFRP composite laminates. Subsequently, the effect of fatigue loading is examined for the same composite laminates. The incorporation of 3 wt. % of Nano-silica is observed to significantly enhance the fatigue strength by 21.6% compared to the neat GFRP composite laminates. As well as the effect of dynamic modulus was also compared for both materials under fatigue loading scenario under the normalized number of cycles. It was observed that modified GFRP composite laminate performs well under fatigue loading as compared with neat GFRP laminate.

In order to expand the range of mechanical joints, the subsequent chapter centered on conducting finite element analysis of glass fiber epoxy pin joints. The pin joints were carefully evaluated to determine their failure modes. Furthermore, a comprehensive

comparison was conducted between two sets of pin joints: Modified GFRP with the addition of Nano-silica and the other Neat epoxy GFRP. The purpose of this comparison was to analyze the impact of Nano-silica on the performance and failure characteristics of the pin joints. Furthermore, the behavior of pin joints under both fatigue and static loading conditions was thoroughly examined.

CHAPTER 5 – FINITE ELEMENT ANALYSIS OF PIN JOINTS

The objective of this chapter is to examine the performance of pin joints made from glass fiber epoxy composites under static and fatigue loading. It explores how geometric factors, specifically the E:D ratio (edge to diameter) and W:D ratio (breadth to diameter), influence the load-bearing strength and damage pattern of pin joints. To conduct this analysis, finite element analysis (FEA) was employed, utilizing the FEA Package. Pin joints are widely used in various engineering applications to connect components and transmit load [200]. Understanding their mechanical behavior is crucial for designing reliable and efficient structures. The main focus of this chapter is to employ FEA to assess the bearing strength and mode of failure of pin joints. Additionally, it aims to investigate how the E:D and W:D ratios affect these factors under both static and fatigue loading conditions. Mechanical joints play a vital role in mechanical assemblies, providing flexibility and load transfer while accommodating relative motion between connected parts [22]. They are commonly used in aerospace, automotive, and various industrial applications [201]. However, factors such as the E:D and W:D ratios can significantly affect the strength, stiffness, and stress distribution in pin joints. Hence, it is crucial to examine the impacts of geometric ratios on the structural performance of pin joints using FEA under fatigue loading conditions. Additionally, the influence of Nano-silica on the failure modes and associated strength of the pin joint was compared across various joint configurations.

5.1 Joint Configurations

As discussed in the previous chapter, the incorporation of Nano-silica resulted in enhanced strength of glass epoxy laminates, reaching its peak at a Nano-silica content of 3 wt. %. Nevertheless, beyond the 3 wt. % Nano-silica content, the strength started to decline, possibly attributable to the agglomeration present within the laminates. Pin joints were fabricated for both neat Glass Fiber Reinforced Polymer (GFRP) and Modified GFRP, which included 3 wt. % of Nano-silica. A comparison was made between these pin joints under static and fatigue loading. A composite plate with specified dimensions for length

(L), breadth (W), and thickness (t) was utilized to construct the joint. The plate featured a single hole with a 4 mm diameter, securely fastened in position with a rigid pin. The hole was centrally located along the plate's centerline at a certain distance from one of the ends. The arrangement of the single-hole pin joint is depicted in Figure 3.6. The joint underwent a tensile load, applied in parallel to the plate and symmetrically with respect to the centerline, effectively eliminating any bending moments around the x, y, or z-axis.

The E:D and W:D proportions were adjusted in the range of 3 to 5. Samples were manufactured for the bidirectional ply orientations, with varying E:D and W:D proportions, while keeping the geometric parameters thickness 't', length 'L', and diameter 'D' unchanged are outlined in Table 5.1. To optimize different geometric parameters and assess their influence on the bearing strength of pin joints under static and fatigue loading conditions, the Taguchi method, employing the "higher the better" attribute, was utilized. This analysis was conducted using the L9 orthogonal array.

Table 5.1 Pin joint configurations at various E:D and W:D proportions.

Specimen No.	E/D	W/D	E (mm)	W (mm)	D (mm)	t (mm)	L (mm)
PJC1	3	3	12	12	4	2.5±0.2	100
PJC2	3	4	12	16	4	2.5±0.2	100
PJC3	3	5	12	20	4	2.5±0.2	100
PJC4	4	3	16	12	4	2.5±0.2	100
PJC5	4	4	16	16	4	2.5±0.2	100
PJC6	4	5	16	20	4	2.5±0.2	100
PJC7	5	3	20	12	4	2.5±0.2	100
PJC8	5	4	20	16	4	2.5±0.2	100
PJC9	5	5	20	20	4	2.5±0.2	100

5.2   Numerical Analysis of Pin Joints under Static Loading

Typically, failure is regarded as the complete loss of function in a structure. Nevertheless, when it comes to composite laminates, there are several occurrences of localized damage prior to the complete loss of overall strength. The laminate ultimately fails due to the gradual accumulation of damage in its fiber and matrix phases. The pin joints were

subjected to numerical analysis through finite element methods, which is a highly adaptable technique that can be employed for evaluating composite laminates [31], [73], [140], [202]. The finite element analysis (FEA) approach enables a detailed examination of stress distribution, displacement, and deformation patterns within the pin joints, providing valuable insights into their mechanical response. Various researchers have proposed multiple techniques for predicting the strength of composite joints [108], [117], [120], [129]. In this study, the characteristic curve method (CCM), combined with the Tsai-Wu failure theory, was employed using FEA package for the numerical analysis of pin joints. This approach enabled the prediction of failure strength and failure modes. The determination of the characteristic length under tension and compression was accomplished using the Characteristic Curve Method (CCM) to generate a curve near to the hole vicinity. Tsai-Wu polynomial equations were employed to calculate the failure index on the characteristic curve, allowing for the prediction of load-bearing capacity and damage mode. The process of determining the characteristic length and failure index was elaborated upon by Singh *et al.* [203].

5.2.1 Finite Element Modeling of Neat GFRP Composite Pin Joint

To simulate the GFRP composite pin joint, an ANSYS Workbench was employed, utilizing a Design modular platform. The process began with generating a surface sketch based on the specified geometric dimensions outlined in Table 5.1. Figure 5.1 depicts the representation of the surface sketch within the design modular.

After the creation of the geometry, engineering data was input into the FEA software to define the material properties of both Neat and modified GFRP composite materials, aligning with experimental findings as per ASTM standards. Subsequently, within the model tab, meshing was conducted using a multi-zone method for body meshing and face meshing near the hole region, as illustrated in Figure 5.2.
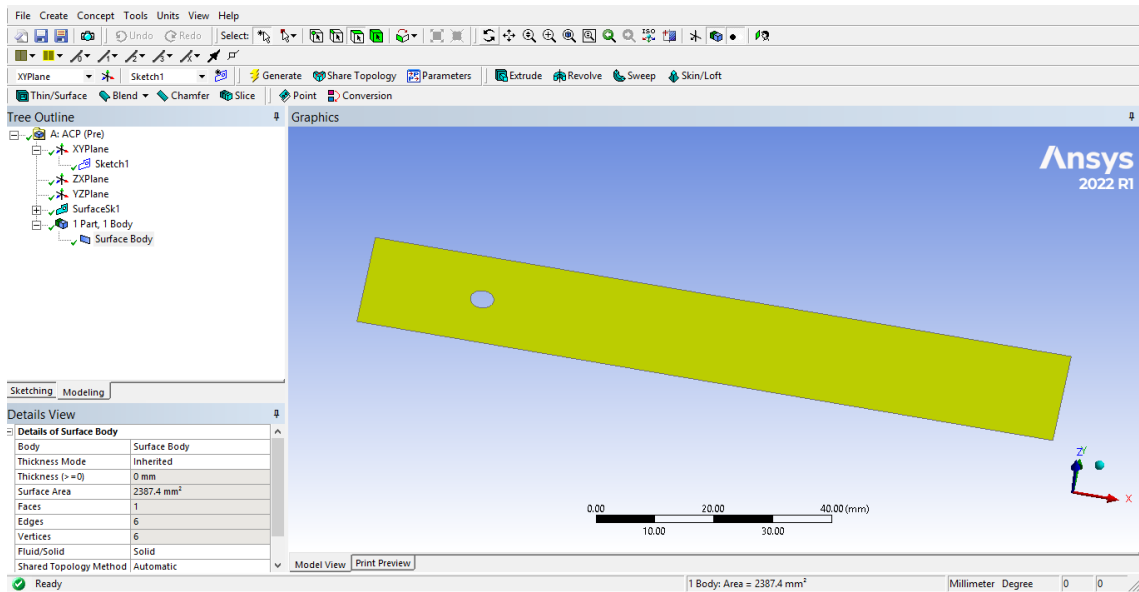
Figure 5.1 Modeling of surface sketch in design modular
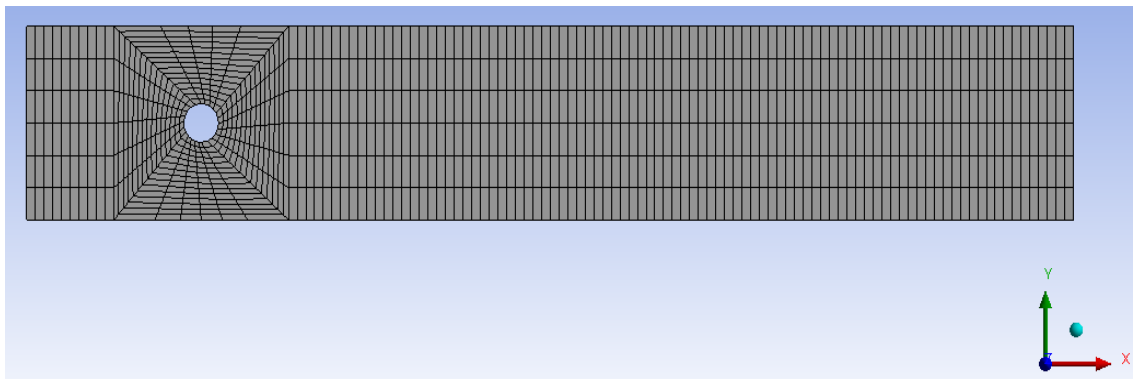
Figure 5.2 Meshing of GFRP pin joints

For the comprehensive modeling of the GFRP pin joint with a ply-wise arrangement, the Ansys Composite PrePost (ACP) module was employed. The detailed modeling of the GFRP composite laminate was achieved by utilizing the ACP module, incorporating a total of 6 plies to construct the composite laminate, as depicted in Figure 5.3.
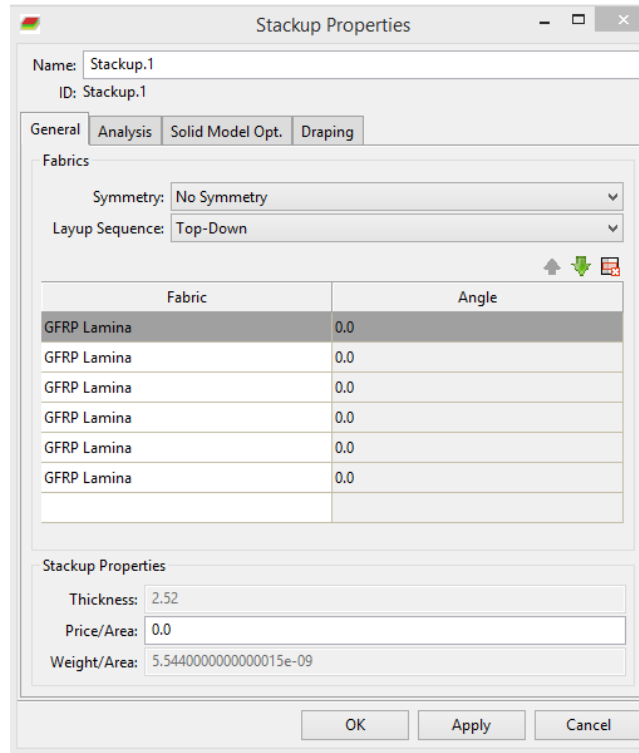
Figure 5.3 Stacking-up of GFRP lamina

Subsequently, within the ACP module, the solid model was meticulously crafted by employing ply orientation selection sets with rosettes. This method was utilized to precisely define the thickness direction, denoted as the z-axis, for the stack-up process. This approach enabled the creation of a modeling group, as visually demonstrated in Figure 5.4. The modeling group represented the organized arrangement of plies within the composite structure, ensuring accurate alignment and orientation for the overall solid model of the GFRP pin joint.
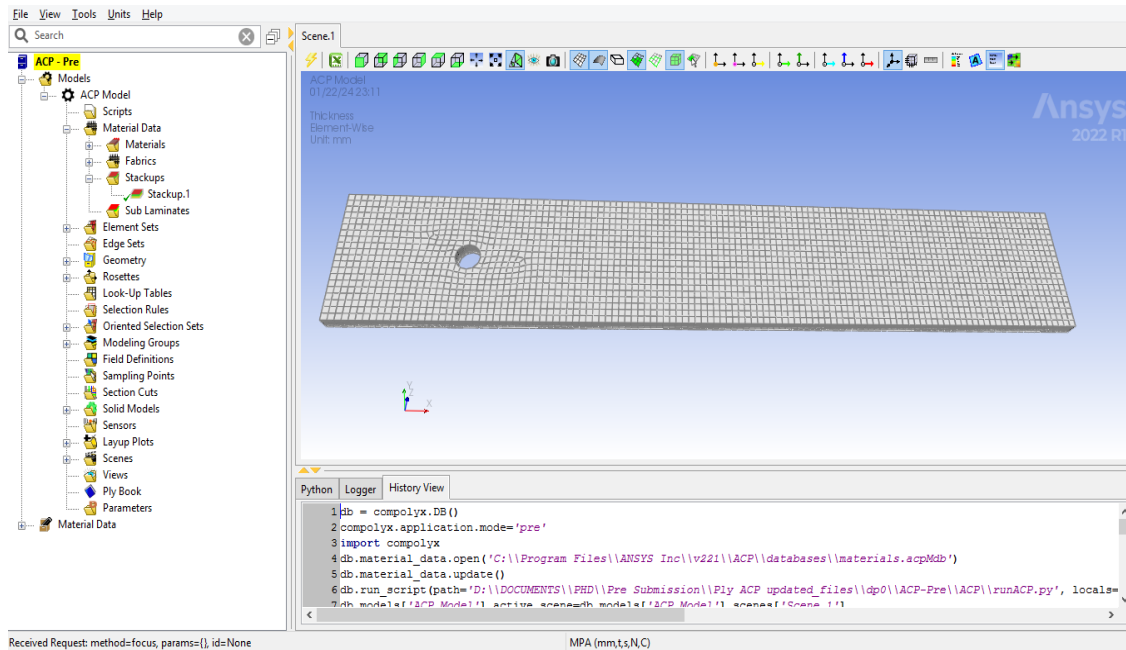
Figure 5.4 Illustration of setup module in ACP (Pre)

Following the preparation of the composite laminate within the ACP (Pre) module, a connection was established between the ACP (Pre) setup and the static structural module. Within the static structural module, specific boundary conditions were defined. It was assumed that perfect bonding existed between each ply, and the ply orientation exhibited symmetry relative to the z = 0 plane. For static loading, the composite plate, featuring a pinned joint, underwent a bearing load denoted as 'P' at the hole region. The opposite end of the joint was considered fixed to simulate static loading conditions. In the case of fatigue loading, cyclic loading was applied at the hole region with a frequency of 2 Hz and a loading ratio (R) of 0.1. This loading scenario was designed to simulate the effects of fatigue on the composite structure. The boundary conditions for analysis, including both static and fatigue loading conditions, are depicted in Figure 5.5.
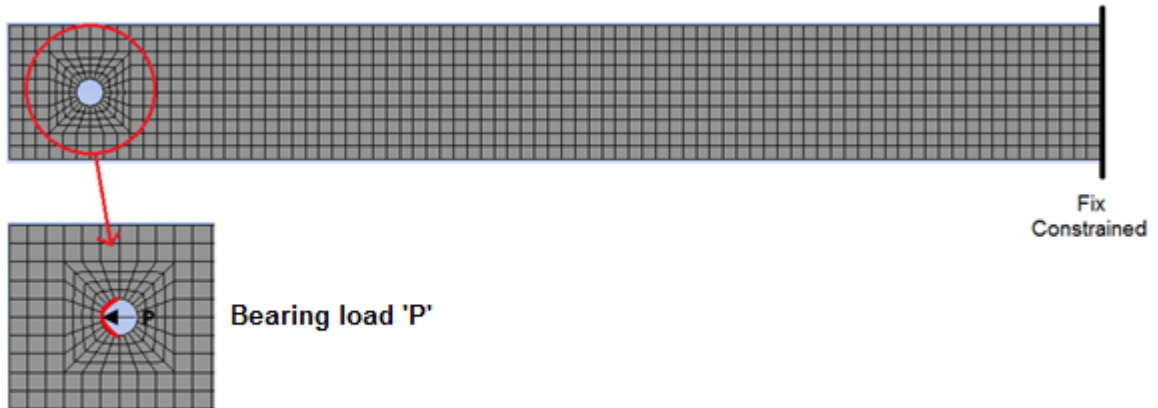
Figure 5.5 Boundary condition of GFRP pin joints

The eight-node hexahedral (brick) element SOLID185 was employed to mesh the 3D model. Each of the eight nodes in the Solid185 element has three translational degrees of freedom (u, v, w) in each of the coordinate directions (x, y, z). A convergence study was also done to refine the mesh size was conducted to explore how discretization affects the stress distribution near the hole.
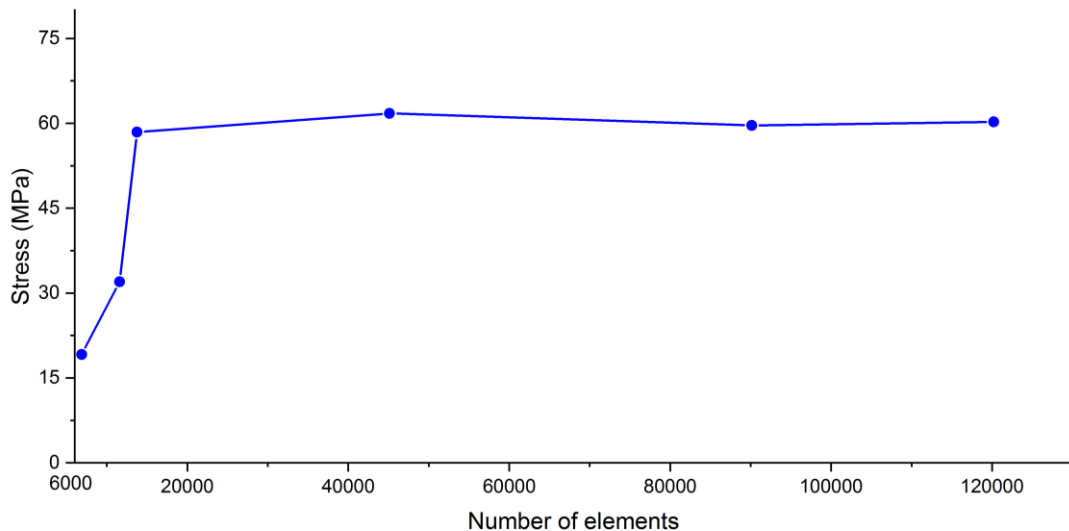
Figure 5.6 Mesh convergence plot at E:D and W:D equals 5.

Figure 5.6 illustrates the convergence plot for stress, showcasing results obtained at different element counts with a 5% tolerance in induced stress at a ratio of E:D and W:D

equal to 5 for the neat GFRP pin joint configuration. The graph distinctly shows that convergence is achieved at 13,765 elements, with the stress level stabilizing at 58.45 MPa. This approach has been consistently applied to all pin joint configurations for both material categories *i.e.* Neat GFRP and Modified GFRP with 3 wt. % of Nano-silica composite pin joints. The examination of the bearing strength of the GFRP composite pin under static loading involved the application of the T-Sai Wu failure theory. This theory was employed to anticipate the failure mode and determine the corresponding bearing strength. Figure 5.7 illustrates the process of defining failure criteria for the reinforced ply in the analysis.
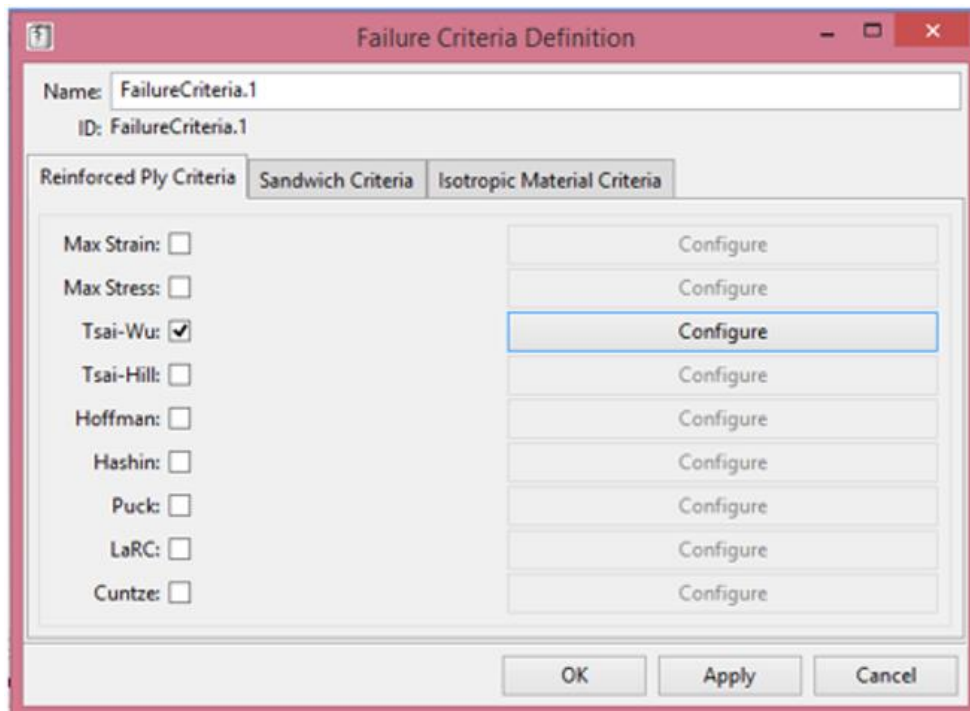
Figure 5.7 Failure criteria definition of reinforced ply

The entire integration process involves linking the ACP (Pre) module with the static structural module. Once the composite laminate is configured within the ACP (Pre) module, this setup is mapped with the static structural module. After the pre-processing phase, the interconnected modules are further linked with the ACP (Post) module to extract results based on specified failure criteria, as depicted in Figure 5.8. This comprehensive

procedure is consistently applied to both neat and GFRP pin joints across all pin joint configurations.
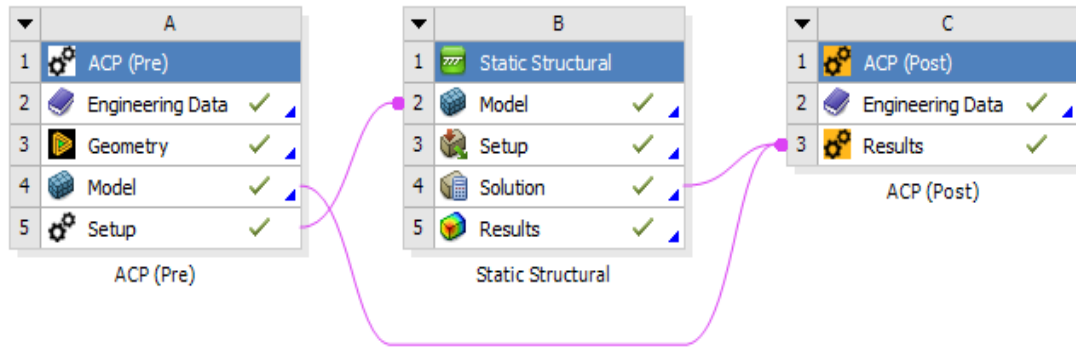
Figure 5.8 FE Analysis of bearing strength of GFRP composite pin joint by utilizing ACP (Pre) - Static structural - ACP (Post) module

By utilizing Named selection, an imaginary characteristic curve was plotted based on the characteristic lengths 'rot' and 'roc'. The failure angle was determined by measuring the FI (Failure Index) value on the characteristic curve. Similarly, r_{ot} and r_{oc} for each configuration have been determined using the finite element method as shown in Table 5.2.

Table 5.2 Characteristic lengths in tension and compression for Neat GFRP at various joint configurations

PJC	E:D	W:D	D (mm)	E (mm)	W (mm)	r_{ot} (mm)	r_{oc} (mm)
PJC1	3	3	4	12	12	1.07	0.19
PJC2	3	4	4	12	16	1.47	0.22
PJC3	3	5	4	12	20	2.90	0.38
PJC4	4	3	4	16	12	1.03	0.11
PJC5	4	4	4	16	16	1.76	0.27
PJC6	4	5	4	16	20	1.73	0.20
PJC7	5	3	4	20	12	1.00	0.36
PJC8	5	4	4	20	16	1.48	0.42
PJC9	5	5	4	20	20	2.05	0.08

Upon determining the characteristic lengths, the equation was employed to generate the characteristic curve. The complete curve was constructed within the modeling software to anticipate the failure mode in the GFRP composite pin joints across different joint

configurations. Figure 5.9 showcases the FI (Failure Index) values around the hole for a particular combination of geometric parameters (at W:D & E:D proportion equals 5). The failure index values and corresponding failure angles were determined by referencing the characteristic curve.
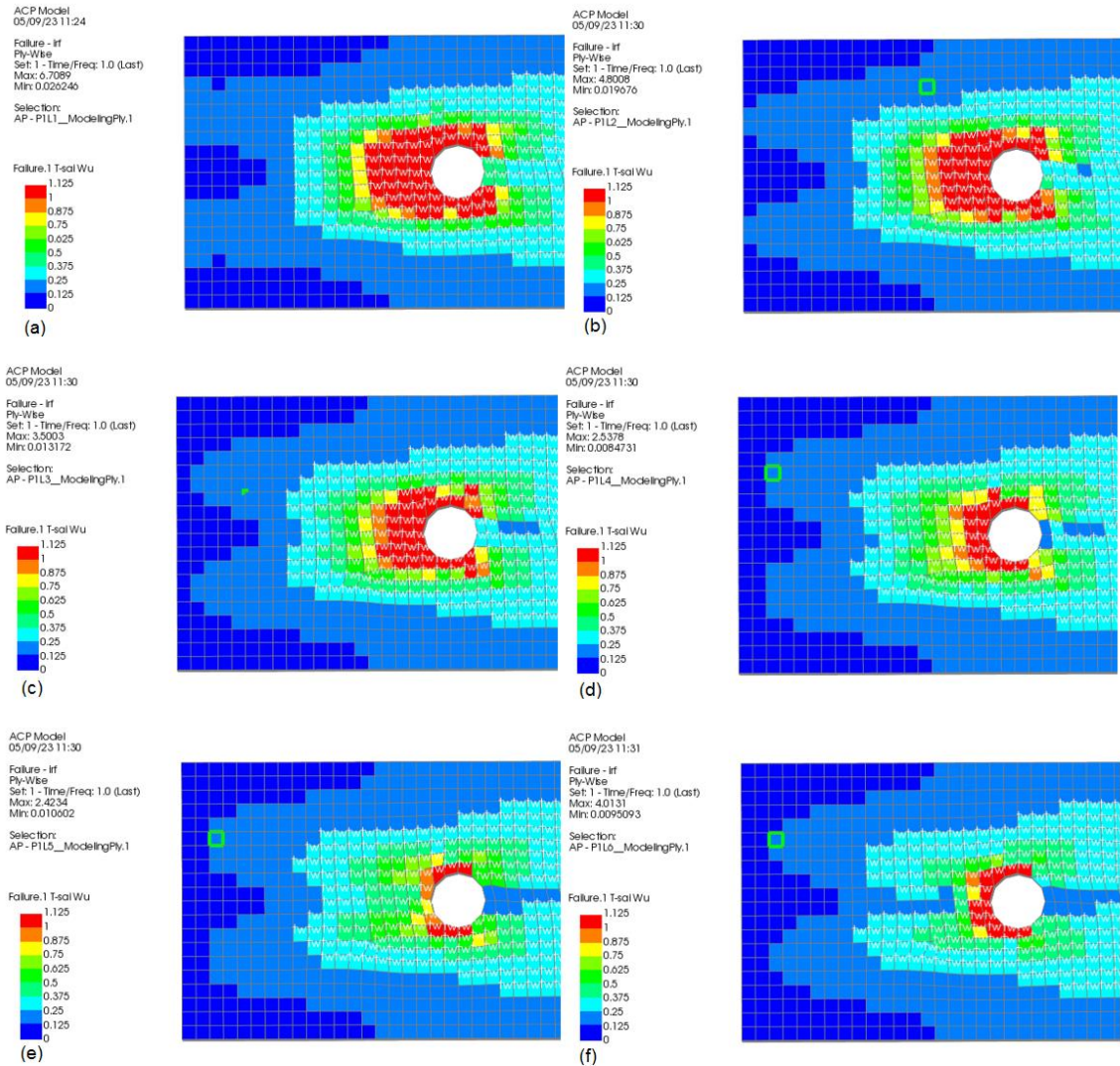
Figure 5.9 FI at E:D & W:D equals 5 for Neat GFRP pin joint at each ply level using Tsai-Wu criteria.

Table 5.3 presents the evaluation of the three primary failures for all pin joint configurations by calculating the FI (Failure Index) and failure angle on the characteristic curve. For all W:D and E:D proportions, the FI value was computed for nodes positioned on the characteristic curve. The failure angle was determined at the point where the FI

value reached its maximum. Such calculations were performed systematically. Fiber failure takes place when the applied tensile stress surpasses the ultimate strength of the fibers. This failure mode is typically characterized by either fiber breakage or fiber pullout. Plies with fibers aligned parallel to the loading direction are more prone to the initiation and propagation of fiber failure. Matrix cracking can occur both within individual plies and at the interfaces between plies. Cracks in the matrix can propagate parallel to the fiber direction or traverse across multiple plies. Matrix cracking can reduce the load-carrying capacity of the laminate and lead to localized stress concentrations. Figure 5.9 (a) to (f) indicates that failure began near the hole's periphery in the loading direction, indicating that the failure angle was between 0º and 15º. The maximum failure index value was found at a failure angle of 10.34º on the characteristic curve, indicating that the composite pin joint failed due to bearing as shown in Figure 5.10.
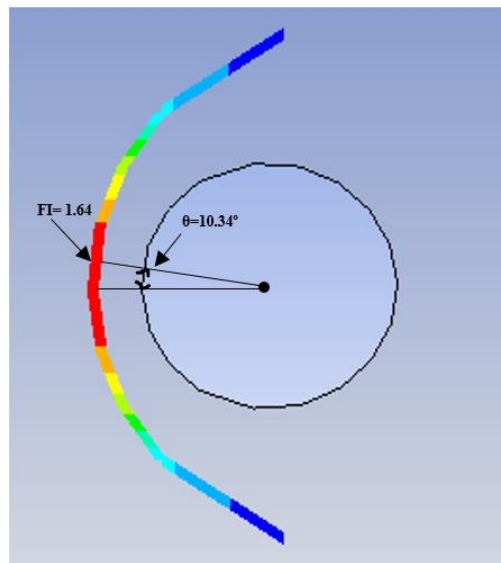
Figure 5.10 Failure index and corresponding failure angle at E:D and W:D proportion equals 5

5.2.1 Finite Element Analysis (FEA) of Modified GFRP Composite Pin Joints

Likewise, Finite Element (FE) analysis was carried out on modified GFRP pin joints by incorporating 3 wt. % of Nano-silica particles. This analysis encompassed all pin joint configurations, and the Tsai-Wu failure theory was utilized in conjunction with the CCM to predict the damage mode and corresponding load-bearing capacity for the specific pin

joint configurations. The damage modes categorized by failure angle for all W:D and E:D proportions are presented in the Table 5.3 for both categories of pin joints *i.e.* Modified GFRP with 3 wt.% of Nano-silica and Neat GFRP composite. According to the data presented in Table 5.3, it can be observed that for a W:D proportion of 3, the predominant failure modes were net tensions (N) across all E:D proportions. When the W:D ratio is 3, the damage modes can vary, either being net tension or a combination of shear-out (S) followed by net tension failure, depends upon the E:D proportion. When the E:D proportion was low, the failure mode was net tension.

Table 5.3 Failure modes of the pin joint specimen predicted through numerical results under static loading

| Specimen | Bearing Load and Failure Mode Predicted Numerically | | | |
| | Neat GFRP | | Modified GFRP | |
	Bearing Load (N)	Failure Mode	Bearing Load (N)	Failure Mode
PJC1	742	N	798	N
PJC2	779	N	911	N+S
PJC3	793	N+S	886	B+S
PJC4	804	N+S	978	N
PJC5	881	B+S	1006	B
PJC6	916	B+S	1089	B
PJC7	719.6	B	881	N+S
PJC8	949.6	B	1119.8	B
PJC9	1029	B	1289.5	B
N; Net-tension, S; Shear-out, B; Bearing				

However, as the E:D ratio increased, it shifted to a mixed mode of failure. When W:D≥4 and E:D≤3, shear-out failure mode occurred. With a further increase in the E/D proportion, the failure mode shifted from shear-out to bearing (B). When both W:D≥4 and E:D≥4, all specimens exhibited a bearing failure mode, which is highly desirable due to its exceptional load-carrying capacity. The experimental and FEM results show minimal discrepancies, primarily attributed to the manual preparation of numerous specimens. Figure 5.11 indicates that the modified GFRP composite demonstrates a bearing failure mode at W:D and E:D values of 5. Furthermore, when comparing the neat and modified GFRP composite pin joints at W:D and E:D proportion equals 5, both demonstrate the identical damage

mode, namely the bearing failure. Furthermore, it is noticeable that the modified GFRP composite shows enhanced resistance to failure in the vicinity of the hole, specifically in terms of bearing strength. This improved resistance can be attributed to the inclusion of Nano-silica in the composite material. The high surface area of Nano-silica particles improves the interaction between the matrix and reinforcement fibers. This enhanced bonding facilitates increased load transfer and improves the bearing strength of composite pin joints [61].

Plywise failure indexed has been demonstrated in Figure 5.11 (a) to (f) to understand how the damage initiates on the ply level, the load is primarily transferred from one ply to another through shear stresses between the plies. As the load is applied, the stress distribution gradually redistributes, causing higher stresses to be transferred to the initial plies. Therefore, the initial plies, such as ply 1, tend to experience higher stress levels compared to the subsequent plies. This redistribution of stress leads to a decrease in the failure index as we move from ply 1 to ply 6. Modified GFRP Pin joints undergo progressive damage accumulation, where the initiation and propagation of damage, such as matrix cracks or fiber breaks, occur gradually. As the loading continues, the damage accumulates, leading to a decrease in the strength and stiffness of the affected plies. Therefore, the plies closer to the loading direction, such as ply 1, are more susceptible to damage accumulation, resulting in a decrease in the ply-wise failure index. As well as Ply 1, being closer to the surface or the load-bearing region, experiences higher stress concentrations compared to the inner plies
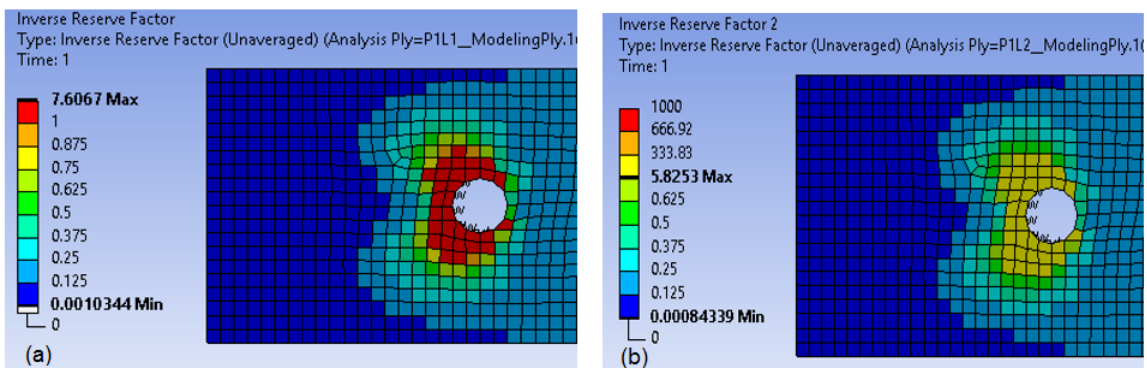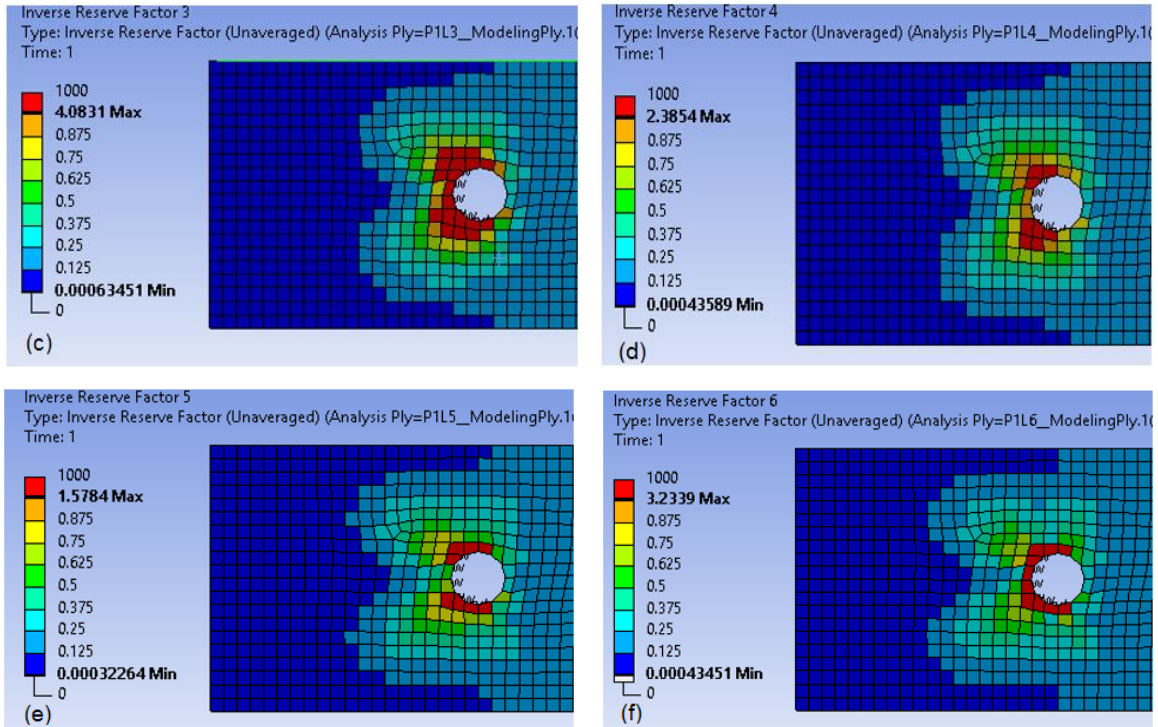
Figure 5.11 Failure indexed using Tsai-Wu failure criteria for Modified GFRP pin joint at E:D & W:D equals 5 at each ply level

5.3 Numerical Analysis of GFRP Pin Joints under Fatigue Loading

The study primarily focuses on conducting numerical analysis of pin joints subjected to fatigue loading. The aim of this analysis is to examine the behavior and performance of pin joints under cyclic loading conditions. The numerical analysis offers valuable insights into the fatigue life, damage modes, and load-bearing strength of the pin joints. On the same L9 orthogonal array has been taken into account for discriminating the geometric parameters for the pin joints as well as two distinct categories of composite material have been considered for the fatigue analysis of pin joints *i.e.* Neat GFRP and modified GFRP composite material.

5.3.1 Finite Element Analysis (FEA) of Neat GFRP Composite Pin Joints

The ultimate bearing load predicted through numerical analysis using FEA has been adopted as the maximum load for fatigue analysis of pin joints as represented in Table 5.3. In this analysis, a load level of 70% of the maximum load has been considered to assess

105

the fatigue performance of the joints. Additionally, the software provides fatigue sensitivity analysis, which evaluates the predicted life of the pin joints when the bearing load varies from 50% to 90% of the predicted bearing load for both categories of materials. The boundary conditions used in the numerical analysis of pin joints under static loading conditions were retained for the fatigue analysis. Cyclic loading was applied in the hole region, while the other side of the plate at the tab region was constrained with fixed support. To explore the impact of fatigue loading on failure mode and life in comparison to static loading, damage, and predicted life were considered for all pin joint configurations. Figure 5.12 represents the geometric model of the pin joint considered for fatigue analysis of the pin joint along with the boundary conditions.
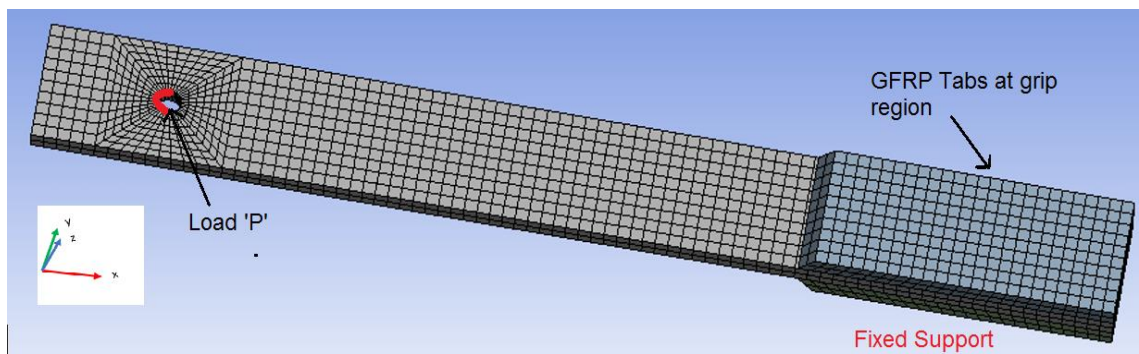
Figure 5.12 Structured meshing at the hole vicinity using the FEA tool for pin joint specimen

Based on the findings from Figure 5.13, it is evident that the W:D proportion carries greater significance compared to the E:D proportion. As the W:D proportion upsurges to 4 and 5 at E:D equals 5, the predominant failure mode shifts from catastrophic failure (net-tension, shear-out, cleavage failure) to progressive damage. In Figure 5.13(a), it can be observed that W:D ratios of 3 and 5 exhibit steep slopes, indicating an adverse impact on the fatigue life of the pin joints and an increased risk of catastrophic failure, especially net-tension failure. Similarly, in Figure 5.13(b), a steep slope is evident at E:D = 4 and W:D = 3, indicating a pronounced effect on the fatigue life of the pin joints. When the W:D ratio increased to 4 and 5 while maintaining the E:D ratio at 4, moderate slopes were observed.
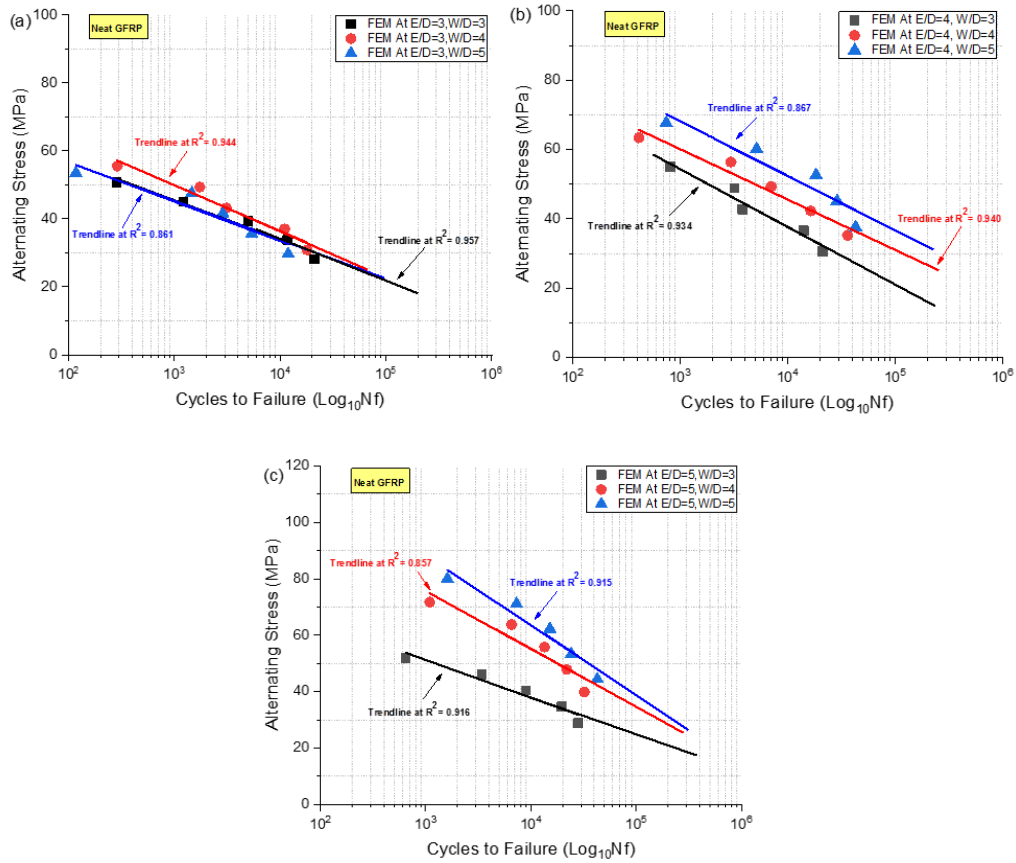
Figure 5.13 SN plot predicted for Neat GFRP using FEA at various pin joint configurations

A moderate slope indicates that the material can withstand a moderate number of cycles before experiencing failure under cyclic loading conditions. A composite with a moderate slope can still exhibit acceptable fatigue performance in many applications under finite design life. Among all the analyzed pin joint configurations for fatigue, those with E:D and W:D values equal to or greater than 4 show a pattern of progressive damage characterized by a shallow slope. Pin joints with higher E:D and W:D proportions demonstrate extended fatigue life, allowing them to withstand more cycles before joint failure. This indicates enhanced durability and resilience of these configurations under cyclic loading condition. The initiation of progressive damage observed under fatigue loading at E:D and W:D equals 5 as demonstrated in Figure 5.14(a).
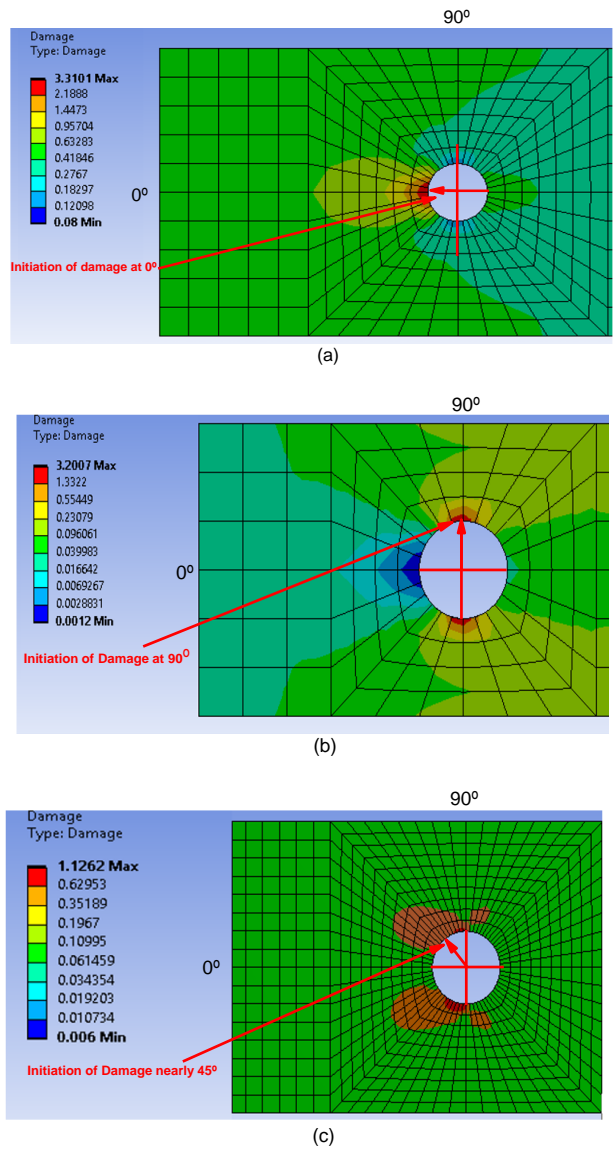
Figure 5.14 Damage initiation in pin joints under fatigue loading with various failure modes observed (a) Bearing, (b) Net-tension, (c) Shear-out failure modes

Bearing failure has been considered as progressive damage which implies failure initiated nearly parallel to the loading direction. As the cyclic loading continues, these cracks grow and coalesce, eventually resulting in bearing failure. Under fatigue loading, the gradual accumulation and propagation of damage within the material over multiple loading cycles. In progressive failure, the initiation of damage occurs predominantly in the direction of the applied load. In net-tension failure, damage initiation occurs at an angle of approximately

90°, perpendicular to the loading direction. Likewise, in shear-out failure, damage initiation is observed at an angle of approximately 45°. Cyclic loading causes progressive degradation of the GFRP composite, reducing its mechanical properties and resulting in failure. GFRP pin joints often exhibit high-stress concentrations near the hole regions. Under cyclic loading, these stress concentrations can reach critical levels, causing the joint to fail catastrophically with either pure tension or shearing mode as represented in Figure 5.14(b) and (c).

5.3.1 Finite Element Analysis (FEA) of Modified GFRP Composite Pin Joints

Different joint configurations were examined using the finite element method to analyze the fatigue performance of a modified GFRP composite pin joint. A similar pattern has been observed in which the failure mode depends on the E:D and W:D proportions. At lesser E:D and W:D proportions, catastrophic damage mode has been observed, while at higher proportions, the damage mode changes to progressive damage mode. From Figure 5.15, it is evident that for higher W:D and E:D proportions, particularly greater than or equal to 4, the slope of the trendline appears less steep when compared to lower W:D and E:D proportions.
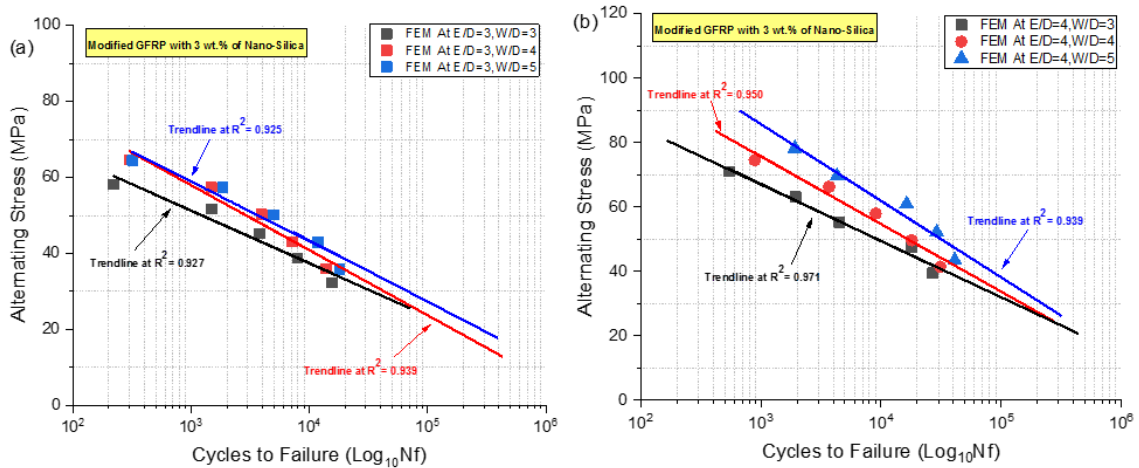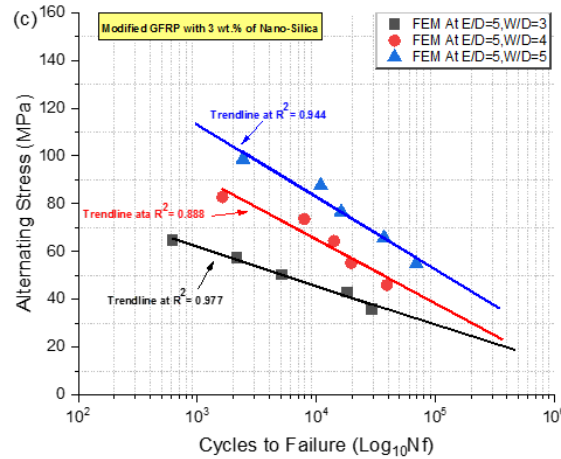
Figure 5.15 SN plot predicted for Modified GFRP using FEA at various pin joint configurations

Conversely, the lower W:D and E:D ratios exhibit a steep slope, indicating a lack of tolerance to withstand fatigue loading. A steep slope signifies poor performance under fatigue loading, whereas a shallow slope indicates good resistance to tolerate fatigue loading. A shallow slope indicates that the material can withstand a higher number of cycles before experiencing failure, especially when subjected to low to moderate stress levels. The behavior of the joint near the hole vicinity is crucial under cyclic loading. During cyclic stress-strain cycles, the absorption of energy by the fiber and matrix near the hole plays a critical role. This energy absorption is responsible for hysteresis loss [83]. As more energy is absorbed, the damage progresses, eventually leading to material failure.

Additionally, the introduction of Nano-silica has shown improvements in both tensile strength and fatigue strength when compared to the Neat GFRP pin joints under the same loading conditions. The inclusion of a suitable amount of Nano-silica particles in the modified GFRP pin joints enhances the interfacial bonding between the fibers and the matrix. This improved bonding is the reason behind the enhancement of fatigue strength in the modified GFRP pin joints. This improved bonding helps in distributing the stress more effectively throughout the material, reducing stress concentration points and preventing crack initiation and propagation during cyclic loading. Table 5.4 represent the various

110

failure modes observed numerically under fatigue loading for Neat and modified GFRP composite pin joints.

Table 5.4 Comparison of numerically observed failure modes under fatigue loading for neat and modified GFRP composite pin joints

Specimen	Neat GFRP	Specimen	Modified GFRP
FPJC1	N	FMPJC1	N
FPJC2	N+S	FMPJC2	N
FPJC3	B+S	FMPJC3	B+S
FPJC4	N+S	FMPJC4	N+S
FPJC5	B+S	FMPJC5	B+S
FPJC6	B	FMPJC6	B
FPJC7	N	FMPJC7	N+S
FPJC8	B	FMPJC8	B
FPJC9	B	FMPJC9	B
N; Net-Tension, S; Sheat-out, B; Bearing			

5.4   Closure

The finite element analysis of Neat GFRP and modified GFRP composite pin joints, considering geometric parameters like E:D and W:D proportions, has yielded valuable insights. The analysis revealed various failure modes in joint configurations subjected to static fatigue loading. In the case of Neat GFRP pin joints, it was observed that a catastrophic failure mode, specifically pure tension and shear damage mode occurred at lower E:D and W:D proportions. In contrast, at higher E:D and W:D proportions, a progressive damage pattern was detected. The behavior of the joint in the vicinity of the hole was found to be crucial when subjected to cyclic loading. In the case of modified GFRP composite pin joints, the incorporation of Nano-silica demonstrated notable improvements in strength. The inclusion of Nano-silica led to improved tensile strength and fatigue strength compared to Neat GFRP pin joints under comparable loading conditions. The finite element analysis yielded valuable insights into the impact of geometric parameters and the influence of Nano-silica on the fatigue behavior of GFRP composite pin joints. At higher W:D and E:D proportions the shallow slope has been

111

observed in modified GFRP pin joints under tension-tension fatigue loading with improved fatigue strength as compared with Neat GFRP pin joints. These findings enhance understanding of the structural behavior and durability of these joints, aiding in the design and optimization of composite structures to enhance reliability and performance. The next chapter focused on conducting experimental analyses of both neat and modified GFRP pin joint configurations under static and fatigue loading conditions. This experimental study aims to complement the results obtained from the FE analysis by providing an understanding of the mechanical behavior and performance of pin joints.

CHAPTER 6 - EXPERIMENTAL ANALYSIS OF PIN JOINTS

The aim of this chapter is to present the experimental analysis conducted on both neat and modified GFRP pin joints subjected to static and fatigue loading. The experimental investigation serves as a complementary study to the previous chapter's finite element analysis, providing valuable insights into the bearing strength and failure modes of pin joints under various joint configurations. The study also investigated how geometric parameters such as E:D and W:D proportions influenced the load-bearing strength and damage modes of pin joints. The study included varying the geometric parameters, namely the E:D ratio and the W/D proportion across a range of values from 3 to 5, respectively.

6.1   Experimental Analysis of Pin Joints under Static Loading

Pin joint samples were fabricated according to the configuration as discussed in the previous chapter illustrated in Figure 3.6. A single hole with a diameter of 4 mm was considered in the plate which was fixed in place using a rigid pin and a fixture was designed for this purpose as shown in Figure 6.1. The joint experienced a tensile load, applied parallel to the plate and symmetrically with respect to the centerline, eliminating any bending moments around the x, y, or z-axis. For the [0°/90°] ply orientations, samples were fabricated with varying E:D and W:D proportions while other geometric parameters thickness 't', length 'L', and diameter 'D' remained unchanged, which are specified in Table 5.1. To obtain the average bearing strength values, each specimen with a specific geometric configuration underwent three tests. The Taguchi method, using the "higher the better" attribute, was utilized to optimize different geometric parameters and assess their influence on the bearing strength of pin joints under static and fatigue loading conditions. This was accomplished using the L9 orthogonal array.
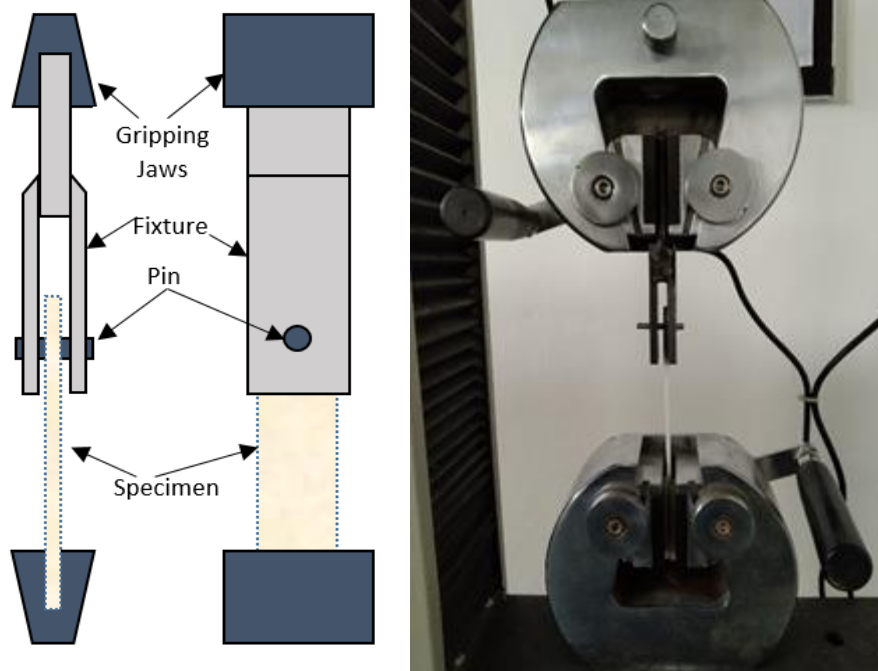
Figure 6.1 Schematic of fixture used for testing pin joints

6.1.1 Experimental Analysis of Neat GFRP Pin Joints

Samples of pin joints were tested to assess their bearing strength and failure modes. The testing specifically focused on neat epoxy glass fiber of stacking sequence $[0°/90°]_{6s}$ ply orientations during the testing. The stress vs. strain plots for various geometric parameters of $[0°/90°]_{6s}$ ply orientation without the addition of Nano-silica is depicted in Figure 6.2. Pin joint failure is typically classified into three main modes: pure tension, shear, and bearing damage mode. Pure tension and shear damage modes occur suddenly and are caused by excessive tensile and shear stresses, respectively, without any prior indication or warning. In contrast, progressive damage mode develops in the material surrounding the contact area between the pin and the laminate as a result of compressive stresses exerted on the hole surface. Bearing failure is desirable due to its higher strength contribution. To prevent other failure modes, it is crucial to implement proper joint geometry design and carefully select the composite material. Optimal proportions of W:D and E:D proportions are essential in order to prevent immediate joint failure. Analyzing the stress vs. strain graphs of the specimens can help easily to identify the primary modes of failure.
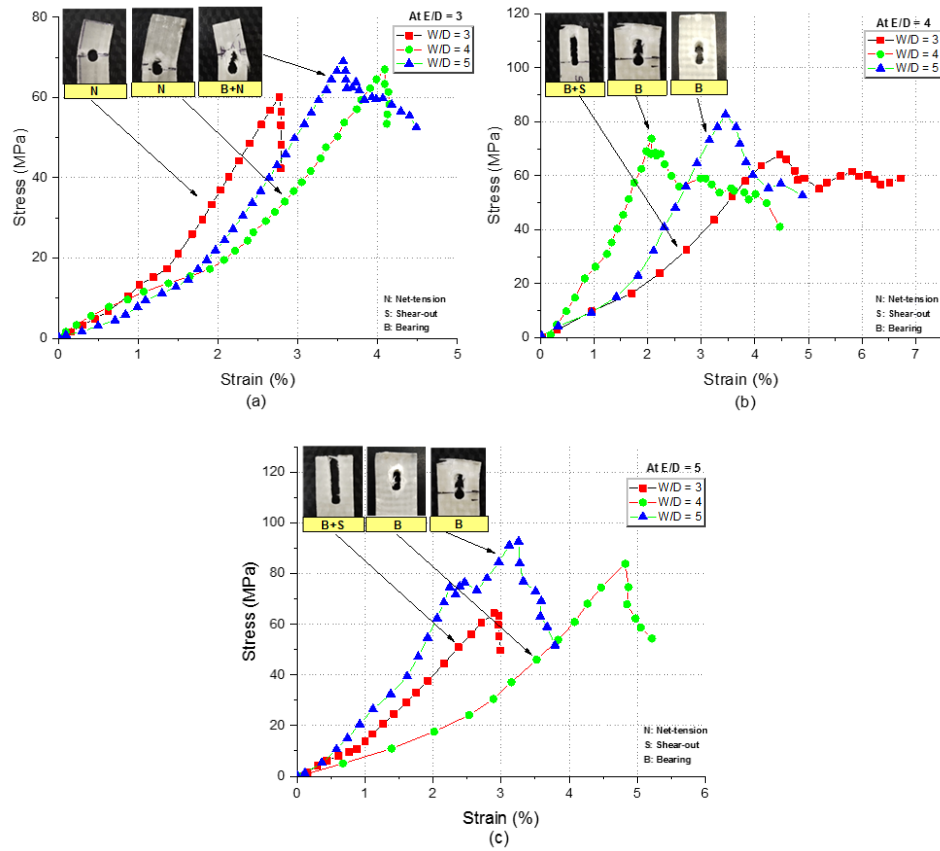
Figure 6.2 Stress-Strain curves of Neat GFRP pin joints where W:D proportion varies from 3 to 5 (a) At E:D=3 (b) At E:D=4, and (c) E:D=5

Figures 6.2 and 6.3 show that a low W:D proportion, particularly at 3, leads to a sudden failure after certain peak points, indicating failure resulting from net tension or shearing. A sudden drop in the curve after a peak point indicates a net tension failure mode. On the contrary, if the curve experiences a sudden decrease after several peak points, it suggests a shear damage mode. The width of the specimen directly influences the net tension failure mode. For W:D proportions of 4 and 5, the values exhibit a partial decrease after the peak point and then progress with a zigzag pattern.
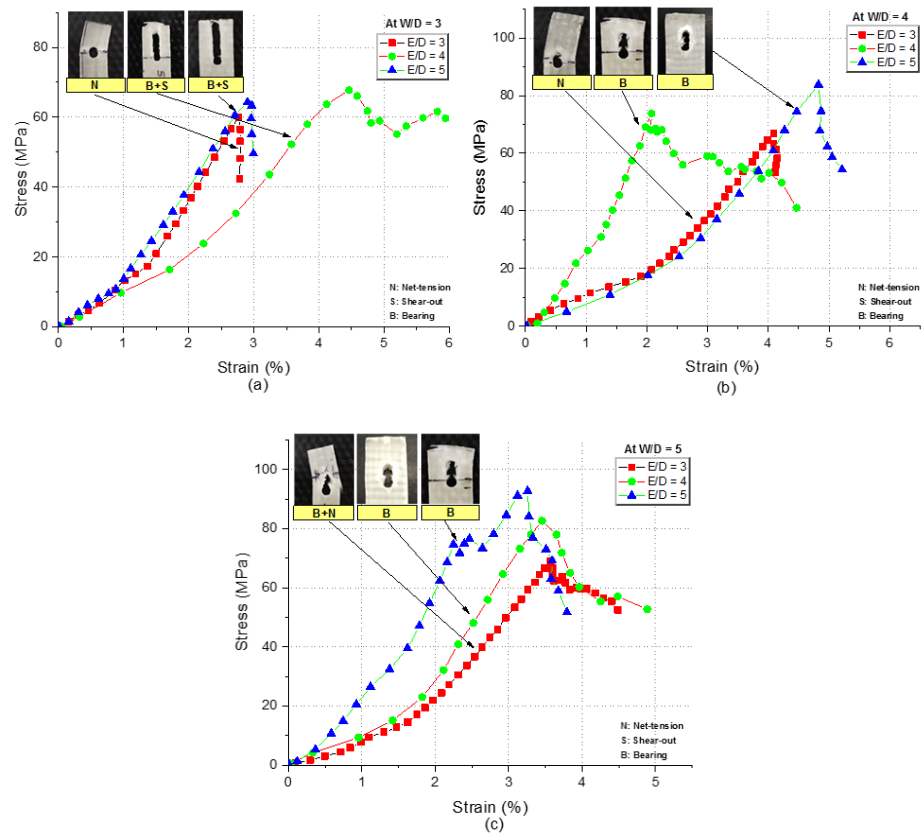
Figure 6.3 Stress-Strain curves of Neat GFRP pin joints where E:D proportion varies from 3 to 5 (a) At W:D=3 (b) At W:D=4, and (c) W:D=5

These factors, including matrix fracture, delamination between laminates, fiber breakages, fiber-matrix interface deformation, and others, could contribute to bearing damage mode. Bearing damage mode was observed when W:D and E:D proportions are 4 or higher, regardless of ply orientations. Pure tension and shear damage modes occur with small W:D and E:D proportions. Choosing the appropriate W:D and E:D proportions is crucial to prevent immediate failure in pin joints. Figures 6.2 and 6.3 demonstrate that the bearing damage mode was observed when W:D and E:D proportions were 4 or higher, respectively.

6.1.2 Experimental Analysis of Modified GFRP Pin Joints

Chapter 4 presents evidence that the inclusion of Nano-silica in glass epoxy composites improves their mechanical properties. The mechanical properties increased as the percentage of Nano-silica by weight increased, reaching a maximum of 3 wt. %. Therefore,

to prepare the pin joints, glass epoxy laminates with 3 wt. % of Nano-silica were utilized. The outcomes of these experiments are shown in Figures 6.4 and 6.5, respectively. Composite pin joints exhibit failure tendencies at low E:D and W:D proportions, primarily due to stress concentrations at the joint edge. With smaller E:D and W:D proportions, the contact area between the joint and the composite laminate become reduced, leading to a concentration of the applied load in a smaller region. The higher stress levels generated can surpass the strength of the composite material, causing the failure of joints. Specifically, low W:D proportion of 3 resulted in net tension and shear damage along with bearing damage mode. Additionally, at low E:D proportions exhibited a combined failure mode of bearing and shear-out.
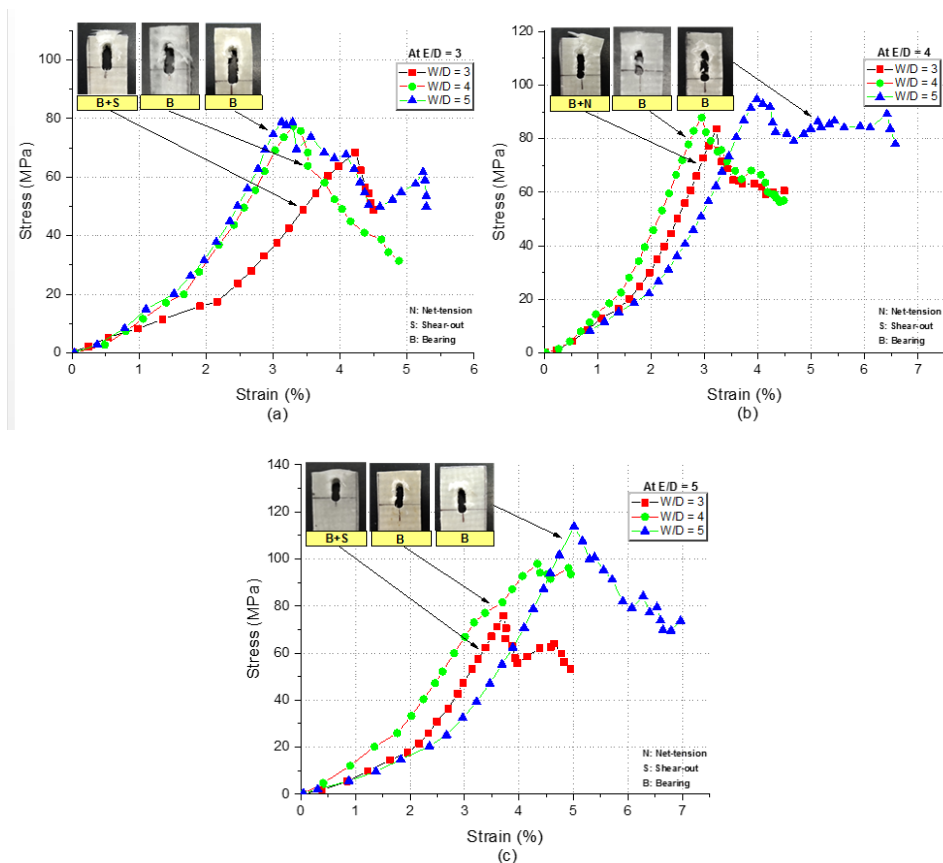
Figure 6.4 Stress-Strain curves of Modified GFRP pin joints: W:D varies 3 to 5 (a) At E:D=3 (b) At E:D=4, and (c) E:D=5

117

The zigzag curve observed in the stress-strain diagram for Neat and modified GFRP pin joints during tensile testing. The zigzag pattern observed in the results may be attributed to the interaction between the fibers and the matrix at the fiber-matrix interface. Under tensile stress, there is a gradual debonding or slippage of the fibers within the matrix, facilitating stress transfer and redistribution. This interfacial behavior can cause fluctuations in the stress-strain curve, resulting in the observed zigzag pattern. As well as pin joints exhibit progressive damage accumulation under tensile loading. As the material undergoes deformation, micro-cracks, and fiber breakage can occur. These localized damage events can cause fluctuations in the stress-strain response.
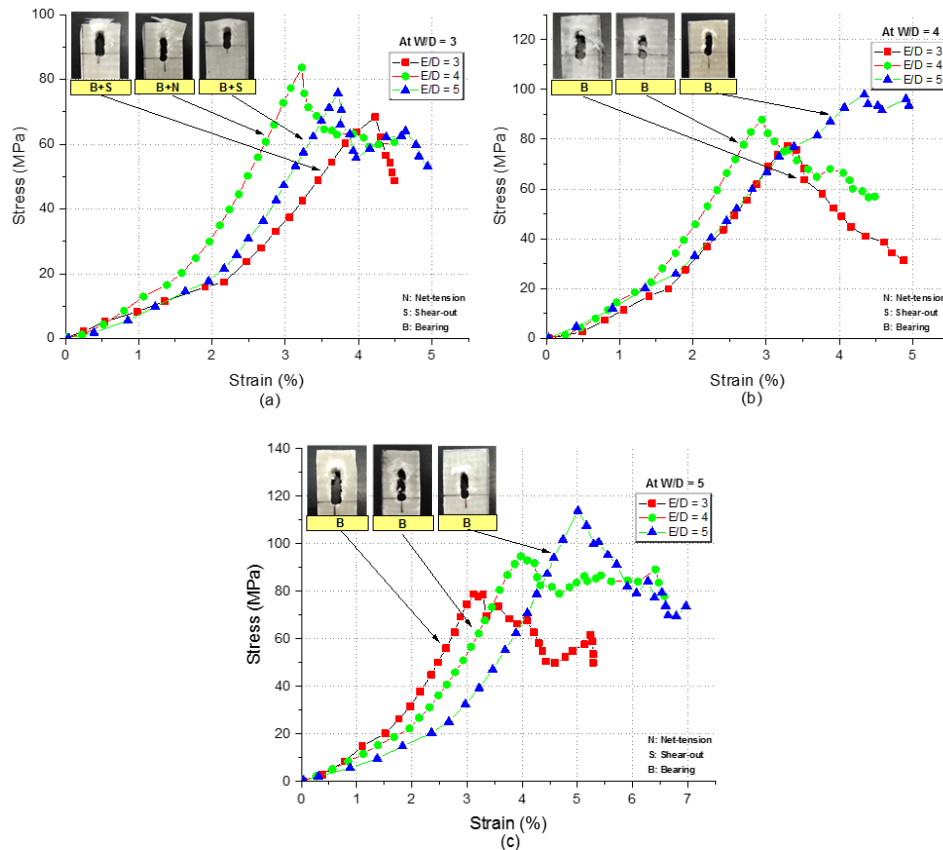
Figure 6.5 Stress-Strain curves of Modified GFRP pin joints: E:D varies 3 to 5(a) At W:D=3 (b) At W:D=4, and (c) W:D=5

In Table 6.1, the average bearing strength for neat and modified GFRP with 3 wt. % Nano-silica is presented for different pin joint configurations along with their corresponding failure modes observed experimentally.

Table 6.1 Average bearing strength for GFRP with 3 wt. % Nano-silica composite pin joints at different joint configurations.

Specimen No.	E:D	W:D	Avg. Bearing Strength Neat GFRP (MPa)	Failure Modes	Avg. Bearing Strength Modified GFRP (MPa)	Failure Modes
PJC1	3	3	60.01	N	68.91	B+S
PJC2	3	4	66.82	N	77.40	B
PJC3	3	5	66.22	B+N	78.96	B
PJC4	4	3	67.50	B+S	83.77	B+N
PJC5	4	4	73.39	B	88.06	B
PJC6	4	5	81.46	B	94.32	B
PJC7	5	3	64.16	B+S	75.88	B+S
PJC8	5	4	82.62	B	97.75	B
PJC9	5	5	92.64	B	113.16	B
N; Net-Tension, S; Sheat-out, B; Bearing						

To prevent immediate failure in composite pin joints, it is essential to carefully select optimal W:D and E:D ratios. Figures 6.4 and 6.5 demonstrate that modified GFRP pin joints often experience failure characterized by bearing combined with net tension or shearing at a low W:D ratio, such as 3. Conversely, a bearing failure mode is observed when W:D $\geq$ 4 and E:D $\geq$ 4, and this damage pattern has been consistently reported by numerous researchers [17], [29], [31], [40]. ANOVA has been applied to study the bearing strength of both neat and modified GFRP composite pin joints under static loading. The objective is to identify the significant geometric parameter and their contributions to the bearing strength of the pin joint. Table 6.2 demonstrates the analysis of variance for neat and modified GFRP pin joints.

Table 6.2 Analysis of Variance for Neat & Modified GFRC pin joints

Neat GFRP Pin Joints						
Source	DF	Adj SS	Adj MS	F value	P value	Contribution (%)
E:D	2	360.77	180.385	12.16967	0.01992	39.61
W:D	2	490.74	245.37	16.55389	0.01162	53.88
Error	4	59.29	14.8225			6.51
Total	8	910.8				100
Modified GFRP Pin Joints						
Source	DF	Adj SS	Adj MS	F value	P value	Contribution (%)
E:D	2	541.03	270.515	18.2503	0.00975	36.80
W:D	2	859.47	429.735	28.99207	0.00416	58.46
Error	4	69.7	17.425			4.74
Total	8	1470.2				100

As W:D is a more signification parameter as compared to the E:D ratio with 53.88% and 58.46% contribution respectively for neat and modified GFRP pin joints. The width of the joint contact area (W) is directly related to the amount of material in contact with the pin. A larger width means a larger contact area, which can distribute the applied load over a larger surface area, potentially reducing stress concentrations. As well as a larger width can contribute to higher shear resistance, which is crucial in resisting transverse forces. Figures 6.6 and 6.7 exhibit that the bearing strength of modified GFRP pin joints with 3 wt. % of Nano-silica is higher compared to that of neat GFRP pin joints, considering the corresponding ply orientations. This is attributed to the enhanced interfacial bonding facilitated by the Nano-silica between the fiber and the polymer.
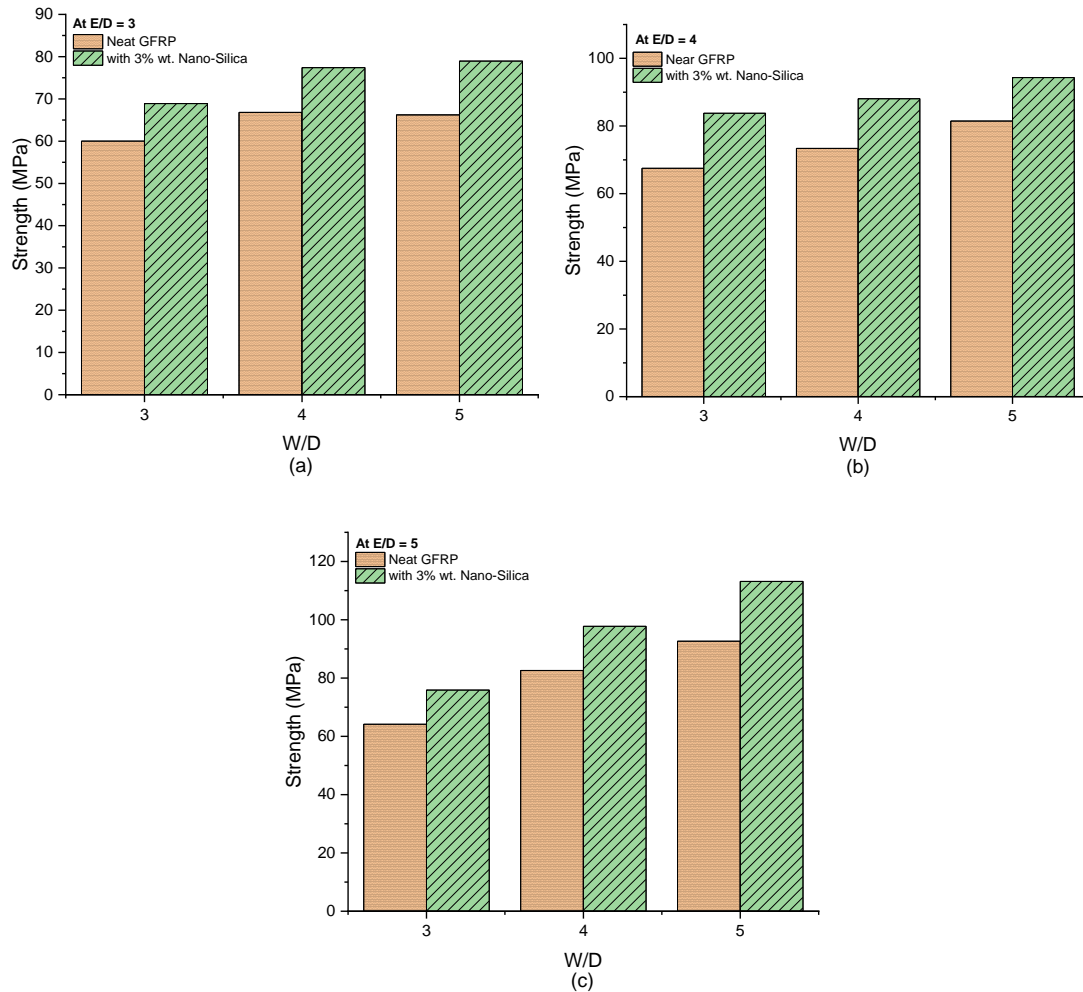
Figure 6.6 Bearing strength of Neat and Modified GFRP pin joints samples at different E:D ratios: (a) W:D=3, (b) W:D=4, and (c) W:D=5

The inclusion of Nanoparticles undeniably improves the mechanical properties of the composite. But the identification of the appropriate amount of Nano-particle to be added to make Nano-composite plays a critical role. SEM investigation conducted in the previous chapter confirmed that the Nano-silica particles are uniformly dispersed, resulting in a strong interfacial bond with the epoxy resin.
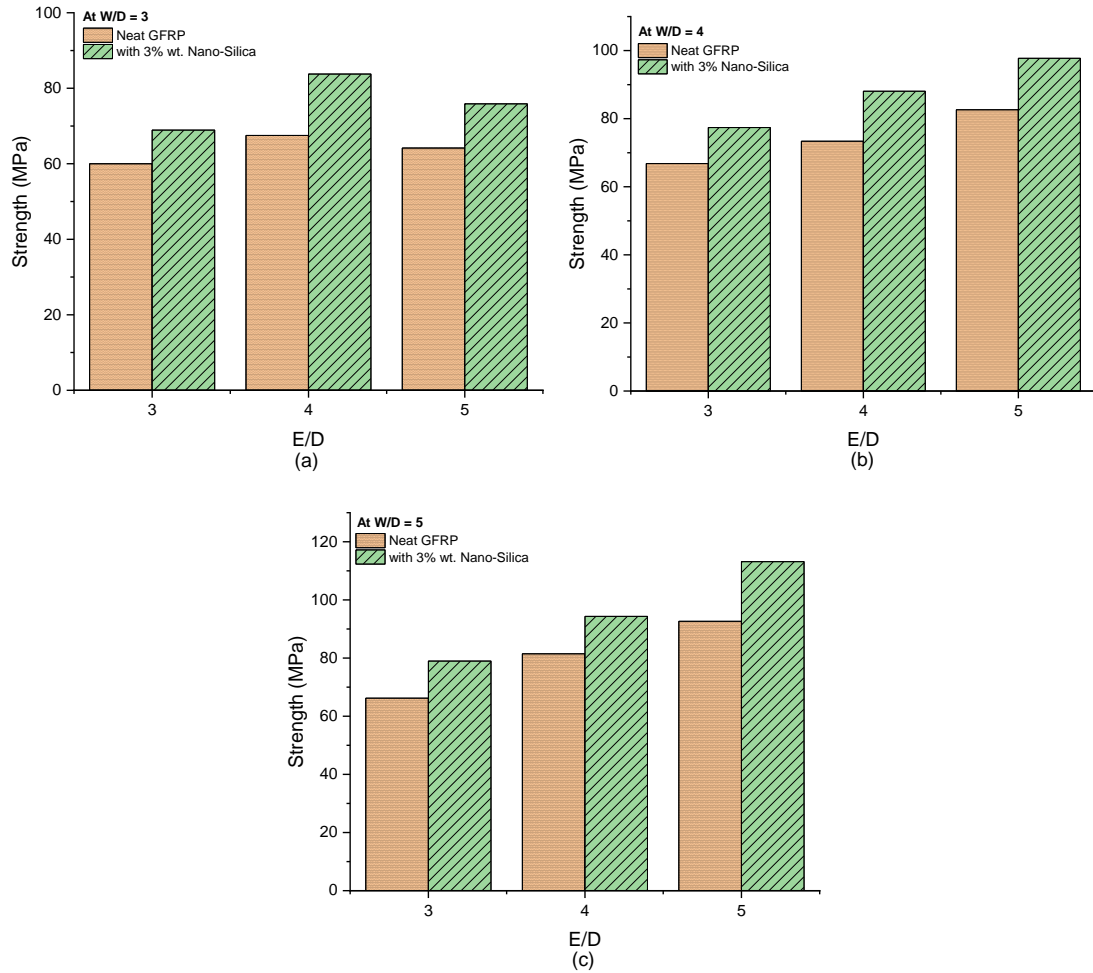
Figure 6.7 Bearing strength of Neat and Modified GFRP pin joints samples at different W:D ratios: (a) E:D=3, (b) E:D=4, and (c) E:D=5

The following section aims to expand the application of mechanical joints by investigating the impact of fatigue loading on pin joints for Neat and Modified GFRP. The analysis will focus on behavior and damage patterns in the pin joint under fatigue loading conditions.

6.2   Experimental Analysis of Pin Joints under Fatigue Loading

Furthermore, experimental tests were performed on pin joint specimens to assess the fatigue behavior of the FRP pin joints under a tension-tension loading scheme. Table 6.3 presents a summary of the average bearing strength for each joint configuration, both with and without the inclusion of Nano-silica, along with their respective standard deviations.

Table 6.3 Summary of mean strength and standard deviation for various pin joint configurations

Joint Configuration	Mean Bearing Strength & Standard Deviation (MPa)	
	Neat GFRP	With 3 wt.% of Nano-silica
FPJC1	60.01 ± 3.67	68.91 ± 4.27
FPJC1	66.82 ± 5.09	77.4 ± 5.60
FPJC3	66.22 ± 6.76	78.96 ± 7.33
FPJC4	67.50 ± 6.45	83.77 ± 4.88
FPJC5	73.39 ± 2.92	88.06 ± 5.24
FPJC6	81.46 ± 6.31	94.32 ± 7.36
FPJC7	64.16 ± 6.45	75.88 ± 4.08
FPJC8	82.62 ± 2.91	97.75 ± 5.77
FPJC9	92.64 ± 3.77	113.16 ± 3.60

.

To evaluate the behavior of pin joints when subjected to fatigue loading, experimental testing was conducted using the Effective Failure Strength (EFS). To calculate the EFS, from the quasi-static tension tests mean failure load was subtracted by the standard deviation. Eq (6.1) shows the expression used to determine effective failure strength for fatigue testing.

$$EFS = Mean\ Failure\ Strength - Standard\ Deviation \qquad (6.1)$$

The specimens were subjected to fatigue testing at five distinct stress levels: 50%, 60%, 70%, 80%, and 90% of the EFS value. Subsequently, the S-N curve was constructed utilizing the curve fitting method. Figure 6.8 depicts a schematic representation of a Dynamic Universal Testing Machine (UTM) along with the fixture setup designed for conducting fatigue tests on different configurations of FRP pin joints. The main focus of this research is to analyze the impact of fatigue loading on different configurations of pin joints. The previous section discussed the static ultimate bearing strength, which serves as a reference for selecting stress amplitudes. It is widely recognized that when subjected to repeated loading, the majority of materials, including fiber-reinforced composites, experience a decrease in strength [83].
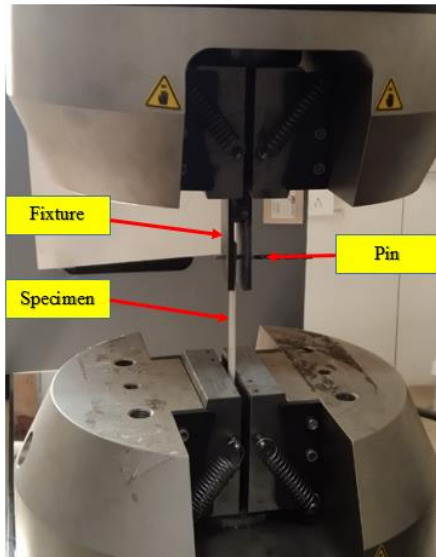
Figure 6.8 Schematic of Dynamic UTM with fixture setup for fatigue test on various pin joints configuration

6.2.1 Fatigue Analysis of Neat GFRP Pin Joints

In the design of pin joint composite structures, it is necessary to incorporate areas with holes, notches, and other types of discontinuities that facilitate the initiation and propagation of cracks. Table 6.4 represents the various stress levels at different pin joint configurations considered for fatigue testing based on Effective failure Strength (EFS). The remaining parameters have been taken the same *i.e.* R =0.1, f = 2 Hz, and the test was conducted at room temperature. The collected data on the number of experimental cycles until failure (N_f) at various stress levels were utilized to analyze the 90% survival life using a two-parameter based Weibull distribution. It helps to predict the fatigue life of joints with various configurations. This distribution has allowed for the prediction of the cycles until failure at different stress levels with a 90% reliability. The Weibull distribution trend line was plotted at a 90% reliability level to extend the SN curve, allowing for the estimation of the fatigue life of joints exposed to tension-tension (T-T) loading at a 2 Hz frequency. Figure 6.9 demonstrates the predicted fatigue life using Weibull along with the experimental data recorded at various stress levels and corresponding damage modes observed under cyclic loading

124

Table 6.4 Various Stress levels based on EFS for fatigue testing of neat GFRP pin joints configuration.

Joint Configuration	EFS (MPa)	50% of EFS (MPa)	60% of EFS (MPa)	70% of EFS (MPa)	80% of EFS (MPa)	90% of EFS (MPa)
FPJC1	56.34	28.17	33.80	39.44	45.07	50.70
FPJC1	61.73	30.86	37.04	43.21	49.38	55.55
FPJC3	59.46	29.73	35.68	41.62	47.56	53.51
FPJC4	61.05	30.52	36.63	42.73	48.84	54.94
FPJC5	70.47	35.23	42.28	49.33	56.37	63.42
FPJC6	75.16	37.58	45.09	52.61	60.13	67.64
FPJC7	57.71	28.85	34.63	40.40	46.17	51.94
FPJC8	79.71	39.85	47.83	55.79	63.76	71.74
FPJC9	88.87	44.43	53.32	62.21	71.09	79.98
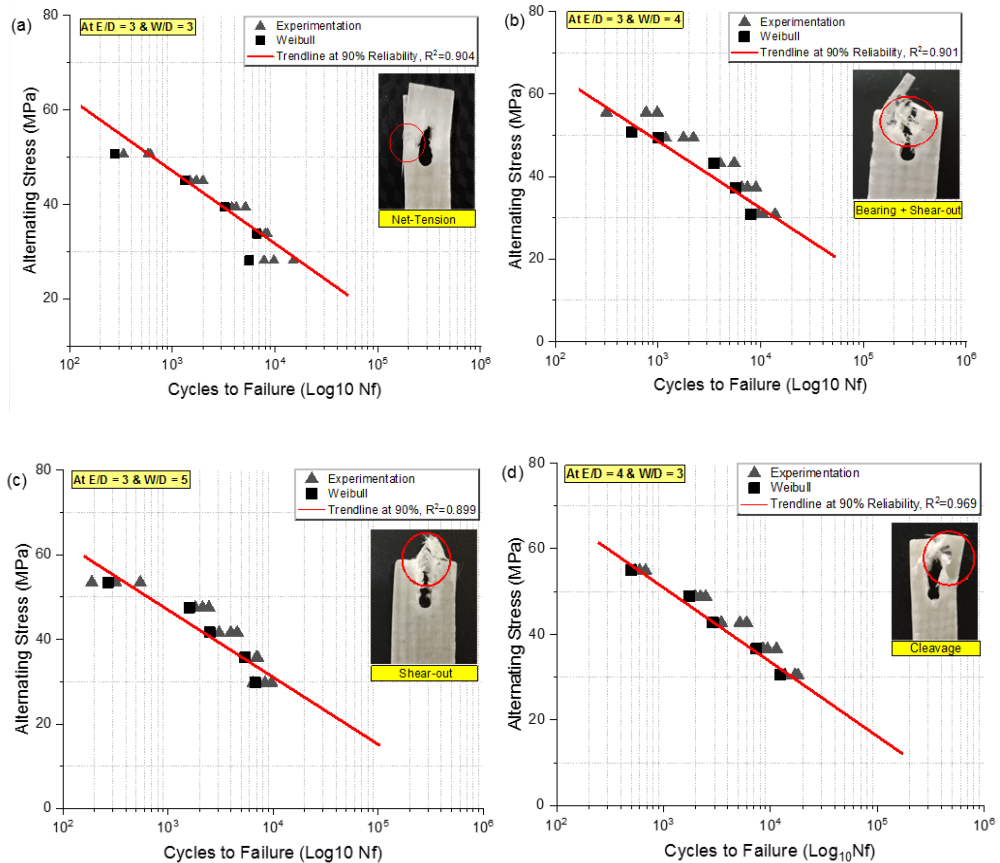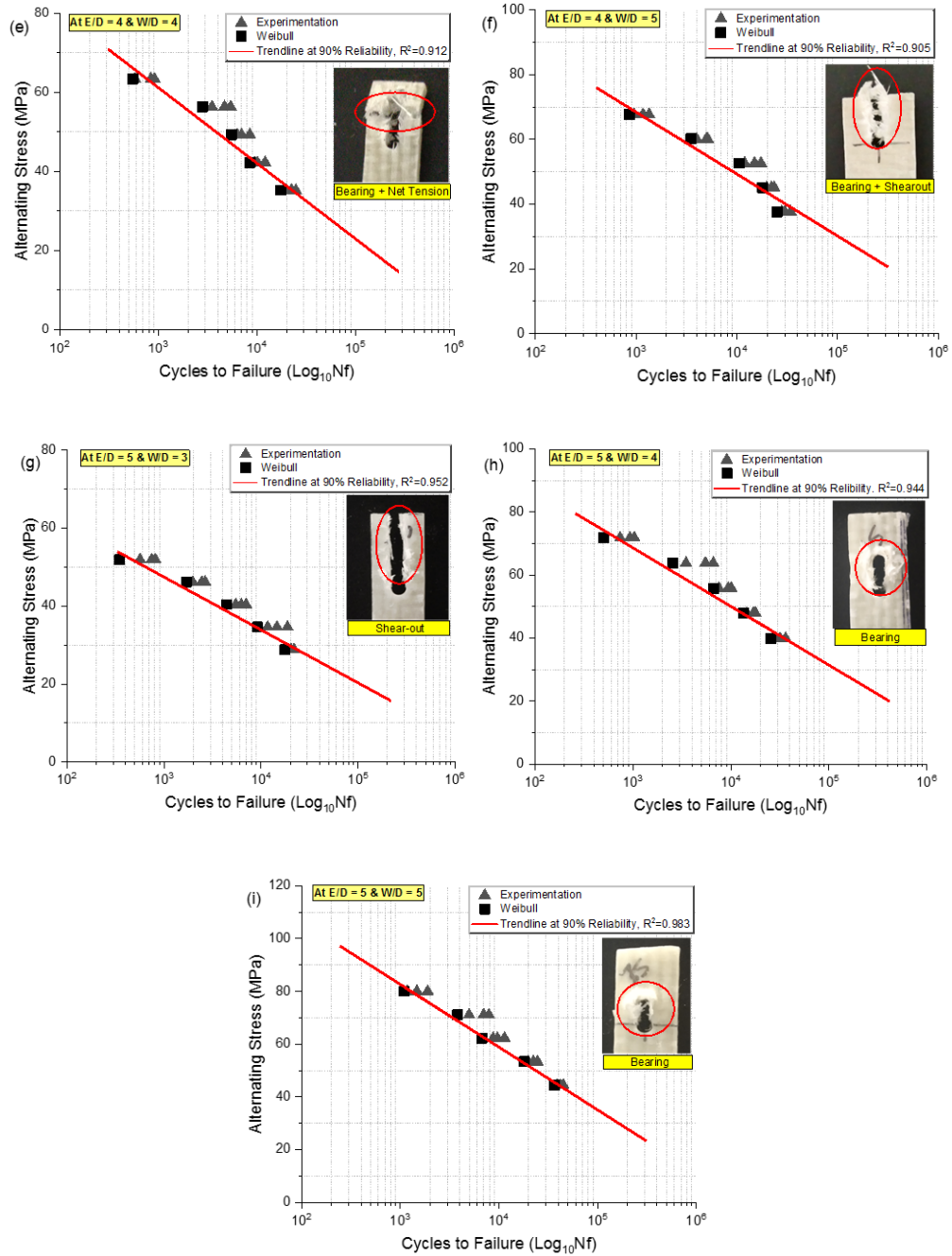
Figure 6.9 S N plot at various Neat GFRP pin joint configurations with the corresponding failure modes observed

It has been observed that Figure 6.10 at lower E:D and W:D proportion under cyclic loading *i.e.* catastrophic failure modes has been observed which fail the specimen without

intimating prior notice. As the E:D and W:D proportion equals or greater than 4. The mode of failure changed from catastrophic to progressive failure mode which is highlighted with the red circle in Figure 6.9.
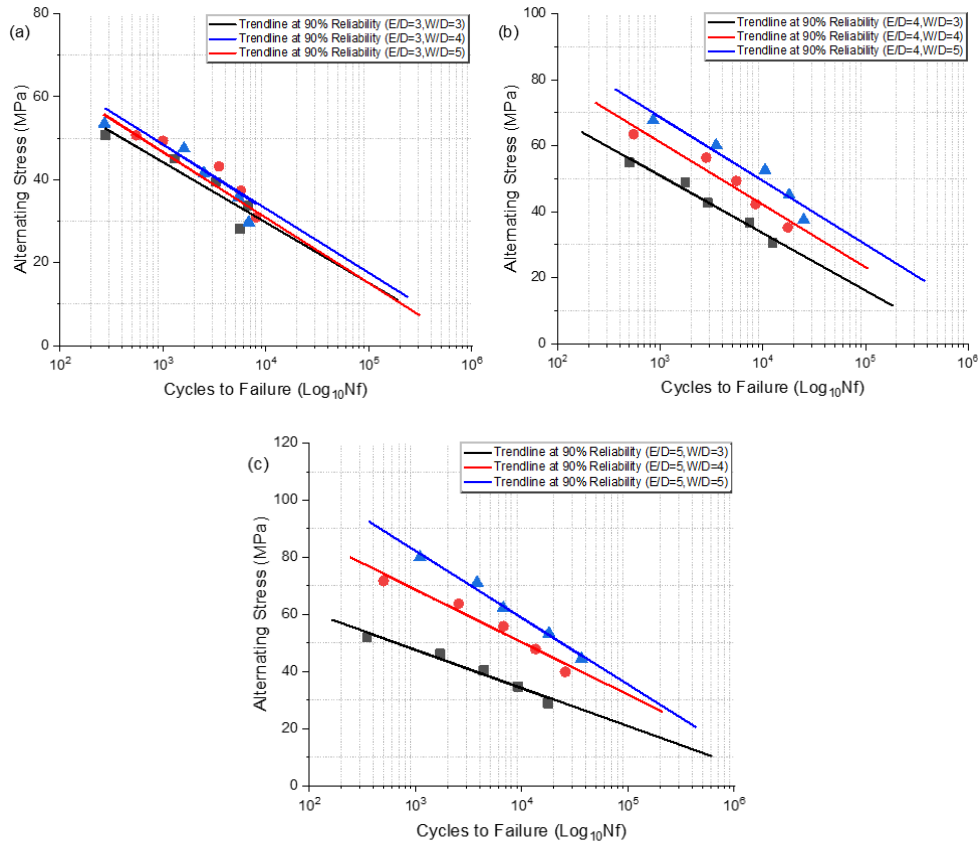
Figure 6.10 SN curve at 90% reliability for Neat GFRP pin joint configurations (a) At E:D=3, (b) At E:D=4, and (c) At E:D=5

Through the static analysis of pin joints with various configurations, it has been observed that the W:D proportion has a more pronounced influence on achieving higher bearing strength, as compared to the E:D proportion. In the fatigue analysis of pin joints exposed to cyclic loading, a similar trend is observed where the E:D proportion has less influence, while the W:D proportion remains more significant. The observation depicted in Figure 6.10 indicates that when the E:D and W:D ratios are 4 or higher (E:D & W:D ≥ 4), the SN curve exhibits a shallow slope, indicating a progressive failure mode. In contrast, at lower E:D and W:D ratios, the SN curve under cyclic loading displays a steeper slope, suggesting

a greater probability of catastrophic failure for the same configuration. If the net tension failure mode predominates, fiber pull-out may be observed as the primary failure mechanism. The cyclic tensile stresses can cause the individual fibers to gradually separate from the matrix, resulting in reduced load-bearing capability. In cases where the shear stresses are extremely high or concentrated in localized regions near the hole vicinity, fiber breakage may occur in addition to or instead of fiber pull-out. The cyclic shear stresses can cause the fibers to fracture due to a reduction in fiber strength due to shearing. Bearing failure primarily involves the compressive loading of the laminate. While fiber pull-out may not be as prevalent in this failure mode, fiber breakage can occur due to the compressive stresses acting on the fibers.

During fatigue tests of glass fiber epoxy composite pin joints, local hysteresis data were collected at regular intervals. The changes observed in the hysteresis curves can be attributed to two factors: effects of creep and damage of material. Creep, arising from either viscoelastic or viscoplastic effects, causes the hysteresis curve to horizontally shift towards higher strains while retaining the same slope. In contrast, damage of material results in a reduction in the slope of the hysteresis curve [204]. To assess the failure behavior of the pin joints, hysteresis curves were recorded at the first and penultimate cycle as shown in Figure 6.11. The hysteresis curves of the specimens showed a decreasing slope and a rightward shift, indicating damage progression and the presence of creep effects in the fiber-reinforced polymer composite. The hysteresis curves exhibited a considerable decrease in slope and a horizontal shift, indicating the initiation and propagation of damage in the composite pin joints. The reduction in dynamic stiffness can be attributed to this damage. One possible explanation for the horizontal shifts in the hysteresis curves at various stress levels is the combination of plastic deformation at the hole region and creep of the polymer resin in GFRP pin joint specimens. Hysteresis plot at W:D and E:D equals 5 as shown in Figure 6.11(a) to (e). The hysteresis curves obtained during the final cycles. The figures clearly indicate that polymer composites undergo progressive damage. The pin joints specimen exhibits increased hysteresis prior to the final fracture. This increase in

hysteresis can be attributed to a series of damages, such as fiber-matrix interactions and other factors.
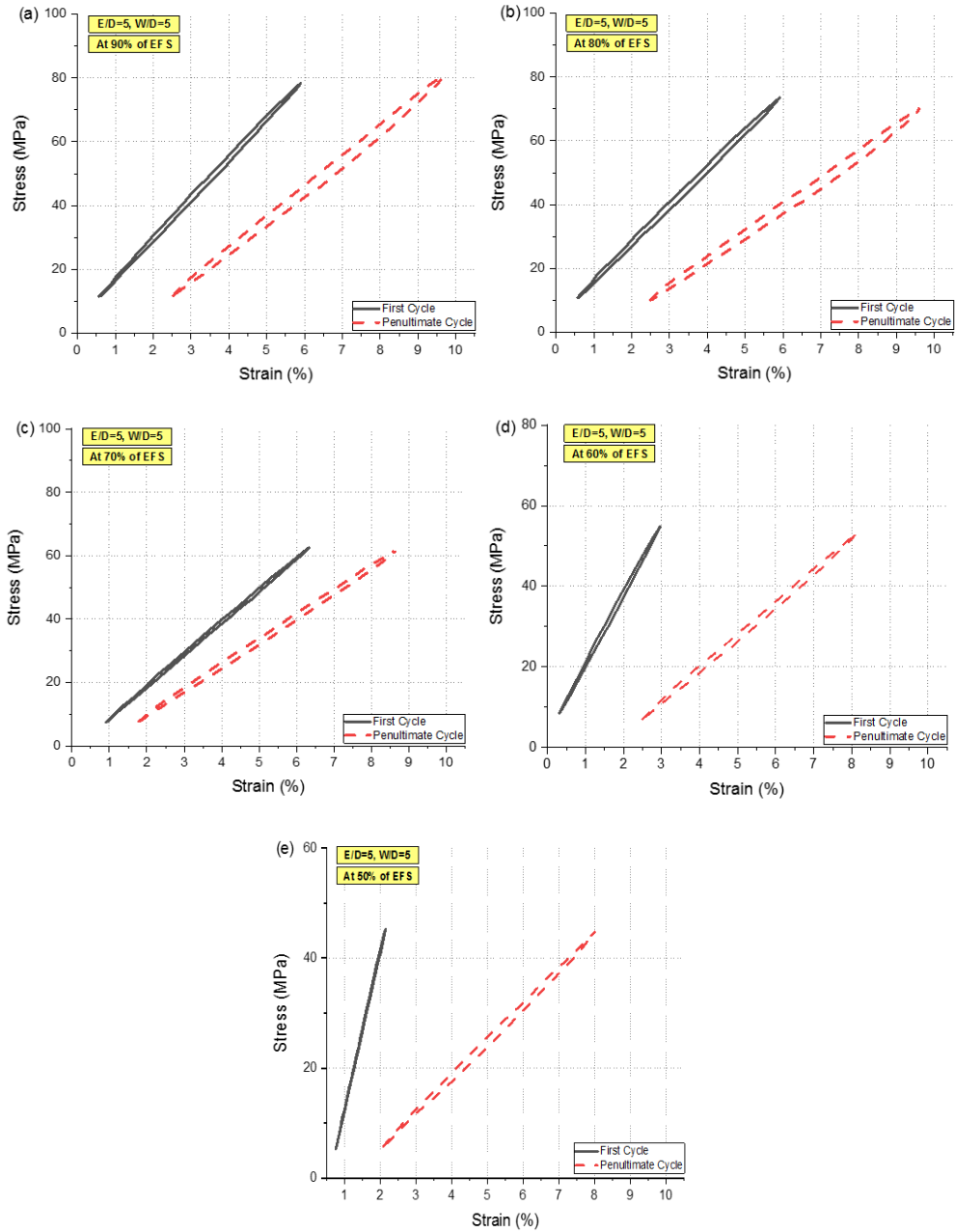
Figure 6.11 Hysteresis curve for Neat GFRP pin joint at E:D and W:D equals 5 at various stress levels (a) At 90% (b) At 80% (c) At 70% (d) At 60% (e) At 50% of EFS

Observing Figure 6.11 (a) to (e) during the initial cycle, it is evident that as the stress levels increase, there is a gradual reduction in the slope of the stress-strain loop. This decline in slope is linked to an accelerated propagation of fiber-matrix damage, caused by higher cyclic stress compared to lower cyclic stress.

6.2.2 Fatigue Analysis of Modified GFRP Pin Joints

Similarly, fatigue analysis was conducted on modified GFRP specimens with 3 wt. % of Nano-silica particles to assess their impact on GFRP composite pin joints. The experiments investigated the impact of Nano-silica particles on the bearing strength and failure behavior of pin joints with various configurations. Table 6.5 represents the various stress levels at each pin joint configuration considered for fatigue testing based on Effective failure Strength (EFS). The test has been conducted with the same environmental condition.

Table 6.5 Various stress levels based on effective failure strength (EFS) for fatigue testing of modified GFRP pin joint configurations.

Joint Configuration	EFS (MPa)	50% of EFS (MPa)	60% of EFS (MPa)	70% of EFS (MPa)	80% of EFS (MPa)	90% of EFS (MPa)
FMPJC1	64.64	32.32	38.784	45.248	51.712	58.176
FMPJC2	71.8	35.9	43.08	50.26	57.44	64.62
FMPJC3	71.63	35.815	42.978	50.141	57.304	64.467
FMPJC4	78.89	39.445	47.334	55.223	63.112	71.001
FMPJC5	82.82	41.41	49.692	57.974	66.256	74.538
FMPJC6	86.96	43.48	52.176	60.872	69.568	78.264
FMPJC7	71.8	35.9	43.08	50.26	57.44	64.62
FMPJC8	91.98	45.99	55.188	64.386	73.584	82.782
FMPJC9	109.56	54.78	65.736	76.692	87.648	98.604

Similarly, the fatigue behavior of each pin joint configuration has been analyzed using a similar methodology. Survival life predictions have been made using two parameters based on Weibull distribution with a 90% reliability level. At lower E/D ratios, a catastrophic failure mode has been observed, which is consistent with the findings in neat GFRP pin joints. In contrast, higher W/D ratios of 4 or greater have shown significantly improved

fatigue strength, as depicted in Figure 6.12 with the red circle, indicating a progressive damage mode. Notably, the modified GFRP pin joints exhibited enhanced fatigue strength compared to the neat GFRP pin joints under fatigue loading for each joint configuration. The infusion of Nano-silica particles with glass epoxy which are generally surface-treated can form chemical bonds with the matrix material in the composite. Chemical interactions, such as covalent or hydrogen bonding, facilitate a robust interface between the Nano-silica particles and the matrix, resulting in enhanced overall strength [205]. As well as due to the small size and high surface area, Nano-silica can physically interlock with the glass fiber and epoxy matrix to form mechanical bonds. This interlocking mechanism enhances the load transfer across the interface and improved the fatigue strength of the composite.
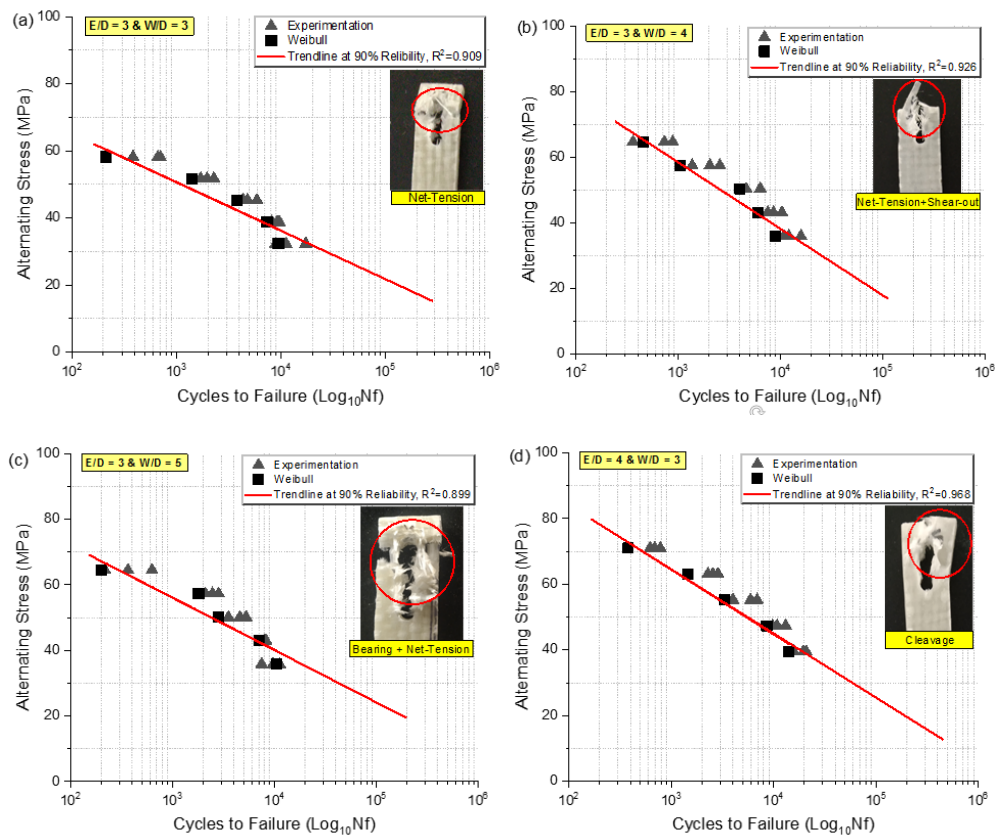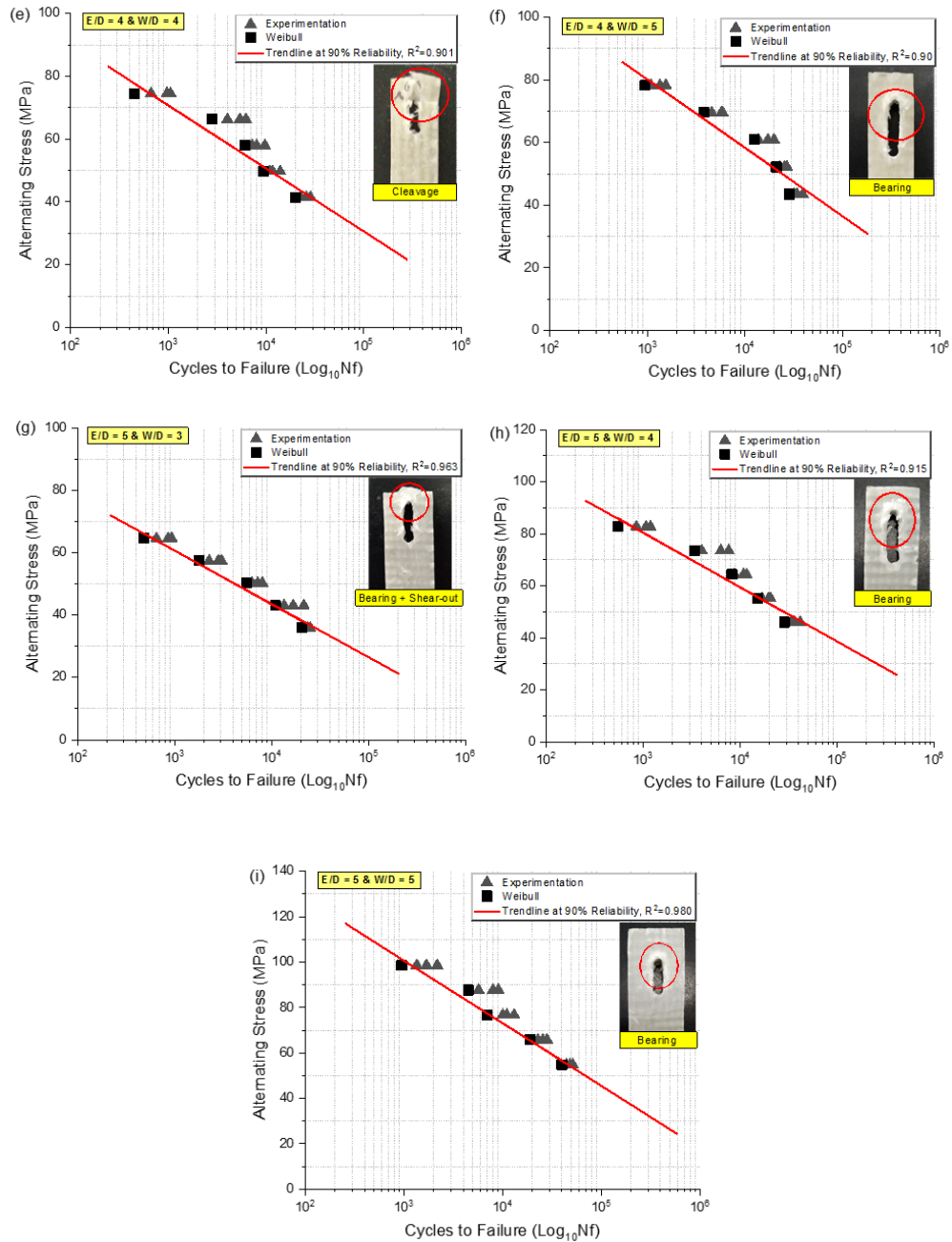
Figure 6.12 S N plot at various modified GFRP with 3 wt. % of Nano-silica pin joint configurations with the corresponding failure modes observed

The comparison between different pin joints, ranging from a W:D proportion of 3 to 5, while keeping the E:D proportion constant, is illustrated in Figure 6.13 (a) to (c). It can be observed from Figure 6.13(a) that at E:D proportion kept 3 and the W:D proportions varied

from 3 to 5, the slope remains quite similar. Consequently, the damage mode is also found to be catastrophic, involving pure tension, shear damage mode, or a combination of both. When the E:D ratio increases to 5 and the W:D ratio increases to 4, the slope of the curve becomes shallower, indicating a longer fatigue life compared to other geometric parameters as shown in Figure 6.13 (c).
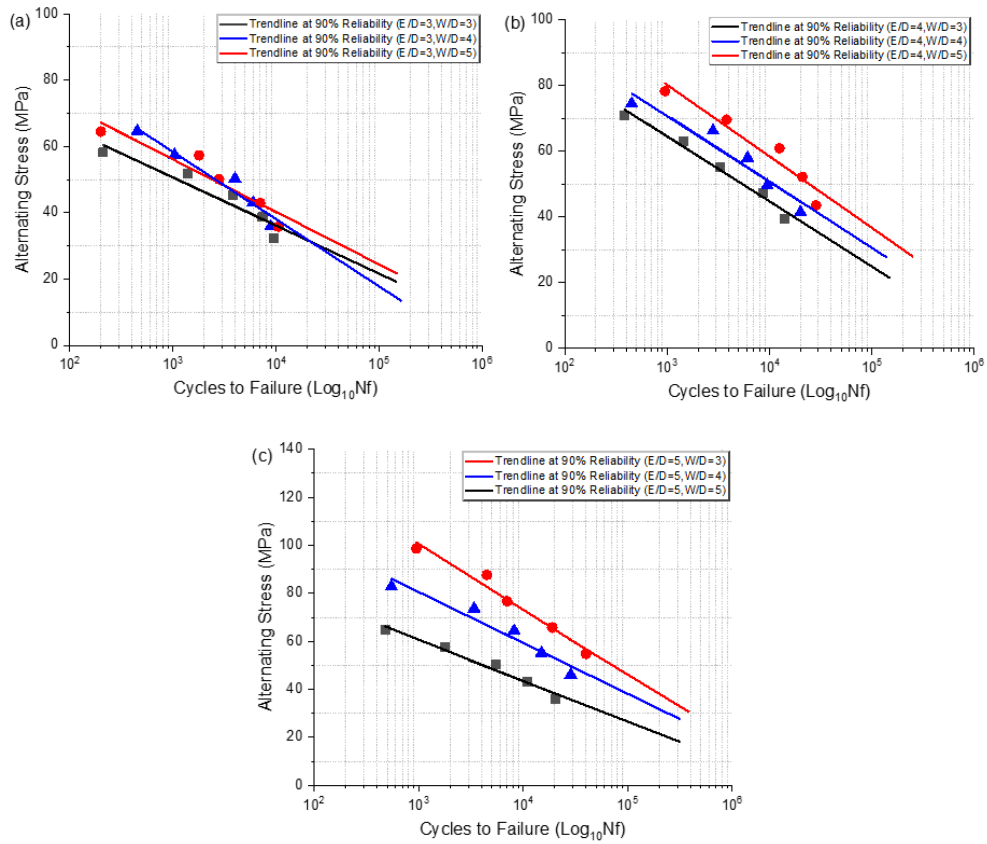
Figure 6.13 S N curve at 90% reliability for Modified GFRP pin joint configurations (a) At E:D=3, (b) At E:D=4, and (c) At E:D=5

For each stress level, hysteresis loops were plotted at E:D = 5 and W:D = 4 to analyze progressive damage and damage initiation under cyclic loading. Comparisons were made using the hysteresis loops from the first and penultimate cycles. It was observed that as the stress level increased, a declining slope was observed shifted towards the rightwards in the graph, as depicted in Figure 6.14 (a) to (e).
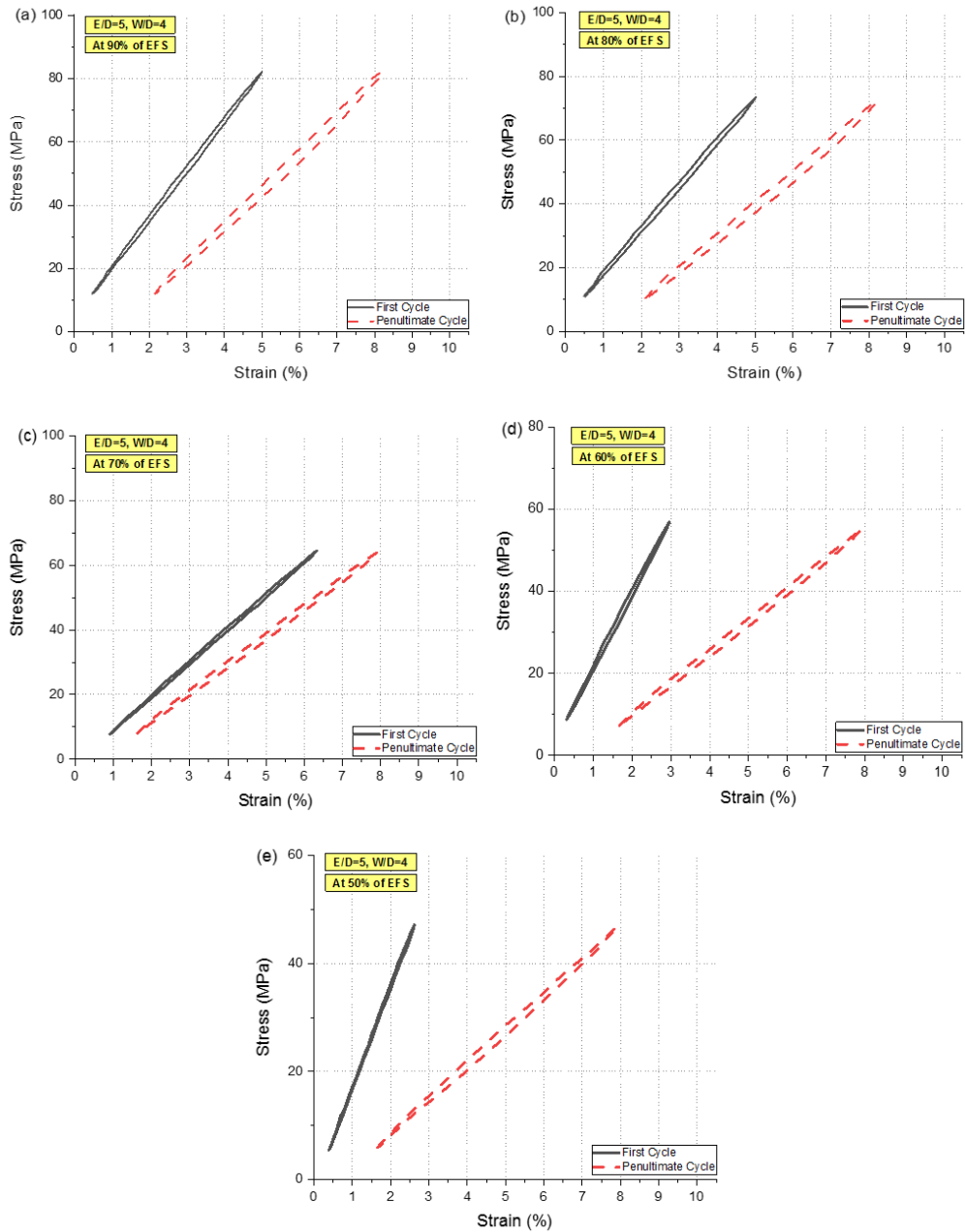
Figure 6.14 Hysteresis curve for Modified GFRP pin joint with 3 wt.% of Nano-silica at E:D=5 and W:D=4 at various stress levels (a) At 90% (b) At 80% (c) At 70% (d) At 60% (e) At 50% of EFS

With an increase in stress level, the initiation of fiber-matrix debonding occurs gradually. Nonetheless, the presence of Nano-silica plays a critical role in interlocking the cracks. Moreover, Nano-silica contributes to the enhancement of interface toughening mechanisms

and acts as a crack arrester, effectively impeding crack propagation and improving the overall fracture toughness of the composite material [164]. This interlocking effect restricts the expansion of progressive damage, leading to extended fatigue life of the joint when compared to the neat GFRP pin joint. Additionally, it was noted that modified GFRP composite pin joints exhibited a smaller hysteresis loop area compared to neat GFRP pin joints with the same joint configuration. The improved fatigue strength observed can be attributed to the inclusion of Nano-silica in the composite material. Nano-silica enhances the fiber-matrix bonding through strong interlocking, thereby increasing the bearing strength to withstand cyclic loads for a greater number of cycles.

6.3 Comparison of Fatigue Life for Neat and Modified GFRP Composite Pin Joints

The previous section and Figure 6.6 demonstrate the improvement in bearing strength of neat and modified GFRP composite pin joints, which can be attributed to the strong adhesion between the fiber matrix and the presence of Nano-silica. Likewise, a similar trend in the fatigue life of pin joints has been investigated for neat and modified GFRP composite pin joints. Fatigue life has been investigated at two different regimes under cyclic loading conditions *i.e.* at Low Cycle Fatigue (LCF) and High Cycle Fatigue (HCF). LCF, which stands for Low-Cycle Fatigue, refers to the fatigue failure that occurs at a relatively small number of loading cycles, typically less than 10^3 cycles. In LCF, the cyclic stresses are typically high, causing plastic deformation in the material. And LCF is commonly observed in applications involving high cyclic stress, such as in structural components, and aerospace applications [206]. In the LCF regime, the failure of pin joints is typically linked to the accumulation of plastic deformation caused by high cyclic loading. In contrast, in the HCF regime, fatigue failure occurs after a large number of loading cycles, typically ranging from 10^5 to 10^6 cycles. In HCF, the cyclic stresses are generally lower, and the material behaves predominantly elastically [93]. The failure in pin joints under the HCF regime is primarily caused by crack initiation and propagation at the hole vicinity due to low cyclic stresses, without significant plastic deformation. The results presented in Figure 6.15(a) illustrate the bearing strength achieved with different pin joint

135

configurations for the Neat GFRP composite, considering both low cycle fatigue (LCF) and high cycle fatigue (HCF) conditions. The results show that at an E:D and W:D proportion of 3, the bearing strength obtained in the LCF regime is approximately 70% of the static bearing strength. Additionally, it was observed that for E:D equal to 3 and W:D equal to 3, 4, and 5, the joints do not provide positive bearing strength under the HCF regime at 10^6 cycles. These joints also experienced early failure due to damage in the fiber matrix. Therefore, it is advisable to avoid using lower E:D and W:D ratios for high-cycle fatigue (HCF) applications. Additionally, the pin joints demonstrated a reduced fatigue life, primarily attributed to the net tension failure mode.
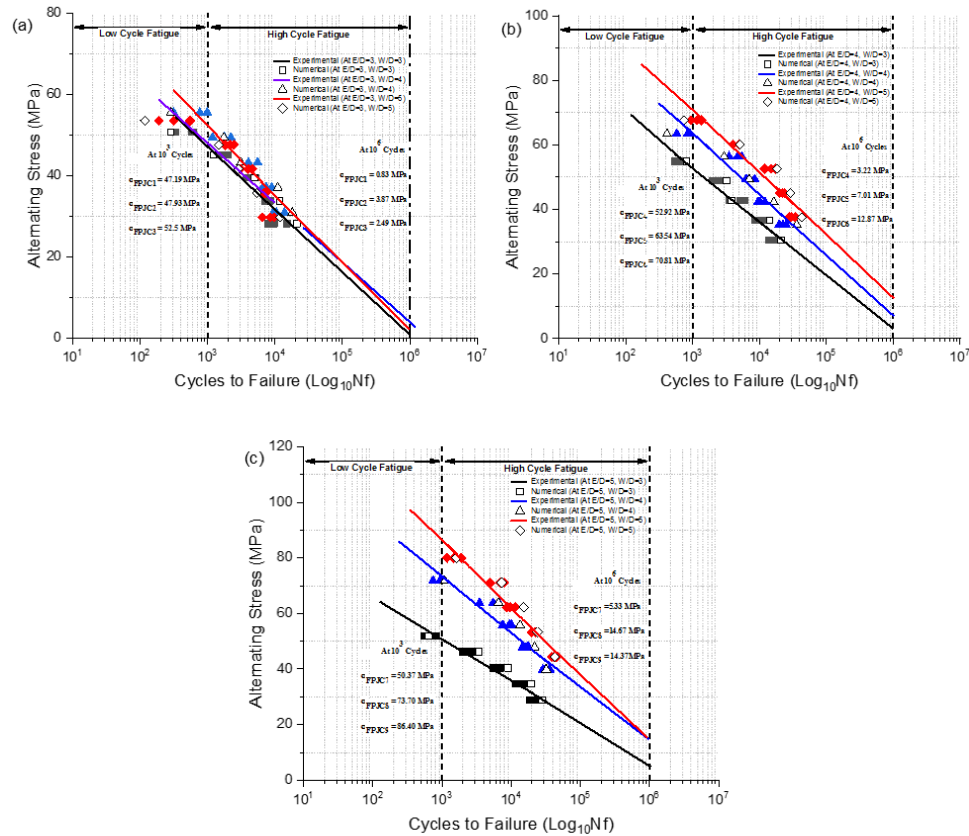
Figure 6.15 Comparison of LCF & HCF life for Neat GFRP pin joint configurations (a) At E:D equals 3, (b) At E:D equals 4, (c) At E:D equals 5 and W:D varies from 3 to 5 respectively

Similarly, as the E:D and W:D proportion increases, there is an enhancement in the bearing strength in both the LCF and HCF regions. For instance, at E:D & W:D proportion equals

136

5, the enhanced strength observed in the low-cycle fatigue (LCF) region is 93% of the static bearing strength, as depicted in Figure 6.15 (c). In contrast, in the high-cycle fatigue (HCF) regime at 10^6 cycles, only approximately 15.5% of the static bearing strength is observed. This indicates that the failure mode observed under high E:D and W:D proportions is characterized by progressive damage. Furthermore, the high number of cycles to failure observed during the experimentation indicates a slow progression of the damage mode, which can be attributed to the relatively low stress levels applied. A similar phenomenon involving enhanced fatigue strength has been examined in modified GFRP pin joint configurations, as depicted in Figure 6.16 (a) to (c).
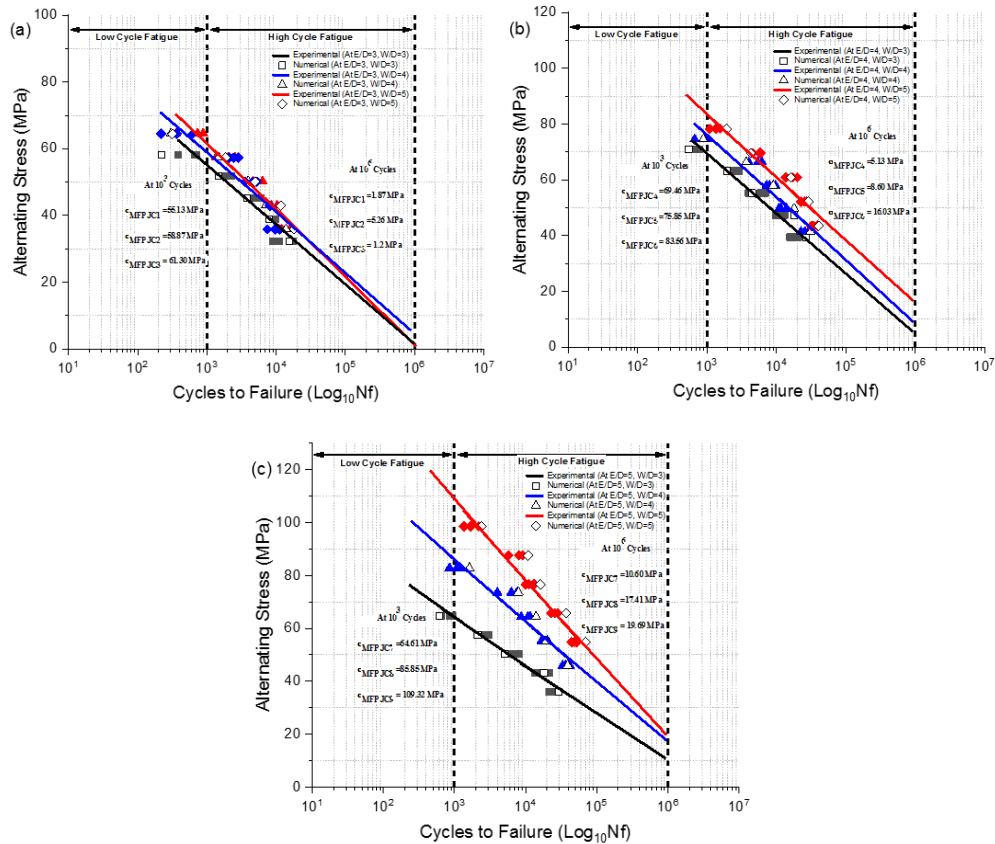
Figure 6.16 Comparison of LCF & HCF life for Modified GFRP pin joint configurations (a) At E:D equals 3, (b) At E:D equals 4, (c) At E:D equals 5 and W:D varies from 3 to 5 respectively

The incorporation of Nano-silica has led to a shift in the damage mode from pure tension to shear damage mode, accompanied by a moderate fatigue life prior to failure. At E:D and

137

W:D proportions equals 5, a noticeable improvement in bearing strength has been observed under fatigue loading in both the low and high cycle fatigue regimes. More precisely, in the Low-Cycle Fatigue (LCF) regime, the bearing strength amounts to 96.6% of the static bearing strength, whereas in the High-Cycle Fatigue (HCF) regime, it decreases to 17.5% of the static bearing strength, as illustrated in Figure 6.16 (c). With an increase in the number of cycles until failure, progressive damage becomes evident. Additionally, a combination of bearing and shear-out failure was observed at a moderate number of cycles until failure. Additionally, at low cycles to failure, a net-tension failure behavior has been observed. When pin joints are subjected to cyclic loading, various damage patterns were observed in the vicinity of the hole. Higher edge and width-to-diameter ratios result in a progressive damage pattern, which is typically expected in pin joint configurations as shown in Figure 6.17. Conversely, when considering a W:D proportion of 3 and E;D proportion of 4, the observed failure mode was a combination of bearing and shear-out failure. This damage mode was characterized by an immediate decrease in dynamic modulus followed by a saturation stage, after which a sudden decrement in modulus occurs. In the case of W:D & E:D proportions equals 3, the dynamic modulus decreases gradually with a steeper trend, indicating that the failure of both the fiber and matrix exceed their tensile strength. Consequently, the specimen experiences a very low dynamic modulus just before its final failure, indicating a catastrophic damage pattern.
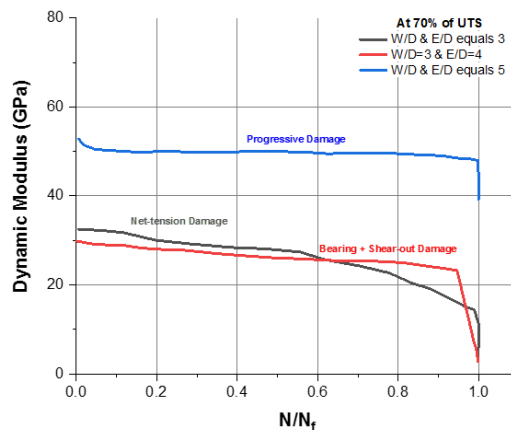
Figure 6.17 Dynamic modulus vs normalized cycles to represent various damage patterns observed in Neat GFRP composite pin joint configuration

Figure 6.18 illustrates a comparison of bearing strength among various joint configurations at both LCF and HCF regions, along with the corresponding static bearing strength. The findings indicate that pin joints fabricated using Modified GFRP exhibit notable improvements in bearing strength compared to those made from Neat GFRP.
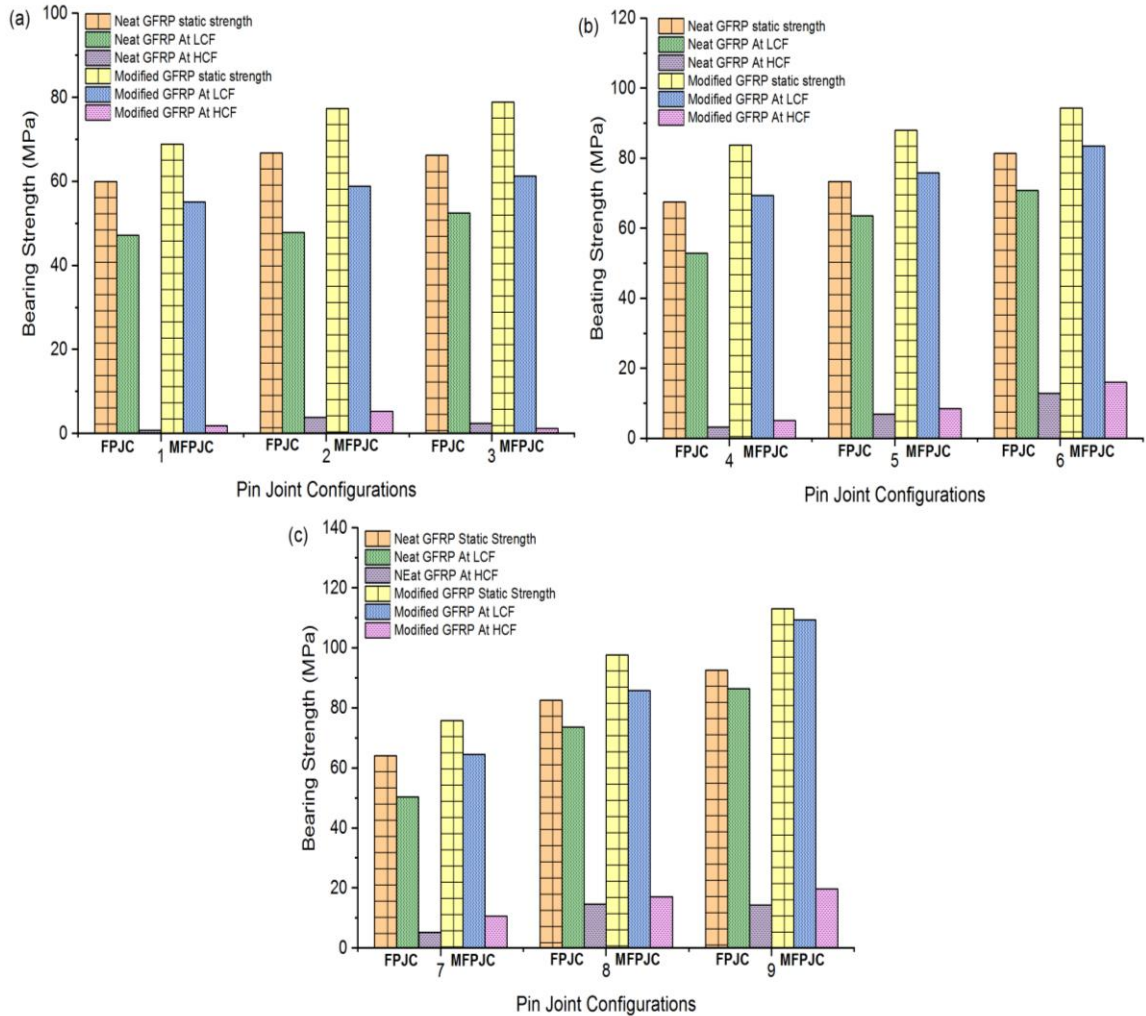
Figure 6.18 Bearing Strength Comparison of Static Tensile Strength, Low and High Cycle Fatigue Strength in Neat and Modified GFRP Composite Pin Joints: (a) E:D=3, (b) E:D=4, (c) E:D=5, and W:D ranges from 3 to 5.

The geometric parameters E:D and W:D are vital considerations in the design of pin joints, as they significantly impact their performance. Generally, increasing the E:D and W:D proportions leads to improved bearing strength of the pin joint. This increase is attributed

139

to improved load distribution, reduced stress concentration, and the transition of improved damage mode from catastrophic to progressive damage. Out of all the pin joint configurations, the joints fabricated from modified GFRP exhibit the highest increase in bearing strength, with an improvement of approximately 28.3% compared to Neat GFRP. The aforementioned observation holds true for E:D and W:D proportions of 5 in the LCF regime. Furthermore, it has been observed that under the HCF regime, when E:D and W:D proportion was set to 5 and 4 respectively, a significant enhancement in bearing strength of 37.02% was achieved compared to the Neat GFRP pin joint. However, this improvement is accompanied by a progressive damage mode.

6.4   Closure

The current chapter focuses on the experimental analysis of pin joints, examining their behavior under static and fatigue loading conditions. The objective is to assess the impact of geometric parameters, namely the E:D and W:D proportions, on pin joints made of both neat and modified GFRP composites. From the results it has been noted that there was an improved bearing strength of 22.15% observed at higher E:D and W:D proportion equals 5. Additionally, fatigue tests were conducted under tension-tension loading conditions with a constant amplitude and a frequency of 2 Hz. The tests were performed at five different stress levels, namely 50%, 60%, 70%, 80%, and 90%. Bearing strength under fatigue loading has been investigated under two regimes *i.e.* LCF and HCF. Neat GFRP exhibited a bearing strength of approximately 70% of the static bearing strength at an E:D and W:D ratio of 3 during the LCF regime, accompanied by a catastrophic failure mode. On the other hand, at E:D and W:D equals 5, a notable improvement in bearing strength of 93% of the static bearing strength was observed under the LCF regime. For Modified GFRP with 3wt. % of Nano-silica, significant improvements in bearing strength were observed under fatigue loading in both LCF and HCF regimes. More specifically, in the LCF regime, the bearing strength achieved 96.6% of the static bearing strength, whereas, in the HCF regime, it dropped to 17.5% of the static bearing strength. With an increase in the number of cycles until failure, progressive damage became evident, and a combination of bearing and shear-out failure was observed at intermediate cycles to failure. Among all the pin joint

configurations, the joints fabricated from Modified GFRP exhibited the highest increase in bearing strength, with an improvement of approximately 28.3% compared to Neat GFRP. This improvement was observed at E:D and W:D proportions of 5 under the LCF regime. Furthermore, in the HCF regime, the highest improvement in bearing strength of 37.02% was observed at an E:D ratio of 5 and a W:D ratio of 4 compared to Neat GFRP. However, this improvement was accompanied by a progressive damage mode. The following chapter presents the findings and offers suggestions for future perspectives based on the results of the present thesis work.

CHAPTER 7 – CONCLUSION AND FUTURE PERSPECTIVES

7.1   Conclusion

The current study focuses on examining the effects of fatigue loading on pin joints made of glass fiber-reinforced epoxy composite. The experimental investigation involved studying the mechanical properties of bi-directional $[0º/90º]_{6s}$ glass fiber epoxy laminate with and without the inclusion of Nano-silica, under fatigue loading conditions. Pin joint specimens with a single hole were prepared using both Neat and Modified GFRP with 3 wt.% of Nano-silica composite laminates. The purpose of the study was to analyze the bearing strength and damage mode of the pin joints under fatigue loading conditions at various joint configurations. The geometric parameters E:D and W:D proportions were varied from 3 to 5 to investigate the influence of the pin joint performance. Notably, the addition of Nano-silica demonstrates a positive influence on the modified glass fiber-reinforced composite laminates, resulting in a notable improvement of 16.25% in tensile strength compared to the neat GFRP composite laminates.

The study revealed that the inclusion of 3 wt. % of Nano-silica improved fatigue strength by 21.6% compared to the neat GFRP composite laminates. Neat GFRP shows lower fatigue resistance and higher vulnerability to failure under cyclic loading with fiber breakage and matrix cracking. In contrast, Modified GFRP exhibits higher fatigue resistance, extended fatigue life, and improved durability under cyclic loading. Observations revealed a combination of fiber breakage, matrix cracking, and fiber pull-out. The stress-strain hysteresis loop in composites indicates energy losses during each cycle, dissipated as heat. Increased hysteresis results from damage, like fiber-matrix interaction failure, weakening the interface's shear strength and disrupting the fiber-matrix bond. Rising stress levels expand the loop's area due to increased friction between surfaces, leading to more energy dissipation. The modified GFRP laminate exhibits a reduced hysteresis loop, accompanied by a gradual decrease in stiffness, leading to an improved fatigue life compared to the neat GFRP laminate.

The behavior of the dynamic modulus with respect to the normalized cycle under fatigue loading at various stress levels differs between neat and modified GFRP pin joints. For neat GFRP pin joints, the dynamic modulus tends to show a more rapid decrease as the normalized cycle increases at all stress levels. This indicates a faster degradation of the material's stiffness with increasing fatigue cycles, regardless of the applied stress level. On the other hand, for modified GFRP pin joints, the dynamic modulus exhibits a relatively slower degradation as the normalized cycle increases, especially at higher stress levels. More sustained dynamic modulus indicates enhanced fatigue resistance. In summary, the modified GFRP pin joints generally demonstrate better fatigue performance with a more gradual reduction in dynamic modulus compared to neat GFRP pin joints.

The study focused on analyzing the bearing strength under low cycle (LCF) and high cycle fatigue (HCF) regimes of neat and modified GFRP pin joints. The damage behavior of pin joints was found to be dependent on geometric and material parameters, specifically W:D and E:D ratios. For small E:D values, net-tension failure was observed, and for small W:D values, shear-out failure occurred abruptly without prior indication. Conversely, the desired progressive mode of failure, bearing mode, was observed in pin joints with W:D and E:D ratios greater or equal to 4, representing non-catastrophic failure. Modified GFRP pin joints showed improved fatigue strength with a shallow slope in the S-N plot at higher W:D and E:D ratios. The addition of Nano-silica enhances bonding between fibers and matrix, effectively resisting crack propagation, making it suitable for fatigue loading, increasing bearing strength, and withstanding cyclic loads for an extended number of cycles. The numerical results closely match the experimental findings.

At E:D and W:D equals 3, Neat GFRP pin joints exhibit a bearing strength in the LCF regime that is about 70% of the static bearing strength. However, at E:D and W:D equals 5, the enhanced strength observed in the LCF regime is 93% of the static bearing strength with a bearing failure mode. Additionally, it was observed that when E:D is equal to 3 and W:D is equal to 3, 4, and 5, the joints do not display positive bearing strength under the HCF regime, leading to catastrophic failure mode. Incorporating Nano-silica shifted the damage mode from pure tension to shear, resulting in a moderate fatigue life before failure.

At E:D and W:D equals 5, extended fatigue life and improved bearing strength were observed due to the addition of Nano-silica compared to neat GFRP with the same geometric configuration, representing 96.6% of static bearing strength under the LCF regime. At E:D and W:D equals 5, the joints made from modified GFRP exhibited the most significant increase in bearing strength *i.e.* 28.3% compared to Neat GFRP under the LCF regime. Similarly, at E:D and W:D equals 5 and 4, respectively, a substantial 37.02% increase in bearing strength was observed compared to the Neat GFRP pin joint under the HCF regime. However, this improvement was accompanied by a progressive damage mode. The study showed that at E:D and W:D equals 5, the dynamic modulus significantly influences the performance of modified GFRP pin joints under fatigue loading. The gradual damage of the dynamic modulus with the slower reduction in material stiffness represents extended fatigue life with improved bearing strength. On the other hand, neat GFRP pin joints exhibited a steeper reduction in dynamic modulus due to the rapid degradation of the material's stiffness with increasing fatigue cycles under various stress levels resulting in shorter fatigue life.

In aircraft structures like fuselage, wings mode from fiber-reinforced polymer composite utilizing pin/rivet joints for connection of structures experiences repeated loading. Likewise, in the marine structure, rivets endure repetitive loading from wave actions, leading to fatigue stress that may result in material degradation and eventual failure over time. This underscores the necessity of fatigue studies to optimize the design and performance of composite pin joints under cyclic loading conditions. Analyzing the impact of fatigue loading on pin joints constructed from glass fiber-reinforced epoxy composite contributes to understanding the behavior of these joints. Additionally, introducing Nano-silica into GFRP pin joints enhances their performance, enabling them to endure a significantly higher fatigue life compared to those made from neat GFRP composite laminate. This insight is particularly valuable for industries focused on structural applications, especially in aviation and marine sectors, facilitating the design of composite joints using modified GFRP with Nano-silica for improved fatigue life and enhanced

toughness would undoubtedly prove valuable for the practical application in workshop practices.

7.2 Recommendation of Future Perspectives

The Potential areas for further development of the present work include:

- The main focus of the current study was the analysis of pin joints in glass fiber-reinforced laminates, considering the presence and absence of Nano-silica. An additional aspect worth exploring involves investigating the influence of temperature conditions on the bearing strength and damage analysis of pin joints in glass fiber-reinforced laminates, considering the presence and absence of Nano-silica.
- The current study has the potential to be expanded to encompass different materials, including various types of fibers and Nano-fillers. This extension is of utmost importance as the fatigue loading significantly affects the strength of composite laminates and their joints, making it imperative to consider the various material parameters.
- The present study has the potential for expansion to investigate the strength and damage modes of adhesively bonded joints under fatigue loading conditions.

REFERENCES

[1]   S. W. Tsai and E. M. Wu, "A General Theory of Strength for Anisotropic Materials," *J. Compos. Mater.*, vol. 5, no. 1, pp. 58–80, Jan. 1971, doi: 10.1177/002199837100500106.

[2]   N. O. T. Measurement, "Sensitive Handbook Composite Materials Handbook Volume 2 . Polymer Matrix Composites," vol. 2, no. June, 2011.

[3]   R. Paul and L. Dai, "Interfacial aspects of carbon composites," *Compos. Interfaces*, vol. 25, no. 5–7, pp. 539–605, Jul. 2018, doi: 10.1080/09276440.2018.1439632.

[4]   I. M. Alarifi, M. Khorami, T. M. A. A. EL-Bagory, and R. Asmatulu, "Dynamic Mechanical Analysis of Epoxy/Synthetic Fiber Composites," in *Handbook of Epoxy/Fiber Composites*, no. January 2022, Singapore: Springer Singapore, 2022, pp. 1–28.

[5]   C. Zweben, "Composite Materials," in *Mechanical Engineers' Handbook*, M. Kutz, Ed. Devon, Pennsylvania: Wiley, 2014.

[6]   T. Ngo, *Introduction to Composite Materials*. Intechopen, 2020.

[7]   S. Bansal and J. S. Saini, "Mechanical and wear properties of SiC/Graphite reinforced Al359 alloy-based metal matrix composite," *Def. Sci. J.*, vol. 65, no. 4, pp. 330–338, 2015, doi: 10.14429/dsj.65.8676.

[8]   K. K. Chawla, *CERAMIC MATRIX COMPOSITES*, Second. Springer, 2013.

[9]   P. Alam, D. Mamalis, C. Robert, C. Floreani, and C. M. Ó Brádaigh, "The fatigue of carbon fibre reinforced plastics - A review," *Compos. Part B Eng.*, vol. 166, no. July 2018, pp. 555–579, 2019, doi: 10.1016/j.compositesb.2019.02.016.

[10]   R. Jones, *Mechanics of composite materials*. New York: Taylor and Francis, 1999.

[11]   J. Bai, "Introduction," in *Advanced Fibre-Reinforced Polymer (FRP) Composites*

for Structural Applications, J. B. T.-A. F.-R. P. (FRP) C. for S. A. Bai, Ed. Woodhead Publishing, 2013, pp. 1–4.

[12] K. K. Chawla, *Composite Materials Science and Engineering*, 3rd ed. USA: Springer, 2012.

[13] M. M. Shokrieh and F. Taheri-Behrooz, "Fatigue life prediction of composite materials based on progressive damage modeling," *Fatigue Life Predict. Compos. Compos. Struct.*, pp. 249–292, 2010, doi: 10.1533/9781845699796.2.249.

[14] A. Aktaş, "Statistical analysis of bearing strength of glass-fiber composite materials," *J. Reinf. Plast. Compos.*, vol. 26, no. 6, pp. 555–564, 2007, doi: 10.1177/0731684407075531.

[15] A. Gupta and M. Singh, "Statistical Investigation on Reliability of Single-Hole Pin Joints Strength and Failure Mechanisms in Glass – Epoxy Composite Laminates," pp. 133–145, 2021.

[16] B. D. Agarwal, L. J. Broutman, and K. Chandrashekhara, *Analysis and Performance of Fiber Composites*, Third. Wiley, 2015.

[17] B. Okutan Baba, "Behavior of pin-loaded laminated composites," *Exp. Mech.*, vol. 46, no. 5, pp. 589–600, 2006, doi: 10.1007/s11340-006-8735-z.

[18] A. B. Strong, *Fundamentals of Composites Manufacturing Second Edition: Materials, Methods and Applications*. Society of Manufacturing Engineers, 2008.

[19] C. E. Chaves and F. F. Fernandez, "A review on aircraft joints design," *Aircr. Eng. Aerosp. Technol.*, vol. 88, no. 3, pp. 411–419, 2016, doi: 10.1108/aeat-10-2012-0184.

[20] J. A. Nairn, "Matrix Microcracking in Composites," *Compr. Compos. Mater.*, vol. 2, pp. 403–432, 2000, doi: 10.1016/b0-08-042993-9/00069-3.

[21] A. Nanda Kishore, S. K. Malhotra, and N. Siva Prasad, "Failure analysis of multi-pin joints in glass fibre/epoxy composite laminates," *Compos. Struct.*, vol. 91, no.

3, pp. 266–277, 2009, doi: 10.1016/j.compstruct.2009.04.043.

[22]   L. Calabrese, V. Fiore, T. Scalici, P. Bruzzaniti, and A. Valenza, "Failure maps to assess bearing performances of glass composite laminates," *Polym. Compos.*, vol. 40, no. 3, pp. 1087–1096, 2019, doi: 10.1002/pc.24806.

[23]   A. Bernasconi, L. M. Martulli, and M. Carboni, "Fatigue crack growth analysis in composite bonded joints by back face distributed strain sensing and comparison with X-ray microtomography," *Int. J. Fatigue*, vol. 154, no. May 2021, p. 106526, 2022, doi: 10.1016/j.ijfatigue.2021.106526.

[24]   Z. Kapidžić, H. Ansell, J. Schön, and K. Simonsson, "Fatigue bearing failure of CFRP composite in biaxially loaded bolted joints at elevated temperature," *Compos. Struct.*, vol. 127, pp. 298–307, 2015, doi: 10.1016/j.compstruct.2015.03.031.

[25]   S. Budhe, M. D. Banea, S. de Barros, and L. F. M. da Silva, "An updated review of adhesively bonded joints in composite materials," *Int. J. Adhes. Adhes.*, vol. 72, pp. 30–42, 2017, doi: https://doi.org/10.1016/j.ijadhadh.2016.10.010.

[26]   F. Asgari Mehrabadi, "Experimental and Numerical Failure Analysis of Adhesive Composite Joints," *Int. J. Aerosp. Eng.*, vol. 2012, pp. 1–10, 2012, doi: 10.1155/2012/925340.

[27]   U. A. Khashaba, T. A. Sebaey, and K. A. Alnefaie, "Failure and reliability analysis of pinned-joints composite laminates: Effects of stacking sequences," *Compos. Part B Eng.*, vol. 45, no. 1, pp. 1694–1703, 2013, doi: 10.1016/j.compositesb.2012.09.066.

[28]   F. Sen, M. Pakdil, O. Sayman, and S. Benli, "Experimental failure analysis of mechanically fastened joints with clearance in composite laminates under preload," *Mater. Des.*, vol. 29, no. 6, pp. 1159–1169, 2008, doi: 10.1016/j.matdes.2007.05.009.

[29]   M. Tercan, O. Asi, and A. Aktaş, "An experimental investigation of the bearing

strength of weft-knitted 1 × 1 rib glass fiber composites," *Compos. Struct.*, vol. 78, no. 3, pp. 392–396, 2007, doi: 10.1016/j.compstruct.2005.10.015.

[30]   X. Li, X. Cheng, Y. Cheng, Z. Wang, and W. Huang, "Tensile properties of a composite–metal single-lap hybrid bonded/bolted joint," *Chinese J. Aeronaut.*, 2020, doi: 10.1016/j.cja.2020.03.042.

[31]   M. Singh, H. Bhunia, and J. S. Saini, "Effect of Ply Orientation on Strength and Failure Mode of Pin Jointed Unidirectional Glass-epoxy Nanoclay Laminates," *Def. Sci. J.*, vol. 65, no. 6, pp. 489–499, 2015, doi: 10.14429/dsj.65.8917.

[32]   R. Karakuzu, N. Taylak, B. M. Içten, and M. Aktaş, "Effects of geometric parameters on failure behavior in laminated composite plates with two parallel pin-loaded holes," *Compos. Struct.*, vol. 85, no. 1, pp. 1–9, 2008, doi: 10.1016/j.compstruct.2007.10.003.

[33]   B. M. Içten, R. Karakuzu, and M. E. Toygar, "Failure analysis of woven kevlar fiber reinforced epoxy composites pinned joints," *Compos. Struct.*, vol. 73, no. 4, pp. 443–450, 2006, doi: 10.1016/j.compstruct.2005.02.016.

[34]   A. Gupta, M. Singh, J. Singh, S. Singh, and C. Prakash, "A critical review on damage modeling and failure analysis of pin joints in fiber reinforced composite laminates," *Polym. Polym. Compos.*, vol. 30, pp. 1–13, 2022, doi: 10.1177/09673911221099764.

[35]   O. Asi, "An experimental study on the bearing strength behavior of Al2O3 particle filled glass fiber reinforced epoxy composites pinned joints," *Compos. Struct.*, vol. 92, no. 2, pp. 354–363, 2010, doi: 10.1016/j.compstruct.2009.08.014.

[36]   B. Okutan and R. Karakuzu, "The strength of pinned joints in laminated composites," *Compos. Sci. Technol.*, vol. 63, no. 6, pp. 893–905, 2003, doi: 10.1016/S0266-3538(02)00313-5.

[37]   W. Hwang and K. S. Han, "Fatigue of Composites—Fatigue Modulus Concept and

Life Prediction," *J. Compos. Mater.*, vol. 20, no. 2, pp. 154–165, 1986, doi: 10.1177/002199838602000203.

[38]   V. B. Bhandari, *Design of Machine Elements*. Tata McGraw-Hill, 2007.

[39]   M. A. McCarthy, C. T. McCarthy, V. P. Lawlor, and W. F. Stanley, "Three-dimensional finite element analysis of single-bolt, single-lap composite bolted joints: Part I - Model development and validation," *Compos. Struct.*, vol. 71, no. 2, pp. 140–158, 2005, doi: 10.1016/j.compstruct.2004.09.024.

[40]   R. Karakuzu, T. Gülem, and B. M. Içten, "Failure analysis of woven laminated glass-vinylester composites with pin-loaded hole," *Compos. Struct.*, vol. 72, no. 1, pp. 27–32, 2006, doi: 10.1016/j.compstruct.2004.10.009.

[41]   R. Karakuzu, C. R. Çalişkan, M. Aktaş, and B. M. Içten, "Failure behavior of laminated composite plates with two serial pin-loaded holes," *Compos. Struct.*, vol. 82, no. 2, pp. 225–234, 2008, doi: 10.1016/j.compstruct.2007.01.002.

[42]   O. Asi, "Effect of different woven linear densities on the bearing strength behaviour of glass fiber reinforced epoxy composites pinned joints," *Compos. Struct.*, vol. 90, no. 1, pp. 43–52, 2009, doi: 10.1016/j.compstruct.2009.01.007.

[43]   A. Aktaş, H. Imrek, and Y. Cunedioğlu, "Experimental and numerical failure analysis of pinned-joints in composite materials," *Compos. Struct.*, vol. 89, no. 3, pp. 459–466, 2009, doi: 10.1016/j.compstruct.2008.09.009.

[44]   R. Karakuzu, O. Demirgoren, B. M. Icten, and M. E. Deniz, "Failure behavior of quasi-isotropic laminates with three-pin loaded holes," *Mater. Des.*, vol. 31, no. 6, pp. 3029–3032, 2010, doi: 10.1016/j.matdes.2009.12.024.

[45]   O. Aluko, "An Analytical Method for Failure Prediction of Composite Pinned Joints," *Lect. Notes Eng. Comput. Sci.*, vol. 2192, no. 1, pp. 2581–2587, 2011.

[46]   A. Aktaş, "Failure analysis of serial pinned joints in composite materials," *Indian J. Eng. Mater. Sci.*, vol. 18, no. 2, pp. 102–110, 2011.

[47] T. Qin, L. Zhao, and J. Zhang, "Fastener effects on mechanical behaviors of double-lap composite joints," *Compos. Struct.*, vol. 100, pp. 413–423, 2013, doi: 10.1016/j.compstruct.2013.01.008.

[48] A. Olmedo, C. Santiuste, and E. Barbero, "An analytical model for predicting the stiffness and strength of pinned-joint composite laminates," *Compos. Sci. Technol.*, vol. 90, pp. 67–73, 2014, doi: 10.1016/j.compscitech.2013.10.014.

[49] K. Turan, M. Gur, and M. O. Kaman, "Progressive failure analysis of pin-loaded unidirectional carbon-epoxy laminated composites," *Mech. Adv. Mater. Struct.*, vol. 21, no. 2, pp. 98–106, 2014, doi: 10.1080/15376494.2012.677109.

[50] C. Atas, "Bearing strength of pinned joints in woven fabric composites with small weaving angles," *Compos. Struct.*, vol. 88, no. 1, pp. 40–45, 2009, doi: 10.1016/j.compstruct.2008.04.002.

[51] F. X. Irisarri, F. Laurin, N. Carrere, and J. F. Maire, "Progressive damage and failure of mechanically fastened joints in CFRP laminates - Part I: Refined Finite Element modelling of single-fastener joints," *Compos. Struct.*, vol. 94, no. 8, pp. 2269–2277, 2012, doi: 10.1016/j.compstruct.2011.07.023.

[52] A. Öndürücü, Ü. Esendemir, and R. F. Tunay, "Progressive failure analysis of glass–epoxy laminated composite pinned-joints," *Mater. Des.*, vol. 36, pp. 617–625, Apr. 2012, doi: 10.1016/j.matdes.2011.11.031.

[53] H. S. Li, S. Xia, and D. M. Luo, "A probabilistic analysis for pin joint bearing strength in composite laminates using Subset Simulation," *Compos. Part B Eng.*, vol. 56, pp. 780–789, 2014, doi: 10.1016/j.compositesb.2013.09.025.

[54] A. A. Pisano, P. Fuschi, and D. De Domenico, "Failure modes prediction of multi-pin joints FRP laminates by limit analysis," *Compos. Part B Eng.*, vol. 46, pp. 197–206, 2013, doi: 10.1016/j.compositesb.2012.09.071.

[55] J. Zhang, F. Liu, L. Zhao, Y. Chen, and B. Fei, "A progressive damage analysis

based characteristic length method for multi-bolt composite joints," *Compos. Struct.*, vol. 108, no. 1, pp. 915–923, 2014, doi: 10.1016/j.compstruct.2013.10.026.

[56] A. V Murthy, B. Dattaguru, H. V. . Narayana, and A. . Rao, "Stress and strength analysis of pin joints in laminated anisotropic plates," *Compos. Struct.*, vol. 19, no. 4, pp. 299–312, Jan. 1991, doi: 10.1016/0263-8223(91)90078-D.

[57] F. Esmaeili and T. N. Chakherlou, "Investigation on the effect of tigthening torque on the stress distribution in double lap simple bolted and hybrid (bolted -bonded) joints," *J. Solid Mech.*, vol. 7, no. 3, pp. 268–280, 2015.

[58] K. V. Arun, D. Sujay Kumar, and M. C. Murugesh, "Influence of bolt configuration and TiO2/ZnS fillers content on the strength of composites fasteners," *Mater. Des.*, vol. 53, pp. 51–57, 2014, doi: 10.1016/j.matdes.2013.06.008.

[59] Y. Zhu, D. Sun, H. Zheng, M. Wei, and L. Zhang, "Improvement in properties of epoxy-based electrophoretic coating by silica/polyurethane nanocomposites," *J. Mater. Sci.*, vol. 42, no. 2, pp. 545–550, Jan. 2007, doi: 10.1007/s10853-006-1066-8.

[60] X. F. Yao, D. Zhou, and H. Y. Yeh, "Macro/microscopic fracture characterizations of SiO2/epoxy nanocomposites," *Aerosp. Sci. Technol.*, vol. 12, no. 3, pp. 223–230, Apr. 2008, doi: 10.1016/j.ast.2007.03.005.

[61] A. Jumahat, C. Soutis, S. A. Abdullah, and S. Kasolang, "Tensile Properties of Nanosilica/Epoxy Nanocomposites," *Procedia Eng.*, vol. 41, pp. 1634–1640, 2012, doi: 10.1016/j.proeng.2012.07.361.

[62] Y. Hua, L. Gu, and H. Watanabe, "Micromechanical analysis of nanoparticle-reinforced dental composites," *Int. J. Eng. Sci.*, vol. 69, pp. 69–76, Aug. 2013, doi: 10.1016/j.ijengsci.2013.04.001.

[63] M. Zelenkova Myskova, J. Zelenka, V. Spacek, and F. Socha, "Properties of Epoxy Systems with Clay Nanocomposites," *Mech. Compos. Mater.*, vol. 39, no. 2, pp.

119–122, 2003, doi: 10.1023/A:1023453210943.

[64]   C.-K. Lam, H. Cheung, K. Lau, L. Zhou, M. Ho, and D. Hui, "Cluster size effect in hardness of nanoclay/epoxy composites," *Compos. Part B Eng.*, vol. 36, no. 3, pp. 263–269, Apr. 2005, doi: 10.1016/j.compositesb.2004.09.006.

[65]   A. J. Brunner *et al.*, "The influence of silicate-based nano-filler on the fracture toughness of epoxy resin," *Eng. Fract. Mech.*, vol. 73, no. 16, pp. 2336–2345, Nov. 2006, doi: 10.1016/j.engfracmech.2006.05.004.

[66]   F. H. Chowdhury, M. V. Hosur, and S. Jeelani, "Investigations on the thermal and flexural properties of plain weave carbon/epoxy-nanoclay composites by hand-layup technique," *J. Mater. Sci.*, vol. 42, no. 8, pp. 2690–2700, Apr. 2007, doi: 10.1007/s10853-006-1370-3.

[67]   P. Jawahar, R. Gnanamoorthy, and M. Balasubramanian, "Tribological behaviour of clay – thermoset polyester nanocomposites," *Wear*, vol. 261, no. 7–8, pp. 835–840, Oct. 2006, doi: 10.1016/j.wear.2006.01.010.

[68]   B. C. Kim, S. W. Park, and D. G. Lee, "Fracture toughness of the nano-particle reinforced epoxy composite," *Compos. Struct.*, vol. 86, no. 1–3, pp. 69–77, Nov. 2008, doi: 10.1016/j.compstruct.2008.03.005.

[69]   S. Sundaram, R. Nagalingam, and R. Satheesh Raja, "Experimental analysis on tensile properties of FRP with nano clay," *Int. J. Adv. Manuf. Technol.*, Dec. 2008, doi: 10.1007/s00170-008-1868-8.

[70]   X. Li, Z.-J. Zhan, G.-R. Peng, and W.-K. Wang, "Nano-disassembling method—A new method for preparing completely exfoliated epoxy/clay nanocomposites," *Appl. Clay Sci.*, vol. 55, pp. 168–172, Jan. 2012, doi: 10.1016/j.clay.2011.11.015.

[71]   M. Singh, J. S. Saini, and H. Bhunia, "Investigation on failure modes for pin joints made from unidirectional glass – epoxy nanoclay laminates," *Fatigue Fract. Eng. Mater. Struct.*, vol. 39, no. 3, pp. 320–334, 2015, doi: 10.1111/ffe.12358.

[72] M. Sekhon, J. S. Saini, G. Singla, and H. Bhunia, "Influence of nanoparticle fillers content on the bearing strength behavior of glass fiber-reinforced epoxy composites pin joints," *Proc. Inst. Mech. Eng. Part L J. Mater. Des. Appl.*, vol. 231, no. 8, pp. 641–656, 2017, doi: 10.1177/1464420715607556.

[73] M. Singh, J. S. Saini, and H. Bhunia, "To study the contribution of different geometric parameters on the failure load for multi holes pin joints prepared from glass / epoxy nanoclay laminates," *J. Compos. Mater.*, vol. 52, no. 5, pp. 629–644, 2018, doi: 10.1177/0021998317712572.

[74] M. Singh, J. S. Saini, H. Bhunia, and P. Singh, "Application of Taguchi method in the optimization of geometric parameters for double pin joint configurations made from glass – epoxy nanoclay laminates," *J. Compos. Mater.*, vol. 51, no. 19, pp. 2689–2706, 2017, doi: 10.1177/0021998316678920.

[75] A. Aktas and R. Karakuzu, "Failure Analysis of Two-Dimensional Carbon-Epoxy Composite Plate Pinned Joint," *Mech. Adv. Mater. Struct.*, vol. 6, no. 4, pp. 347–361, 2010.

[76] V. Singh, M. Singh, J. S. Saini, R. Badhwar, A. Gupta, and N. Chauhan, "Effect of Nanoclay in Unidirectional Carbon–Epoxy Laminated Composites," *Lect. Notes Mech. Eng.*, pp. 159–170, 2020, doi: 10.1007/978-981-15-4059-2_13.

[77] M. M. Singh *et al.*, "Determination of Strength Parameters of Glass Fibers Reinforced Composites for Engineering Applications," *Silicon*, vol. 12, no. 1, pp. 1–11, 2020, doi: 10.1007/s12633-019-0078-3.

[78] I. Burhan and H. S. Kim, "S-n curve models for composite materials characterisation: An evaluative review," *J. Compos. Sci.*, vol. 2, no. 3, 2018, doi: 10.3390/jcs2030038.

[79] M. Quaresimin and M. Ricotta, "Life prediction of bonded joints in composite materials," *Int. J. Fatigue*, vol. 28, no. 10 SPEC. ISS., pp. 1166–1176, 2006, doi: 10.1016/j.ijfatigue.2006.02.005.

[80] W. Ferdous *et al.*, "Testing and modelling the fatigue behaviour of GFRP composites – Effect of stress level, stress concentration and frequency," *Eng. Sci. Technol. an Int. J.*, no. xxxx, pp. 1–10, 2020, doi: 10.1016/j.jestch.2020.01.001.

[81] I. N. Yadav and K. B. Thapa, "Fatigue damage model of woven glass-epoxy fabric composite materials," *J. Mater. Res. Technol.*, vol. 9, no. 1, pp. 301–306, 2020, doi: 10.1016/j.jmrt.2019.10.058.

[82] S. Zhou, Y. Li, K. Fu, and X. Wu, "Progressive fatigue damage modelling of fibre-reinforced composite based on fatigue master curves," *Thin-Walled Struct.*, vol. 158, no. November 2019, p. 107173, 2021, doi: 10.1016/j.tws.2020.107173.

[83] T. A. Ansari, K. K. Singh, and M. S. Azam, "Observations of fatigue damage development in woven glass fi ber-reinforced polymer composite using transmission light photography technique," *Polym. Polym. Compos.*, vol. 30, pp. 1–10, 2022, doi: 10.1177/09673911221101300.

[84] I. K. Giannopoulos, D. Doroni-Dawes, K. I. Kourousis, and M. Yasaee, "Effects of bolt torque tightening on the strength and fatigue life of airframe FRP laminate bolted joints," *Compos. Part B Eng.*, vol. 125, 2017, doi: 10.1016/j.compositesb.2017.05.059.

[85] M. Nakada *et al.*, "Statistical tensile and flexural fatigue lives of unidirectional CF/PP laminates," *J. Reinf. Plast. Compos.*, p. 073168442311599, Feb. 2023, doi: 10.1177/07316844231159951.

[86] P. T. Curtis, "The fatigue behaviour of fibrous composite materials," *J. Strain Anal. Eng. Des.*, vol. 24, no. 4, pp. 235–244, 1989, doi: 10.1243/03093247V244235.

[87] M. Genedy, S. Daghash, E. Soliman, and M. M. Reda Taha, "Improving fatigue performance of GFRP composite using Carbon Nanotubes," *Fibers*, vol. 3, no. 1, pp. 13–29, 2015, doi: 10.3390/fib3010013.

[88] C. Kassapoglou, "Fatigue life prediction of composite structures under constant

amplitude loading," *J. Compos. Mater.*, vol. 41, no. 22, pp. 2737–2754, 2007, doi: 10.1177/0021998307078735.

[89] R. Starikov, "Experimental Investigation of Fatigue Behaviour in Composite Bolted Joints," The Royal Institute of Technology, Stockholm, Sweden, 1999.

[90] H. Mao and S. Mahadevan, "Fatigue damage modelling of composite materials," *Compos. Struct.*, vol. 58, no. 4, pp. 405–410, 2002, doi: 10.1016/S0263-8223(02)00126-5.

[91] I. De Baere, W. Van Paepegem, C. Hochard, and J. Degrieck, "On the tension-tension fatigue behaviour of a carbon reinforced thermoplastic part II: Evaluation of a dumbbell-shaped specimen," *Polym. Test.*, vol. 30, no. 6, pp. 663–672, 2011, doi: 10.1016/j.polymertesting.2011.05.005.

[92] C. Gerendt, A. Dean, T. Mahrholz, N. Englisch, S. Krause, and R. Rolfes, "On the progressive fatigue failure of mechanical composite joints: Numerical simulation and experimental validation," *Compos. Struct.*, vol. 248, no. March, p. 112488, 2020, doi: 10.1016/j.compstruct.2020.112488.

[93] R. Ben Sghaier, N. Majed, H. Ben Dali, and R. Fathallah, "High cycle fatigue prediction of glass fiber-reinforced epoxy composites: reliability study," *Int. J. Adv. Manuf. Technol.*, vol. 92, no. 9–12, pp. 4399–4413, 2017, doi: 10.1007/s00170-017-0496-6.

[94] S. S. Samareh-Mousavi, S. Mandegarian, and F. Taheri-Behrooz, "A nonlinear FE analysis to model progressive fatigue damage of cross-ply laminates under pin-loaded conditions," *Int. J. Fatigue*, vol. 119, no. October 2018, pp. 290–301, 2019, doi: 10.1016/j.ijfatigue.2018.10.010.

[95] B. Dindar and N. B. Bektaş, "Experimental investigation of fatigue and mechanical properties of unidirectional composite plates filled nanoparticles," *Acta Phys. Pol. A*, vol. 134, no. 1, pp. 285–288, 2018, doi: 10.12693/APhysPolA.134.285.

[96] P. Van Der Sypt, M. Chérif, and C. Bois, "Analysis of the fatigue behaviour of laminated composite holes subjected to pin-bearing loads," *Int. J. Fatigue*, vol. 103, pp. 86–98, 2017, doi: 10.1016/j.ijfatigue.2017.05.025.

[97] U. Javaid, C. Ling, and P. Cardiff, "Mechanical performance of carbon-glass hybrid composite joints in quasi-static tension and tension-tension fatigue," *Eng. Fail. Anal.*, vol. 116, no. June, 2020, doi: 10.1016/j.engfailanal.2020.104730.

[98] J. Maljaars and M. Euler, "Fatigue S-N curves of bolts and bolted connections for application in civil engineering structures," *Int. J. Fatigue*, vol. 151, no. April, p. 106355, 2021, doi: 10.1016/j.ijfatigue.2021.106355.

[99] F. M. González Ramírez *et al.*, "Experimental characterization of Mode I fatigue delamination growth onset in composite joints: A comparative study," *Mater. Des.*, vol. 160, pp. 906–914, 2018, doi: 10.1016/j.matdes.2018.10.007.

[100] N. H. Padmaraj, K. M. Vijaya, and P. Dayananda, "Experimental study on the tension-tension fatigue behaviour of glass/epoxy quasi-isotropic composites," *J. King Saud Univ. - Eng. Sci.*, vol. 32, no. 6, pp. 396–401, 2020, doi: 10.1016/j.jksues.2019.04.007.

[101] A. D'Amore, M. Giorgio, and L. Grassia, "Modeling the residual strength of carbon fiber reinforced composites subjected to cyclic loading," *Int. J. Fatigue*, vol. 78, pp. 31–37, 2015, doi: 10.1016/j.ijfatigue.2015.03.012.

[102] H. T. Hahn and R. Y. Kim, "Fatigue Behavior of Composite Laminate," *J. Compos. Mater.*, vol. 10, no. 2, pp. 156–180, 1976, doi: 10.1177/002199837601000205.

[103] G. C. Tsai, J. F. Doyle, and C. T. Sun, "Frequency Effects on the Fatigue Life and Damage of Graphite/Epoxy Composites," *J. Compos. Mater.*, vol. 21, no. 1, pp. 2–13, 1987, doi: 10.1177/002199838702100101.

[104] H. T. Han, S. W. Choi, and G. S. Lim, "The Effect of Loading Parameters on Fatigue of Composite Laminates: Part II," 2001.

[105] A. Gillet, P. F. Rancescato, and P. Saffre, "Single- and Multi-objective Optimization of Composite Structures: The Influence of Design Variables," *J. Compos. Mater.*, vol. 44, no. 4, pp. 457–480, 2010, doi: 10.1177/0021998309344931.

[106] P. P. Camanho and M. Lambert, "A design methodology for mechanically fastened joints in laminated composite materials," *Compos. Sci. Technol.*, vol. 66, pp. 3004–3020, 2006, doi: 10.1016/j.compscitech.2006.02.017.

[107] J. Zhang and J. Rowland, "Damage modeling of carbon-fiber reinforced polymer composite pin-joints at extreme temperatures," *Compos. Struct.*, vol. 94, no. 8, pp. 2314–2325, 2012, doi: 10.1016/j.compstruct.2012.03.011.

[108] F. Chang, R. A. Scott, and G. S. Springer, "Strength of mechanically fastended composite joints," *J. Compos. Mater.*, vol. 8, pp. 253–265, 1974.

[109] P. P. Camanho and F. L. Mathew, "A Progressive Damage Model for Mechanically Fastened Joints in Composite Laminates," *J. Compos. Mater.*, vol. 33, no. 24, pp. 2248–2280, 1999, doi: 10.1177/002199839903302402.

[110] W.-H. Chen and S.-S. Lee, "Numerical and Experimental Failure Analysis of Composite Laminates with Bolted Joints under Bending Loads," *J. Compos. Mater.*, vol. 29, no. 1, pp. 15–36, Jan. 1995, doi: 10.1177/002199839502900102.

[111] L. B. Lessard and M. M. Shokrieh, "Two-Dimensional Modeling of Composite Pinned-Joint Failure," *J. Compos. Mater.*, vol. 29, no. 5, pp. 671–697, Mar. 1995, doi: 10.1177/002199839502900507.

[112] T. Kermanidis, G. Labeas, K. I. Tserpes, and S. Pantelakis, "Finite element modeling of damage accumulation in bolted composite joints under incremental tensile loading," *Eur. Congr. Comput. Methods Appl. Sci. Eng. ECCOMAS 2000*, no. September, pp. 11–14, 2000.

[113] S. J. Kim, J. S. Hwang, and J. H. Kim, "Progressive Failure Analysis of Pin-Loaded Laminated Composites Using Penalty Finite Element Method," *AIAA J.*, vol. 36, no.

1, pp. 75–80, Jan. 1998, doi: 10.2514/2.354.

[114] P. F. Liu and J. Y. Zheng, "Recent developments on damage modeling and finite element analysis for composite laminates: A review," *Mater. Des.*, vol. 31, no. 8, pp. 3825–3834, 2010, doi: 10.1016/j.matdes.2010.03.031.

[115] A. C. Orifici, I. Herszberg, and R. S. Thomson, "Review of methodologies for composite material modelling incorporating failure," *Compos. Struct.*, vol. 86, no. 1–3, pp. 194–210, 2008, doi: 10.1016/j.compstruct.2008.03.007.

[116] S. D. Thoppul, J. Finegan, and R. F. Gibson, "Mechanics of mechanically fastened joints in polymer-matrix composite structures - A review," *Compos. Sci. Technol.*, vol. 69, no. 3–4, pp. 301–329, 2009, doi: 10.1016/j.compscitech.2008.09.037.

[117] M. Dano, E. Kamal, and G. Gendron, "Analysis of bolted joints in composite laminates : Strains and bearing stiffness predictions," *Compos. Struct.*, vol. 79, pp. 562–570, 2007, doi: 10.1016/j.compstruct.2006.02.024.

[118] J. M. Whitney and R. J. Nuismer, "Stress Fracture Criteria for Laminated Composites Containing Stress Concentrations," *J. Compos. Mater.*, vol. 8, no. 3, pp. 253–265, Jul. 1974, doi: 10.1177/002199837400800303.

[119] S. E. Yamada and C. T. Sun, "Analysis of Laminate Strength and Its Distribution," *J. Compos. Mater.*, vol. 12, no. 3, pp. 275–284, 1978, doi: 10.1177/002199837801200305.

[120] J. Kweon, H.-S. Ahn, and J.-H. Choi, "A new method to determine the characteristic lengths of composite joints without testing," *Compos. Struct.*, vol. 66, pp. 305–315, 2004, doi: 10.1016/j.compstruct.2004.04.053.

[121] H. Hamada, Z.-I. Maekawa, and K. Haruna, "Strength Prediction of Mechanically Fastened Quasi-Isotropic Carbon/Epoxy Joints," *J. Compos. Mater.*, vol. 30, no. 14, pp. 1596–1612, 1996.

[122] J. Singh, K. Singh, and J. S. Saini, "Efficiency and Stiffness of the Single Lap Bolt

Joints in Glass Epoxy Composites," *Def. Sci. J.*, vol. 69, no. 3, pp. 280–289, 2019, doi: 10.14429/dsj.69.13348.

[123] A. Atas and C. Soutis, "Subcritical damage mechanisms of bolted joints in CFRP composite laminates," *Compos. Part B Eng.*, vol. 54, pp. 20–27, 2013, doi: 10.1016/j.compositesb.2013.04.071.

[124] A. Atas, "Strength prediction of mechanical joints in composite laminates based on subcritical damage modelling," The University of Sheffield, 2012.

[125] A. Ataş, "Failure analysis of bolted joints in cross-ply composite laminates using cohesive zone elements," *Comput. Mater. Contin.*, vol. 34, pp. 199–225, Jan. 2013.

[126] A. Ataş, G. F. Mohamed, and C. Soutis, "Progressive failure analysis of bolted joints in composite laminates," *Plast. Rubber Compos.*, vol. 41, no. 4–5, pp. 209–214, Jun. 2012, doi: 10.1179/1743289811Y.0000000038.

[127] L. J. Hart-Smith, "Bolted joints in graphite-epoxy composites," 1976. doi: NASA Langley report NASA CR-144899.

[128] A. Ataş and C. Soutis, "Strength prediction of bolted joints in CFRP composite laminates using cohesive zone elements," *Compos. Part B Eng.*, vol. 58, pp. 25–34, 2014, doi: 10.1016/j.compositesb.2013.10.017.

[129] Q. Yang and B. Cox, "Cohesive models for damage evolution in laminated composites," *Int. J. Fract.*, vol. 133, no. 2, pp. 107–137, 2005, doi: 10.1007/s10704-005-4729-6.

[130] I. S. Raju and T. K. O' Brien, "Fracture mechanics concepts, stress fields, strain energy rel," in *Delamination Behaviour of Composites*, 2008, pp. 3–27.

[131] E. F. Rybicki and M. F. Kanninen, "A finite element calculation of stress intensity factors by a modified crack closure integral," *Eng. Fract. Mech.*, vol. 9, no. 4, pp. 931–938, 1977, doi: https://doi.org/10.1016/0013-7944(77)90013-3.

[132] S. T. Pinho, C. G. Dávila, P. P. Camanho, L. Iannucci, and P. Robinson, "Failure

Models and Criteria for FRP Under In-Plane or Three-Dimensional Stress States Including Shear Non-linearity," *Nasa/Tm-2005-213530*, no. February, p. 68, 2005, doi: NASA/TM-2005-213530.

[133] C. G. Davila, P. P. Camanho, and C. A. Rose, "Failure Criteria for FRP Laminates," *J. Compos. Mater.*, vol. 39, no. 4, pp. 323–345, 2005, doi: 10.1177/0021998305046452.

[134] P. P. Camanho, C. G. Davila, T. S. Pinho, L. Iannucci, and P. Robinson, "Prediction of in situ strengths and matrix cracking in composites under transverse tension and in-plane shear," *Compos. Part A Appl. Sci. Manuf.*, vol. 37, no. 2, pp. 165–176, 2006, doi: 10.1016/j.compositesa.2005.04.023.

[135] C. T. Sun and S. G. Zhou, "Failure of Quasi-Isotropic Composite Laminates with Free Edges," *J. Reinf. Plast. Compos.*, vol. 7, no. 6, pp. 515–557, Nov. 1988, doi: 10.1177/073168448800700602.

[136] S. W. Tsai and H. T. Hahn, *Introduction to Composite Materials*. Technomic Publishing Company, Connecticut, 1980.

[137] S. Soni, "A new look at commonly used failure theories in composite laminates," *24th Struct. Struct. Dyn. Mater. Conf.*, 1983, doi: 10.2514/6.1983-837.

[138] M. Toyoda, "Strength characteristics of composite materials," *Weld. Int.*, vol. 5, no. 5, pp. 341–345, 1991, doi: 10.1080/09507119109446748.

[139] I. Goldenblat and V. A. Kopnov, "Strength of glass-reinforced plastics in the complex stress state," *Polym. Mech.*, vol. 1, no. 2, pp. 54–59, 1965, doi: 10.1007/BF00860685.

[140] B. M. Içten and R. Karakuzu, "Progressive failure analysis of pin-loaded carbon-epoxy woven composite plates," *Compos. Sci. Technol.*, vol. 62, no. 9, pp. 1259–1271, 2002, doi: 10.1016/S0266-3538(02)00071-4.

[141] B. Okutan, "The effects of geometric parameters on the failure strength for pin-

loaded multi-directional fiber-glass reinforced epoxy laminate," *Compos. Part B Eng.*, vol. 33, no. 8, pp. 567–578, 2002.

[142] Z. Hashin, "Failure criteria for unidirectional fiber composites," *J. Appl. Mech. Trans. ASME*, vol. 47, no. 2, pp. 329–334, 1980, doi: 10.1115/1.3153664.

[143] D. L. Flaggs, "Experimental Determination of the In Situ Transverse Lamina Strength in Graphite / Epoxy Laminates," *J. Compos. Mater.*, vol. 16, pp. 103–116, 1982.

[144] S. Goswami, "A Finite Element Investigation on Progressive Failure Analysis of Composite Bolted Joints Under Thermal Environment," *J. Reinf. Plast. Compos.*, vol. 24, no. 2, pp. 161–171, Jan. 2005, doi: 10.1177/0731684405042958.

[145] P. P. Camanho and F. L. Matthews, "Stress analysis and strength prediction of mechanically fastened joints in FRP: A review," *Compos. Part A Appl. Sci. Manuf.*, vol. 28, no. 6, pp. 529–547, 1997, doi: 10.1016/S1359-835X(97)00004-3.

[146] U. M. Yan, H. T. Sun, W. D. Wei, and F. K. Chang, "Response and Failure of Composite Plates With a Bolt-Filled Hole," no. June, 1998.

[147] Z. Hashin and A. Rotem, "A Fatigue Failure Criterion for Fiber Reinforced Materials," *J. Compos. Mater.*, vol. 7, no. 4, pp. 448–464, Oct. 1973, doi: 10.1177/002199837300700404.

[148] M. V. Kozlov and S. V. Sheshenin, "Modeling the Progressive Failure of Laminated Composites," *Mech. Compos. Mater.*, vol. 51, no. 6, pp. 695–706, 2016, doi: 10.1007/s11029-016-9540-0.

[149] A. Puck and H. Schürmann, "Failure analysis of FRP laminates by means of physically based phenomenological models," *Compos. Sci. Technol.*, vol. 62, no. 12-13 SPECIAL ISSUE, pp. 1633–1662, 2002, doi: 10.1016/S0266-3538(01)00208-1.

[150] H. M. Deuschle and B.-H. Kroplin, "3D Failure Analysis of UD Fibre Reinforced

Composites: Puck's theory within FEA.pdf>," 2010.

[151] P. Ladevèze, G. Lubineau, and D. Violeau, "A computational damage micromodel of laminated composites," *Int. J. Fract.*, vol. 137, no. 1–4, pp. 139–150, 2006, doi: 10.1007/s10704-005-3077-x.

[152] C. T. Herakovich, *Mechanics of Fibrous Composites*. Wiley, 1997.

[153] J. A. Nairn and S. Hu, "The initiation and growth of delaminations induced by matrix microcracks in laminated composites," *Int. J. Fract.*, vol. 57, no. 1, pp. 1–24, 1992, doi: 10.1007/BF00013005.

[154] L. Pierre, "Multiscale computational damage modelling of laminate composites," *CISM Int. Cent. Mech. Sci. Courses Lect.*, vol. 474, pp. 171–212, 2005, doi: 10.1007/3-211-38102-3_5.

[155] C. V. Singh and R. Talreja, *A multiscale approach to modeling of composite damage*. Elsevier, 2016.

[156] G. J. Dvorak and N. Laws, "Analysis of Progressive Matrix Cracking In Composite Laminates II. First Ply Failure," *J. Compos. Mater.*, vol. 21, no. 4, pp. 309–329, Apr. 1987, doi: 10.1177/002199838702100402.

[157] O. Allix and P. Ladevèze, "Interlaminar interface modelling for the prediction of delamination," *Compos. Struct.*, vol. 22, no. 4, pp. 235–242, 1992, doi: 10.1016/0263-8223(92)90060-P.

[158] Z. Hashin, "Analysis of cracked laminates: a variational approach," *Mech. Mater.*, vol. 4, no. 2, pp. 121–136, 1985, doi: 10.1016/0167-6636(85)90011-0.

[159] F. Turan, K. Gurkan, M. Gudu, A. Durmus, and Y. Taskin, "A statistical approach to predict fatigue failure of leaf springs manufactured with carbon nanotube incorporated epoxy-woven glass fiber composites," *Polym. Compos.*, 2023.

[160] V. S. Uppin *et al.*, "Mechanical Response of Glass–Epoxy Composites with Graphene Oxide Nanoparticles," *Materials (Basel).*, vol. 15, no. 23, p. 8545, Nov.

2022, doi: 10.3390/ma15238545.

[161] B. Bittmann, F. Haupert, and A. K. Schlarb, "Preparation of TiO2/epoxy nanocomposites by ultrasonic dispersion and their structure property relationship," *Ultrason. Sonochem.*, vol. 18, no. 1, pp. 120–126, Jan. 2011, doi: 10.1016/j.ultsonch.2010.03.011.

[162] R. K. Nayak, A. Dash, and B. C. Ray, "Effect of Epoxy Modifiers (Al 2 O 3 /SiO 2 /TiO 2) on Mechanical Performance of epoxy/glass Fiber Hybrid Composites," *Procedia Mater. Sci.*, vol. 6, no. Icmpc, pp. 1359–1364, 2014, doi: 10.1016/j.mspro.2014.07.115.

[163] K. Devendra and T. Rangaswamy, "Strength Characterization of E-glass Fiber Reinforced Epoxy Composites with Filler Materials," *J. Miner. Mater. Charact. Eng.*, vol. 01, no. 06, pp. 353–357, 2013, doi: 10.4236/jmmce.2013.16054.

[164] S. Garg and M. Pant, "Meshfree Methods: A Comprehensive Review of Applications," *Int. J. Comput. Methods*, vol. 15, no. 04, p. 1830001, Oct. 2017, doi: 10.1142/S0219876218300015.

[165] S. Garg and M. Pant, "Numerical simulation of thermal fracture in functionally graded materials using element-free Galerkin method," *Sādhanā*, vol. 42, no. 3, pp. 417–431, 2017, doi: 10.1007/s12046-017-0612-1.

[166] S. Garg and M. Pant, "Numerical simulation of adiabatic and isothermal cracks in functionally graded materials using optimized element-free Galerkin method," *J. Therm. Stress.*, vol. 40, pp. 1–20, Mar. 2017, doi: 10.1080/01495739.2017.1287534.

[167] M. F. Uddin and C. T. Sun, "Strength of unidirectional glass/epoxy composite with silica nanoparticle-enhanced matrix," *Compos. Sci. Technol.*, vol. 68, no. 7, pp. 1637–1643, 2008, doi: https://doi.org/10.1016/j.compscitech.2008.02.026.

[168] S. Mutalikdesai, A. Hadapad, S. Patole, and G. Hatti, "Fabrication and Mechanical Characterization of Glass fibre reinforced Epoxy Hybrid Composites using Fly

ash/Nano clay/Zinc oxide as filler," *IOP Conf. Ser. Mater. Sci. Eng.*, vol. 376, no. 1, pp. 1–7, 2018, doi: 10.1088/1757-899X/376/1/012061.

[169] K. M. Mini, M. Lakshmanan, L. Mathew, and M. Mukundan, "Effect of fibre volume fraction on fatigue behaviour of glass fibre reinforced composite," *Fatigue Fract. Eng. Mater. Struct.*, vol. 35, no. 12, pp. 1160–1166, 2012, doi: 10.1111/j.1460-2695.2012.01709.x.

[170] I. De Baere, W. Van Paepegem, M. Quaresimin, and J. Degrieck, "On the tension – tension fatigue behaviour of a carbon reinforced thermoplastic part I : Limitations of the ASTM D3039 / D3479 standard," *Polym. Test.*, vol. 30, no. 6, pp. 625–632, 2011, doi: 10.1016/j.polymertesting.2011.05.004.

[171] R. Karakuzu, Z. Aslan, and B. Okutan, "The effect of ply number, orientation angle and bonding type on residual stresses of woven steel fiber reinforced thermoplastic laminated composite plates subjected to transverse uniform load," *Compos. Sci. Technol.*, vol. 64, no. 7–8, pp. 1049–1056, 2004, doi: 10.1016/j.compscitech.2003.09.014.

[172] L. Liu, B.-M. Zhang, D.-F. Wang, and Z.-J. Wu, "Effects of cure cycles on void content and mechanical properties of composite laminates," *Compos. Struct.*, vol. 73, no. 3, pp. 303–309, 2006, doi: https://doi.org/10.1016/j.compstruct.2005.02.001.

[173] M. Nalbant, H. Gökkaya, and G. Sur, "Application of Taguchi method in the optimization of cutting parameters for surface roughness in turning," *Mater. Des.*, vol. 28, no. 4, pp. 1379–1385, 2007, doi: https://doi.org/10.1016/j.matdes.2006.01.008.

[174] R. K. Pandey and S. S. Panda, "Multi-performance optimization of bone drilling using Taguchi method based on membership function," *Measurement*, vol. 59, pp. 9–13, 2015, doi: https://doi.org/10.1016/j.measurement.2014.09.038.

[175] J. A. Ghani, I. A. Choudhury, and H. H. Hassan, "Application of Taguchi method in the optimization of end milling parameters," *J. Mater. Process. Technol.*, vol. 145,

no. 1, pp. 84–92, 2004, doi: https://doi.org/10.1016/S0924-0136(03)00865-3.

[176] E. M. Anawa and A. G. Olabi, "Using Taguchi method to optimize welding pool of dissimilar laser-welded components," *Opt. Laser Technol.*, vol. 40, no. 2, pp. 379–388, 2008, doi: https://doi.org/10.1016/j.optlastec.2007.07.001.

[177] Y. Zheng, R. Ning, and Y. Zheng, "Study of SiO2 nanoparticles on the improved performance of epoxy and fiber composites," *J. Reinf. Plast. Compos.*, vol. 24, no. 3, pp. 223–233, 2005, doi: 10.1177/0731684405043552.

[178] Z. Ahmad, M. I. Sarwar, and J. E. Mark, "Dynamic-mechanical thermal analysis of aramid-silica hybrid composites prepared in a sol-gel process," *J. Appl. Polym. Sci.*, vol. 63, no. 10, pp. 1345–1352, Mar. 1997, doi: https://doi.org/10.1002/(SICI)1097-4628(19970307)63:10<1345::AID-APP14>3.0.CO;2-3.

[179] T. Skinner, S. Datta, A. Chattopadhyay, and A. Hall, "Fatigue damage behavior in carbon fiber polymer composites under biaxial loading," *Compos. Part B Eng.*, vol. 174, no. May, p. 106942, 2019, doi: 10.1016/j.compositesb.2019.106942.

[180] T. khezri, M. Sharif, and B. Pourabas, "Polythiophene–graphene oxide doped epoxy resin nanocomposites with enhanced electrical, mechanical and thermal properties," *RSC Adv.*, vol. 6, no. 96, pp. 93680–93693, 2016, doi: 10.1039/C6RA16701B.

[181] C. Monteserín *et al.*, "Effects of Graphene Oxide and Chemically-Reduced Graphene Oxide on the Dynamic Mechanical Properties of Epoxy Amine Composites," *Polymers*, vol. 9, no. 9. 2017, doi: 10.3390/polym9090449.

[182] D. D. Le Pevelen, "Small Molecule X-Ray Crystallography, Theory and Workflow," in *Encyclopedia of Spectroscopy and Spectrometry*, Elsevier, 2010, pp. 2559–2576.

[183] F. Ali, N. Ali, M. Altaf, A. Said, S. S. Shah, and M. Bilal, "Epoxy Polyamide Composites Reinforced with Silica Nanorods: Fabrication, Thermal and Morphological Investigations," *J. Inorg. Organomet. Polym. Mater.*, vol. 30, no. 10,

pp. 3869–3877, 2020, doi: 10.1007/s10904-020-01518-5.

[184] C. Van Dinh, "Evaluation of an Epoxy-Based Nanosilicacomposite Lining in H2SO4 Solution for Anticorrosion of Sewerage Concrete Structures," *J. Nanomater.*, vol. 2020, 2020, doi: 10.1155/2020/4090856.

[185] H. Liu *et al.*, "Fatigue modeling for carbon/epoxy unidirectional composites under various stress ratios considering size effects," *Int. J. Fatigue*, vol. 120, no. October 2018, pp. 184–200, Mar. 2019, doi: 10.1016/j.ijfatigue.2018.11.009.

[186] R. Starikov and J. Schön, "Experimental study on fatigue resistance of composite joints with protruding-head bolts," *Compos. Struct.*, vol. 55, no. 1, pp. 1–11, 2002, doi: 10.1016/S0263-8223(01)00127-1.

[187] J. I. MCCool, *Using the Weibull Distribution*. Wiley, 2012.

[188] E. Barbero, J. Fernández-Sáez, and C. Navarro, "Statistical analysis of the mechanical properties of composite materials," *Compos. Part B Eng.*, vol. 31, no. 5, pp. 375–381, 2000, doi: 10.1016/S1359-8368(00)00027-5.

[189] R. Bedi and R. Chandra, "Fatigue-life distributions and failure probability for glass-fiber reinforced polymeric composites," in *Special Issue on the 12th European Conference on Composite Materials, ECCM 2006*, 2009, vol. 69, no. 9, pp. 1381–1387, doi: 10.1016/j.compscitech.2008.09.016.

[190] P. D. Mangalgiri, "Composite materials for aerospace applications," *Bull. Mater. Sci.*, vol. 22, no. 3, pp. 657–664, 1999, doi: 10.1007/BF02749982.

[191] G. P. Pandian, D. Das, C. Li, E. Zio, and M. Pecht, "A critique of reliability prediction techniques for avionics applications," *Chinese J. Aeronaut.*, vol. 31, no. 1, pp. 10–20, 2018, doi: https://doi.org/10.1016/j.cja.2017.11.004.

[192] K. K. Singh and A. Gaurav, "Effectiveness of short and straight carbon nanotubes on dispersion state and static / dynamic mechanical properties of woven glass fibre-reinforced polymer laminates," *J. Mater. Des. Appl.*, vol. 233, no. 8, pp. 1661–1677,

2019, doi: 10.1177/1464420718780890.

[193] S. B. Ratner and V. I. Korobov, "Self-heating of plastics during cyclic defformation," *Polym. Mech.*, vol. 1, no. 3, pp. 63–68, 1965, doi: 10.1007/BF00858807.

[194] J. L. Thomason and L. Yang, "Temperature dependence of the interfacial shear strength in glass – fibre polypropylene composites," *Compos. Sci. Technol.*, vol. 71, no. 13, pp. 1600–1605, 2011, doi: 10.1016/j.compscitech.2011.07.006.

[195] R. Chandra, S. P. Singh, and K. Gupta, "Damping studies in fiber-reinforced composites - a review," *Compos. Struct.*, vol. 46, pp. 41–51, 1999.

[196] J. Petermann and K. Schulte, "The effects of creep and fatigue stress ratio on the long-term behaviour of angle-ply CFRP," *Compos. Struct.*, vol. 57, no. 1, pp. 205–210, 2002, doi: https://doi.org/10.1016/S0263-8223(02)00084-3.

[197] J. Brunbauer and G. Pinter, "Fatigue life prediction of carbon fibre reinforced laminates by using cycle-dependent classical laminate theory," *Compos. Part B Eng.*, vol. 70, pp. 167–174, 2015, doi: https://doi.org/10.1016/j.compositesb.2014.11.015.

[198] A. Benaarbia, A. Chrysochoos, and G. Robert, "Thermomechanical behavior of PA6.6 composites subjected to low cycle fatigue," *Compos. Part B Eng.*, vol. 76, pp. 52–64, 2015, doi: 10.1016/j.compositesb.2015.02.011.

[199] G. Ligia and R. Deodato, *Physicochemical behavior and supramolecular organization of polymers*. 2009.

[200] H. A. Whitworth, M. Othieno, and O. Barton, "Failure analysis of composite pin loaded joints," *Compos. Struct.*, 2003, doi: 10.1016/S0263-8223(02)00056-9.

[201] A. Gupta and M. Singh, "Reliability analysis to improve performance of multi-pin glass fiber-epoxy laminated composite joints using Weibull distribution," *World J. Eng.*, vol. 20, no. 4, pp. 621–630, 2023, doi: 10.1108/WJE-11-2021-0631.

[202] W. Ferdous *et al.*, "Testing and modelling the fatigue behaviour of GFRP composites – Effect of stress level, stress concentration and frequency," *Eng. Sci. Technol. an Int. J.*, no. xxxx, pp. 1–10, 2020, doi: 10.1016/j.jestch.2020.01.001.

[203] M. Singh, "Study of Nanocomposite Laminates and Failure Analysis of Pin Joints," Thapar Institute of Engineering and Technology, 2018.

[204] S. Stelzer, S. Ucsnik, and G. Pinter, "Fatigue behaviour of composite-composite joints reinforced with cold metal transfer welded pins," *Int. J. Fatigue*, vol. 81, pp. 37–47, 2015, doi: 10.1016/j.ijfatigue.2015.06.004.

[205] C. M. Manjunatha, S. Sprenger, A. C. Taylor, and A. J. Kinloch, "The tensile fatigue behavior of a glass-fiber reinforced plastic composite using a hybrid-toughened epoxy matrix," *J. Compos. Mater.*, vol. 44, no. 17, pp. 2095–2109, 2010, doi: 10.1177/0021998309360943.

[206] C. L. Liu, Z. Z. Lu, Y. L. Xu, and Z. F. Yue, "Reliability analysis for low cycle fatigue life of the aeronautical engine turbine disc structure under random environment," *Mater. Sci. Eng. A*, vol. 395, no. 1–2, pp. 218–225, Mar. 2005, doi: 10.1016/j.msea.2004.12.014.

LIST OF ABBREVIATIONS

ANOVA	Analysis of Variance
ASTM	American Society for Testing & Materials
B	Bearing
CMCs	Ceramic Matrix Composites
EFS	Effective Failure Strength
FEA	Finite Element Analysis
FEM	Finite Element Method
FI	Failure Index
FRC	Fiber reinforced Composite
FRP	Fiber reinforced polymer
GFRP	Glass fiber-reinforced polymer
GSM	Gram per meter square
HCF	High Cycle Fatigue
LCF	Low Cycle Fatigue
MMCs	Metal Matrix Composites
N	Net-Tension
Oas	Orthogonal Arrays
PEA	Polyetherimide
PMCs	Polymer Matrix Composites
PEEK	Polyetheretherketone
PPS	Polyphenylene sulfide
S	Shear-out
S/N	Signal-to-Noise Ratio
SEM	Scanning Electron Microscopy
UTM	Universal Testing Machine
UTS	Ultimate Tensile Strength
XRD	X-Ray diffraction

NOMENCLATURE

2D	Two-Dimensional
3D	Three-Dimensional
D	Diameter
E	Distance from free edge to hole diameter
E_{11}	Longitudinal Modulus
E_{22}	Transverse Modulus
G_{12}	Shear Modulus
L	Length from hole to other side of Plate
n	Scale Parameter
N	No. of Cycles
N_f	Cycles to Failure
P_{max}	Maximum Stress
R	Stress ratio
r_{oc}	Characteristic length in compression
r_{ot}	Characteristic length in tension
S	Shear stress
t	thickness of laminate
W	Width of plate
wt.%	Weight percent
X_c	Longitudinal strength in compression
Xt	Longitudinal strength in tension
Y_c	Transverse strength in compression
Y_t	Transverse strength in tension
β	Shape Parameters
γ	Position Parameter
θ	Failure Angle
ν_{12}	Poisson's ratio
σ_{11}	Maximum principal stress
σ_{22}	Minimum principal stress

LIST OF PUBLICATIONS

1	**Paper Title**	Comparative study of failure analysis in glass fiber reinforced laminated pin joints under cyclic and static loading conditions				
	Journal	Journal of Composite Materials **(SCI-E)**				
	Volume	-	**Issue**	-	**Year**	2024
	Publication Date	25nd January 2024				
	DOI	10.1177/00219983241230386				
2	**Paper Title**	Effect of Nano-silica on fatigue behavior of glass fiber-reinforced epoxy composite laminates : A Weibull distribution approach				
	Journal	Polymer Composites **(SCI-E)**				
	Volume	44	**Issue**	12	**Year**	2023
	Publication Date	21st September 2023				
	DOI	10.1002/pc.27761				
3	**Paper Title**	Investigation of failure behavior of glass fiber reinforced epoxy laminate under fatigue loading				
	Journal	World Journal of Engineering **(E-SCI)**				
	Volume	-	**Issue**	-	**Year**	2023
	Publication Date	20th December 2023				
	DOI	10.1108/WJE-09-2023-0367				
4	**Paper Title**	A critical review on damage modeling and failure analysis of pin joints in fiber reinforced composite laminates				
	Journal	Polymers and Polymer Composite **(SCI-E)**				
	Volume	30	**Issue**	-	**Year**	2022
	Publication Date	8th June 2022				
	DOI	10.1177/09673911221099764				
5	**Paper Title**	Reliability analysis to improve performance of multi-pin glass fiber-epoxy laminated composite joints using Weibull distribution				
	Journal	World Journal of Engineering **(E-SCI)**				
	Volume	30	**Issue**	-	**Year**	2022
	Publication Date	31st January 2022				
	DOI	10.1108/WJE-11-2021-0631				
6	**Paper Title**	Statistical Investigation on Reliability of Single-Hole Pin Joints Strength and Failure Mechanisms in Glass–Epoxy Composite Laminates				
	Journal	Recent Trends in Engineering Design, Lecture Notes in Mechanical Engineering – Springer **(Scopus)**				
	Volume	-	**Issue**	-	**Year**	2021
	Publication Date	26th June 2021				
	DOI	10.1007/978-981-16-1079-0_15				

7	**Paper Title**	Effect of Nanoclay in Unidirectional Carbon–Epoxy Laminated Composites			
	Journal	Advances in Materials Science and Engineering, Lecture Notes in Mechanical Engineering – Springer **(Scopus)**			
	Volume	-	**Issue** -	**Year**	2020
	Publication Date	22nd May 2020			
	DOI	10.1007/978-981-15-4059-2_13			

LIST OF CONFERENCES

1	**Paper Title**	Effect of Nanoclay in Unidirectional Carbon–Epoxy Laminated Composites				
	Conference	International Conference on Functional Materials, Manufacturing, and Performances (ICFMMP-2019)				
	Date	12-13	**Month**	September	**Year**	2019
	Venue	Lovely Professional University, Phagwara, Punjab				
2	**Paper Title**	Statistical Investigation on Reliability of Single-Hole Pin Joints Strength and Failure Mechanisms in Glass–Epoxy Composite Laminates				
	Conference	International Conference on Advances in Sustainable Technologies (ICAST - 2020)				
	Date	6-7th	**Month**	November	**Year**	2020
	Venue	Lovely Professional University, Phagwara, Punjab				
3	**Paper Title**	A compendium on composite laminated adhesive bonded joints and their structural application				
	Conference	International Conference on Materials for Emerging Technologies-2021 (ICMET-2021)				
	Date	18-19	**Month**	February	**Year**	2021
	Venue	Lovely Professional University, Phagwara, Punjab				
4	**Paper Title**	Multi-Objective Optimization of Glass-Epoxy Composite Laminated Pin Joint for Structural Application				
	Conference	4th International Conference on Functional Materials, Manufacturing and Performances-2023 (ICFMMP-2023)				
	Date	25-26	**Month**	August	**Year**	2023
	Venue	Lovely Professional University, Phagwara, Punjab				

LIST OF INTELLECTUAL PROPERTY RIGHTS

1	**Title**	A Fiber-Reinforced Composite Door Hinge Closure for Fatigue Loading Application				
	IPR Type	Patent				
	Publication Date	06	**Month**	June	**Year**	2022
	Application No.	202211029897				
	Field of Invention	Polymer Technology				
2	**Title**	A Novel Water Storage Tank				
	IPR Type	Patent				
	Publication Date	20	**Month**	January	**Year**	2023
	Application No.	202311003023				
	Field of Invention	Mechanical Engineering				
3	**Title**	Design Simulation and Optimization of Composite Laminated Pin Joints in Structural Application				
	IPR Type	Patent				
	Publication Date	19	**Month**	May	**Year**	2023
	Application No.	202311020892				
	Field of Invention	Mechanical Engineering				
4	**Title**	Experimental and numerical study of glass/epoxy composite (GFRP) laminated pin joints under fatigue loading				
	IPR Type	Copyright (Graphical Abstract)				
	Publication Date	30	**Month**	November	**Year**	2022
	Dairy No.	24688/2022-CO/L				

LIST OF MANUSCRIPT
(ACCEPTED/COMMUNICATED/DRAFTED)

1	**Title of Manuscript**	Effect of Nano-silica on the fatigue behavior of Glass Reinforced epoxy composite pin joints
	Target Journal	International Journal of Fatigue **(SCI-E)**
	Status	Manuscript Communicated
2	**Title of Manuscript**	Investigation of the Geometric Parameters on the Performance of Glass Fiber Reinforced Polymer laminated Mechanical Joints under Fatigue Loading
	Target Journal	Polymer Composites **(SCI-E)**
	Status	Manuscript Communicated